2020•2021

Faculteit Industriële Ingenieurswetenschappen

master in de industriële wetenschappen: energie

Masterthesis

Validation of Different Power Loss Models for a Bidirectional Isolated Dual-Active-Bridge DC-DC Converter used in Ultra-fast, Modular Electric Vehicle Chargers

PROMOTOR :

Prof. dr. ir. Wilmar MARTINEZ

PROMOTOR :

ir. Camilo SUAREZ

Dries Willems, Jaan Wouters

Scriptie ingediend tot het behalen van de graad van master in de industriële wetenschappen: energie, afstudeerrichting elektrotechniek

Gezamenlijke opleiding UHasselt en KU Leuven

UHASSELT KU LEUVEN

UHASSELT KU LEUVEN

2020•2021

Faculteit Industriële Ingenieurswetenschappen

master in de industriële wetenschappen: energie

Masterthesis

Validation of Different Power Loss Models for a Bidirectional Isolated Dual-Active-Bridge DC-DC Converter used in Ultra-fast, Modular Electric Vehicle Chargers

PROMOTOR :

Prof. dr. ir. Wilmar MARTINEZ

PROMOTOR :

ir. Camilo SUAREZ

Dries Willems, Jaan Wouters

Scriptie ingediend tot het behalen van de graad van master in de industriële wetenschappen: energie, afstudeerrichting elektrotechniek

UHASSELT KU LEUVEN

Preface

This master's thesis constitutes the final assessment criterium in the framework of the Master program in Energy and Electrical Engineering Technology at Hasselt University in association with KU Leuven. We chose this subject because we are very interested in the automotive sector and especially in fully electric vehicles. The time needed to almost fully charge an EV has always been a much-discussed topic and is often seen as a disadvantage compared to conventional cars which use fossil fuel. We consider being able to contribute to this research as a great honor and that's what motivated us to complete this thesis successfully.

Of course, this was not an easy journey, and that's why we want to first of all thank our promotors Prof. Dr. Ir. Wilmar Martinez and Ir. Camilo Suarez for the good guidance during the making of this thesis. They always made sure we could rely on their expertise in power electronics when implementing the programmed models and analyzing the experimental results. Both of them also took the time to monthly meet with us and help us in determining our next steps. Beyond all this, they also took the time to read through our entire thesis and provided continuous feedback. Another special thanks to Camilo Suarez for constructing a high power, experimental DAB converter, which could be used for measurements.

Prof. Dr. Jeroen Lievens is the next person we would like to thank. He gave us the necessary information and tips to construct a professional paper and also provided plenty of feedback about the scription and poster.

Next, we wanted to thank KULeuven at EnergyVille for letting us use their offices and conference rooms. This gave us a safe place to meet during the COVID-19 pandemic, so all of the communication and work did not have to take place via online meetings. This also helped us in understanding each other more clearly, which prevented many mistakes from being made.

Finally, a special thanks to our family and friends for supporting us whenever needed.

We learned a lot from making this thesis and hope you can do the same by reading it.

May this thesis be useful for readers and for future research about similar topics or any other related field.

Table of contents

List of Tables

List of Figures

List of Designators and Abbreviations

AC	alternating current
A_{eff}	effective area
α	Steinmetz coefficient
A_{wire}	cross-section area of wire
β	Steinmetz coefficient
B_{max}	peak magnetic flux density
C_{ds}	drain source capacitance
C_f	capacitance of the freewheeling diode
C_{gd}	gate drain capacitance
C_{gs}	gate source capacitance
C_{iss}	input capacitance
C_{oss}	output capacitance
C_{rss}	reverse transfer capacitance
C_s	snubber capacitor
D	duty cycle
DAB	Dual active bridge
DC	Direct current
DPS	dual phase shift
EMF	electromagnetic flux
EPS	extended phase shift
ESS	Energy storage system
EV	electric vehicle
FEV	fully electric vehicles
f_s	switching frequency
HEV	hybrid electric vehicles
$I_{avg,t_{dead}}$	average current during dead time
$I_{channel}$	current through the channel of the mosfet
ICS	input current sharing
I_d	drain current
I_{DC}	average direct current through transformer
i_{FET}	current through MOSFET
IGBT	insulated gate bipolar transistor
I_{L1}	maximum reverse current through diodes in primary bridge
I_{L2}	maximum reverse current through diodes in secondary bridge
IPOP	input parallel/output parallel
$I_{reverse}$	reverse current
I_{RMS}	rms value of switch current
ISOP	input parallel/output series
IVS	input voltage sharing
k_e	Eddy current constant
k_i	Steinmetz coefficient
K_I	coefficient for current dependency of switching losses
K_V	coefficient for voltage dependency of switching losses
L_d	drain inductance
L_s	source inductance

l_{turn}	length of one turn around the core
MOSFET	metal-oxide semiconductor field effect transistor
n	amount of turns of winding
OCS	output current sharing
OVS	output voltage sharing
P_{cond}	conduction losses
P_{copper}	copper losses
P_{in}	input power
P_{iron}	iron losses
P_{ohm}	ohmic losses
P_{out}	output power
P_{sw}	switching losses
P_{unk}	unknown losses
Q_{rr}	reverse recovery charge
$R_{SBD,on}$	on-state resistance of the Schottky barrier diode
$R_{ds,on}$	on-state resistance of the MOSFET
$R_{g,ext}$	external resistance of gate
ρ	specific resistivity of wire material
RMS	root mean square
R_{wire1}	resistance op primary winding
R_{wire2}	resistance op secondary winding
SBD	schottky barrier diode
SiC	silicon carbide
SPS	single phase shift
SR	synchronous rectification
t_b	beginning of switching transition
t_{core}	thickness of transformer core
t_{dead}	dead time
t_e	end of switching transition
t_{fr}	forward recovery time
t_{off}	turn off event time
t_{on}	turn on event time
TPS	triple phase shift
t_{rr}	reverse recovery time
T_s	switching period
$V_{SBD,on}$	forward voltage drop from SBD
V_{core}	volume of transformer core
V_{ds}	drain source voltage
V_{DSS}	drain source breakdown voltage
VFD	voltage where Coss drops significantly
V_{gs}	gate source voltage
V_{in}	input voltage
V_{miller}	voltage at miller plateau
V_{out}	output voltage
V_{th}	threshold voltage
ZCS	zero current switching
ZVS	zero voltage switching

Abstract

Due to the rapid electrification of vehicles, EnergyVille is researching 350kW modular, Ultra-fast chargers consisting of multiple DAB converters. Thanks to these kinds of converters, the charger is able to output multiple voltage and current levels independently of each other. This allows the charger to adapt to the vehicles' specifications to ensure optimal fast charging.

To reduce the size of the converter, a high switching frequency is used, which causes large switching losses. These switching losses prove difficult to estimate in high power components due to their parasitic elements. Nowadays, these losses are always verified experimentally via a prototype. The goal of this masters' thesis is to establish different models to estimate the switching losses based on datasheet parameters of the components.

These models are set up in Python and are validated through an experimental setup. Specifically, different operating points of the converter are set and the switching losses are determined via the measured values. Since the models differ in complexity, it is interesting to see which model is the most accurate. Additionally, a model is created to estimate the other converter losses throughout this operating range.

The experimental verification shows that the most complex model, model 3, is the most accurate compared to the experimental results. Therefore, it is used to determine the switching losses throughout the entire operating range.

Abstract Nederlands

Door de snelle elektrificatie van voertuigen doet EnergyVille onderzoek naar 350kW modulaire, ultrasnelle laders bestaande uit meerdere DAB-converters. Dankzij deze converters kan de lader verschillende uitgansspanningen en -stromen onafhankelijk van elkaar bereiken. Zo kan de oplader zich aanpassen aan de specificaties van de auto om een zo optimaal mogelijk laadproces te garanderen.

Om de omvang van de omvormer te verkleinen wordt een hoge schakelfrequentie gebruikt, met grote schakelverliezen tot gevolg. Deze verliezen zijn moeilijk in te schatten door de parasitaire elementen in de vermogen elektronica. Tegenwoordig worden deze experimenteel berekend via een prototype. Het doel van deze thesis is het verifiëren van verschillende modellen die deze verliezen inschatten via de datasheetparameters van de componenten.

De modellen zijn opgezet met Python en worden gevalideerd door middel van een experimentele opstelling. Concreet worden van verschillende werkingspunten van de omvormer de schakelverliezen bepaald via de meetresultaten. Omdat de modellen verschillen in complexiteit, is het interessant om te zien welk model het meest nauwkeurig is. Daarnaast wordt er ook een model gemaakt om de andere converterverliezen binnen dit werkingsgebied te schatten.

Uit de experimentele verificatie blijkt dat het meest complexe model het meest nauwkeurig is in vergelijking met de meetresultaten. Deze wordt daarom gebruikt om de schakelverliezen over het hele werkgebied te bepalen.

1. Introduction

1.1. Situation

Since renewable energy and sustainability are receiving more and more attention, it has become a priority for the industry to obtain the highest possible efficiency for all known and new processes. Charging electric vehicles also attracts a lot of attention in this domain. Due to recent increase in popularity of electrified forms of transport, the demand increases for high power DC chargers that can charge a large portion of the battery of these vehicles in a short period of time. More and more automobile manufacturers are opting for partially electric (HEV) or even fully electric (FEV) vehicles, of which the batteries have specifications tailored to the manufacturer or even the model. As a result, high power DC chargers that can work on different operating points and can meet these various specifications, are becoming necessary for use in smart charging stations.

EnergyVille in Thorpark, Genk is researching the use of 350kW DC chargers with modular construction [1]. Such modularity allows chargers to adapt to the specifications of the battery, making the charging itself more efficient and allowing the battery to last longer. In order to charge all current electric vehicles, this charger must have a voltage range from 200V to 900V and cover a current range from 5A to 500A.

This modular charger is made up of modules with the same or different power outputs. These modules contain a Dual Active Bridge converter (DAB) [1]–[3]. The DAB converter has always the same, simple setup that most of the times consists of MOSFETs, diodes and a galvanic isolation, in this case a transformer. These modules can be connected in different ways and can each be operated individually. This way, the output power can be set as desired, while the efficiency is kept as high as possible. The modular charger has the ability to charge multiple vehicles at the same time. This charger can split its modules and power output between the two vehicles in order to make optimal use of the installed charging capacity.

Additionally, these chargers can be used for charging electric heavy-duty vehicles in the future, such as trucks and lorries [1]. These vehicles will have larger batteries and therefore it will take longer to charge these batteries. This means these chargers will be very cost-effective for trucks since a great enough portion of the battery can be charged in the short rest-period the truck drivers have, without the need of stopping them early to rest again.

Finally, These DAB converters can also be used in smart energy storage systems (ESS) and grid support applications [4]. In some cases, an ESS can even be connected to de DC link of the converter, eliminating the need for a separate battery inverter.

1.2. Problem definition

One of the motives for private individuals and companies to switch from fossil fuels to electricity in terms of mobility and transport is the savings on tax and fuel costs. The latter in particular can be strongly influenced by the charging process of the battery of the

vehicles. When charging with a low-efficiency charger, a large part of the absorbed electrical energy will be lost and therefore no longer usable. These losses imply bigger heatsinks or more expensive cooling which makes the charger technology more expensive and also larger in size [5], [6]. Such losses are not present when refueling with fossil fuel. That is the reason why it is very important that high-power chargers achieve a very high efficiency. For ultra-fast chargers (350kW) the efficiency is determined so that most commercial car batteries can be charged to 80% in less than 15 min. The DAB converter has to deal with several losses which can cause a modular, high power charger to not reach a high enough efficiency. These losses consist of the switching losses of the MOSFETs and their antiparallel diodes and the magnetic losses of the transformer, which forms the center of the circuit of the converter. However, determining these losses at the design stage has proven to be difficult. This is especially true for the switching losses. These losses are most of the time determined by building a prototype converter and calculating them based on measurements. This is a costly and time consuming process. The need arises for a fast and effective way to estimate the losses based on the datasheet parameters of the converter components. This helps eliminating potential components which would cause high losses and saves time and costs on building prototypes. It also helps in understanding the efficiency at different operating points, which can be used to further improve the power management of the charger among its multiple converters.

Therefore, the following was chosen as the research question: "What is the accuracy of existing MOSFET switching models and can they be used to estimate the switching losses of a DAB converter operating under wide voltage and load conditions?"

1.3. Goals

The purpose of this thesis is to investigate how accurate existing switching loss models are in estimating the switching losses which occur during the operation of a DAB converter. This is the first objective of this thesis.

Additionally, a model which estimates the efficiency of the converter is also made. The losses of the converter depend on the output power of at any given time. It is important to be able to determine the efficiency of a single converter over its entire operating range before deciding the amount of modules which make up a 350kW charger for a desired level of efficiency. This is because the efficiency of the charger depends on the sum of the losses of all active modules together as stated in [5]. This also allows further research into control patterns for series or parallel connected converters [7]. Therefore, making a model which estimates the total losses of the converter is the second objective of this thesis.

These models are implemented or created in Python, as this is an open-source programming tool and can be accessed by all.

This thesis can be used as a guide for further research to design a modular, high power DC charger by EnergyVille.

1.4. Method

This thesis mainly focuses on taking steps towards creating a model which accurately estimates the losses in a single DAB converter. The information around the different kind of losses present in the converter, given by [5], serves as the starting point of the literature study. In [5], a Matlab model is constructed which returns the components which will make up the DAB converter with the highest efficiency.

However, this model does not take the complexity of the switching losses into account. For this reason, this thesis is focused mainly on the verification of existing switching models. Additionally, these models are used in a self-made model which models all the losses of the converter. Finally, this model is also verified with experimental results.

2. Literature study

2.1. The DAB Converter Topology

2.1.1 Overall Circuit Topology

According to [8], dual active bridge bidirectional isolated power converters in general are a necessary tool to control the power flow at different DC voltage levels. The dual active bridge consists of a full H-bridge that acts as a DC-AC converter and is connected to the primary winding of a high frequency isolating transformer. The secondary winding of this transformer is connected to another full H-bridge that works as an AC-DC converter. Both H-bridges consist most of time of 4 power MOSFETS with each a freewheeling diode placed in antiparallel. This topology is shown in Figure 1.

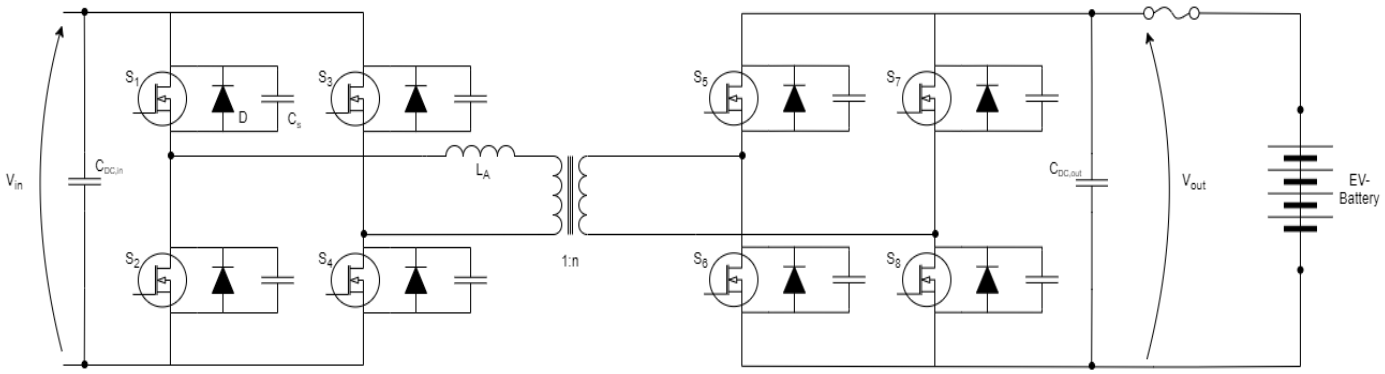

Figure 1: Topology of a bidirectional, isolated dual-active-bridge DC/DC-Converter.

The DAB converter is bidirectional, meaning that the power can flow in both directions and it can work as both a buck or a boost converter [8]. The secondary full bridge is galvanically isolated from the primary via the transformer. This transformer often has a winding ratio $n = 1:1$. However this is not always the case, as in this thesis. It is possible to have snubber capacities parallel over each MOSFET/diode pair, this is done in order to achieve less switching losses, which will be discussed later on, and to get a smaller ripple in the current of the DC-link capacitances [9].

2.1.2 Electronic Components

2.1.2.1 Power Diode

Often a silicon carbide (SiC) Schottky barrier diode (SBD) is normally chosen as the anti-parallel freewheeling diode, placed across each power MOSFET in the full H-bridges. However, in the converter used for this thesis, the internal body diode of the MOSFET will be used to conduct reverse currents. But for completeness of this thesis, a short introduction will be given about the basic working principles behind a SiC SBD.

A normal silicon diode is a device that is able to let current flow in only one direction thanks to the formation of a depletion region between the two differently doped layers as shown in Figure 2.

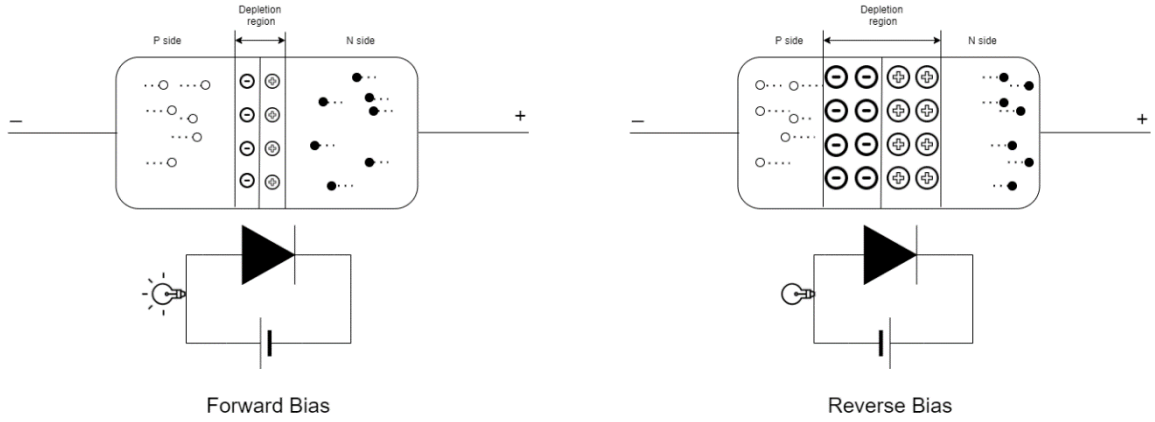

Figure 2: Visual representation of shrinking and widening of the depletion region when applying a forward and reverse bias respectively [10].

This property is ideal to let current bypass a switching device after it is turned off and an inductive load causes a rise in voltage across the switching device, which might potentially damage it. Diodes start conducting after a certain voltage across it, has been reached. This voltage is also called the barrier voltage. After this point the forward current increases rapidly as the voltage across the diode increases further. When this voltage becomes reverse biased, almost no current will be able to flow through the device. However, at a certain point the reverse voltage can become too high and the diode will break down, allowing a large reverse current to flow through the device and damaging it in turn. These characteristics are shown in the graph in Figure 3.

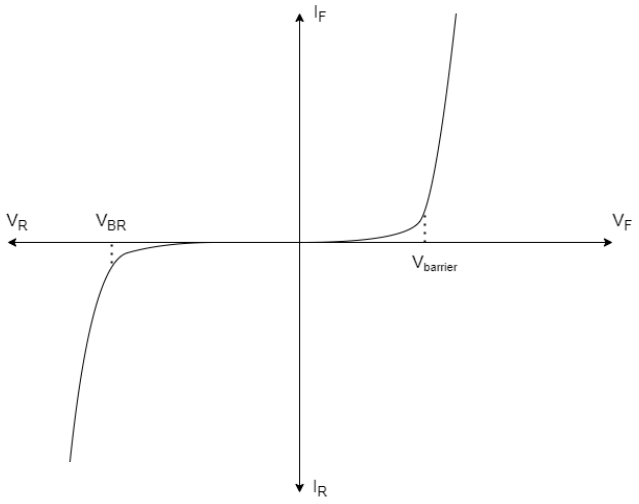

Figure 3: Typical V-I characteristic curve of a normal silicon diode [10].

For high power applications, power diodes are considered because of their higher breakdown voltages and reasonably low barrier potential voltage at high power levels [11, p. 524] [10, pp. 1–70]. But recent innovations in wide-bandgap silicon carbide technology

allowed the use of SiC power diodes, which have superior switching characteristics and operate better in high power and high temperature applications [12].

In order to have even better switching characteristics, SBDs are often used in these converters. These kinds of diodes are formed by joining metal layer together with a semiconductor material. This causes the diode to have a smaller depletion region. This in turn means the diode will have a lower capacitance, lower forward voltage drops at nominal currents and will be able to conduct larger forward currents. This makes it an ideal component for high frequency applications like DAB converter. Thanks to the use of SiC technology in the SBD, blocking voltages from 500V to 10kV with a minimum of 100 A/cm² of maximum forward current density can be managed by a 4H-SiC SBD rectifier [13]. A section of this component can be seen in Figure 4.

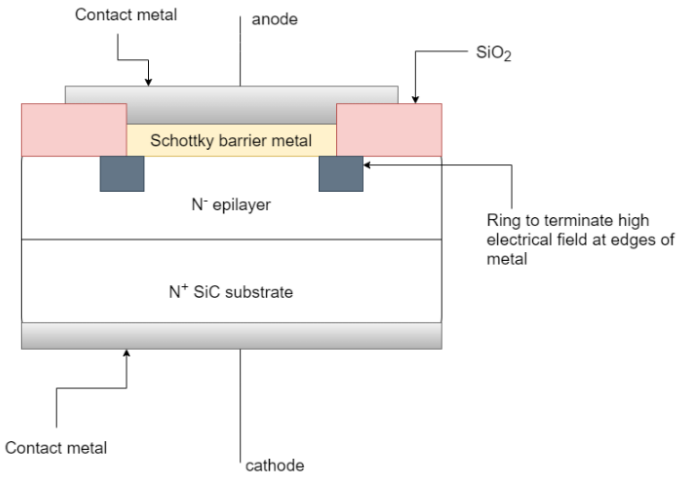

Figure 4: Section of a SiC-Schottky barrier diode [13].

A third reason to use an SBD is because it has superior switching characteristics compared to the intrinsic body diode which is incorporated into the MOSFET structure. The smaller recovery charge (Q_{rr}) and a lower forward voltage drop ($V_{SBD,on}$) of the SBD prevent the intrinsic diode in the power MOSFET from activating during the dead time (t_{dead}). A comparison between these two types of freewheeling diodes is made in [14]–[16]. But, as mentioned before, the converter used in this thesis does use the intrinsic body diode of the switching device. This is done because this diode structure still shows a decent performance at high frequencies and helps in reducing costs and chip count of the module even though a better efficiency would be reached by utilizing a SiC SBD [14] .

2.1.2.2 Power MOSFET

According to [3][5][6], a MOSFET is a semiconductor device that allows current to pass by applying a positive or negative bias to the gate connection of these devices, depending on the type of material which makes up the channel of the MOSFET, which can be a P-type material or an N-type material. P-channel devices require a negative bias to be applied to the gate, whereas N-channel devices require a positive bias. In this thesis, N-channel MOSFETs will be used in order to keep the driving circuit less complicated. As soon as a

positive or negative bias is applied to the gate of the device, a conductive channel will form between the source and the drain and allow current to pass through from the drain connection to the source connection of the device and vice versa as shown in Figure 5.

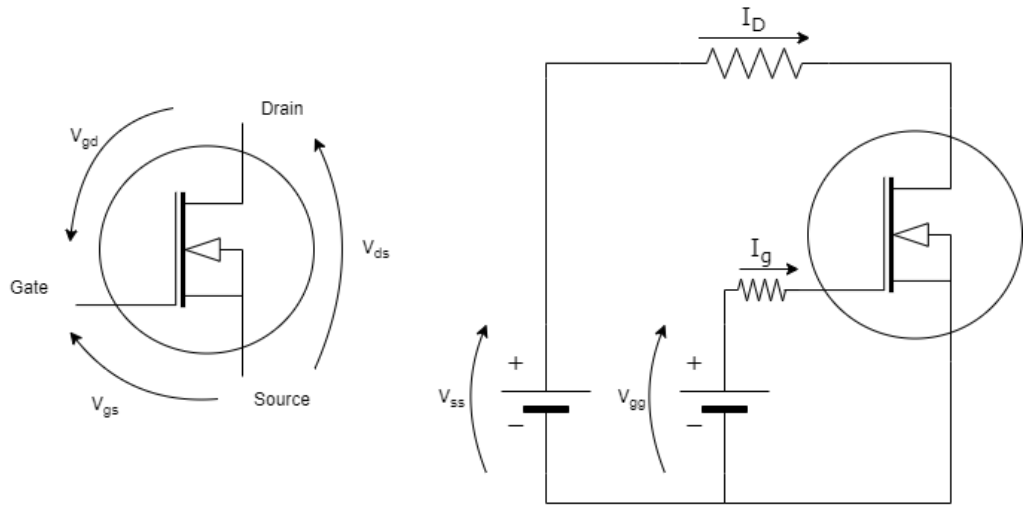

Figure 5: Connections and Operation of an N-channel MOSFET.

A MOSFET begins conducting current as soon as the gate-source voltage (V_{gs}) reaches a certain threshold value (V_{th}). The current which begins to flow through the channel depends on both the value of V_{ds} and V_{gs}. After a certain point where $V_{gs} - V_{th} < V_{ds}$, the current becomes only dependable on V_{gs}. At a further point, V_{ds} will surpass the drain-source breakdown voltage (V_{DSS}). This causes avalanche breakdown to occur in the drain-body junction of the device. At this point, the device will begin conducting large currents, which will in turn damage the device. These characteristics are shown in the graph in Figure 6.

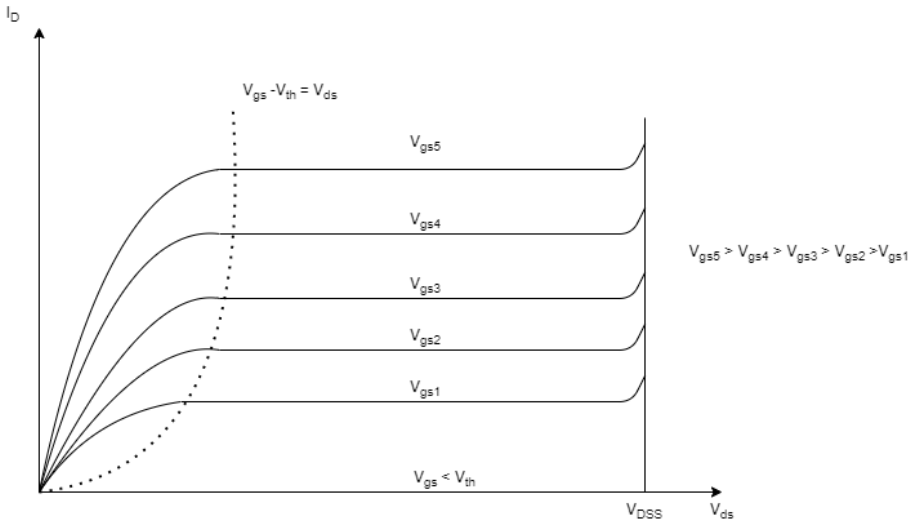

Figure 6: Typical V-I characteristic of MOSFET [10].

Most normal Si MOSFETs will not be able to support the high voltages and currents which occur in DAB converters with a higher power output, like the prototype used in this thesis. For this reason, SiC power MOSFETS will be used. These devices are best used for their

fine properties in high temperature applications [18], [19]. According to [9], [20], the use of MOSFETs instead of IGBTs is more convenient since it works better at higher switching frequencies, which will in turn allow a single module to have a higher power to volume ratio because the inductor size decreases as the switching frequency increases. Si-IGBT-based converters only work best at switching frequencies ranging from 20 kHz to 25 kHz.

2.1.2.3 Transformer

A high-frequency transformer can be found in the heart of the converter. This transformer ensures a galvanic isolation between the input, often the utility grid, and the output of the converter, in this thesis the battery of an EV. According to [5] extra auxiliary inductors are often added in series to the transformer in case the leakage inductance of the transformer is not sufficiently high enough. The core is often made from material, which allows the flux to flow through it and through the secondary windings. The flux also induces an EMF in the secondary windings, which is equal to the secondary open-circuit voltage. When a load is connected like in Figure 7, current will be able to flow in the secondary winding [5], [21].

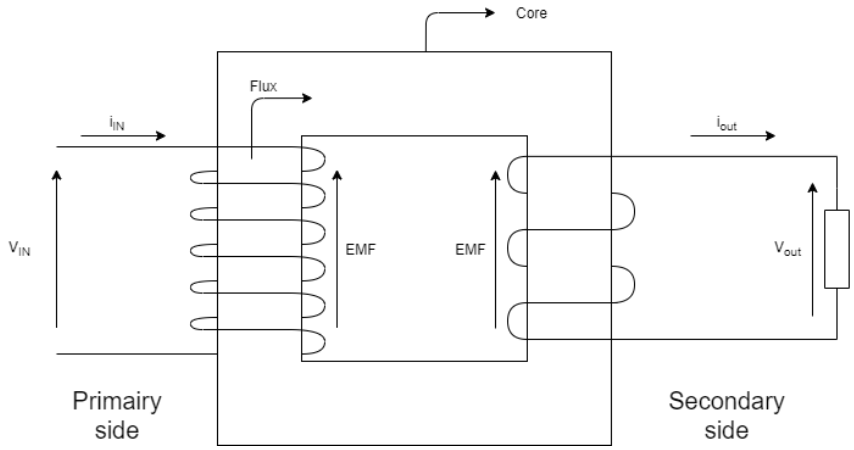

Figure 7: Operation of a transformer.

2.2. Loss Analysis

2.2.1 Overall Losses

The DAB converter has several losses, which can be divided into three categories like in [9]: ohmic losses (P_{ohm}), iron losses (P_{iron}) and switching losses (P_{sw}). The ohmic losses can be further divided into conduction losses (P_{cond}), copper losses (P_{copper}) and unknown losses (P_{unk}). The power MOSFETs are responsible for some conduction losses and switching losses. According to [9] these losses represent 60% of the total losses of the converter and both are about equal in size. The copper and iron losses are almost completely located in the magnetic components of the converter and they contain about 30% of the total losses. Finally, the unknown losses are all the power losses from which the origins are most of the time known, but the value cannot be determined. Their total

value can only be calculated by subtracting all other losses from the total losses. A visual classification and relation is given in Figure 8.

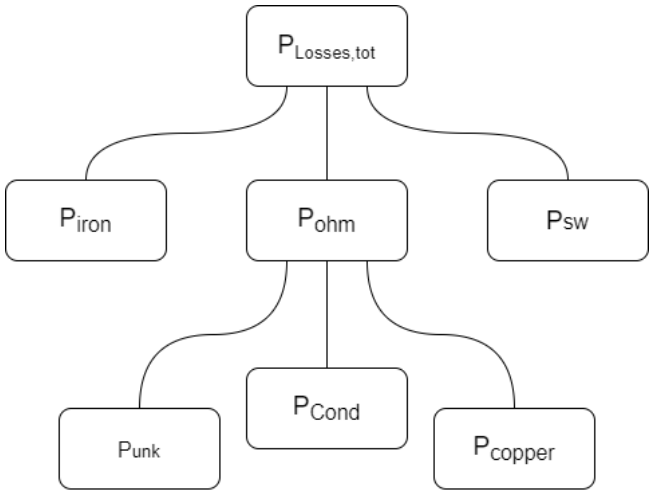

Figure 8: Schematic representation of the losses in a DAB converter [9].

2.2.2 Conduction Losses

2.2.2.1 Schottky diode

Conduction losses are the most dominant losses in the converter, often containing more than one third of the total losses in the converter. These losses occur when the power MOSFET and power diode are in the on-state and thus conducting the freewheeling during t_{dead}. This freewheeling current, which occurs when a MOSFET is turned off, is caused by the inductive loads connected to the switching devices. In this case, the inductive load is the isolation transformer.

A model to calculate the conduction losses in a SiC-Schottky barrier diode (SBD) is presented in [22].

$$P_{cond,SBD} = V_{SBD,on} \cdot (I_o - i_{FET}) \quad (1)$$

Where $V_{SBD,on}$ is the forward voltage drop of the SBD, I_o the sum of the current through the Schottky diode and MOSFET at any given time and i_{FET} the current through the MOSFET at any given time during t_{dead}.

In [23] a more accurate estimation of the conduction losses are made. The on-state resistance and voltage drop of a SBD are calculated, taking into account their temperature dependency. Note that both $V_{SBD,on}$ and $R_{SBD,on}$ of a SiC SBD at $T > 50°C$ are higher than those of a Si PN diode, meaning lower conduction losses. However, the Si PN diode does have a much larger reverse recovery charge Q_{rr}, causing it to have higher switching losses than the SBD, which has a negligible Q_{rr}. Which will be discussed later on.

In [5], [24], [25], it is expected that the SBD only conducts during the dead time t_{dead}, when all switches in the full bridge are turned off. The conduction losses in a single SBD are calculated using the average current ($I_{avg,t_{dead}}$) during that time. This value is determined based on t_{dead}, the peak current value in the primary while the SBD conduct (I_L) and the switching frequency (f_s).

As stated before, the converter used in this thesis does not employ the use of SiC SBDs to conduct the freewheeling current. Instead, synchronous rectification will be used. This will be explained later on.

2.2.2.2 SiC power MOSFET

Conduction losses occur in the power MOSFETs when they are turned on and conducting. During this time (t_{on}), a forward voltage drop exists across this device because of the resistance caused by all of its internal layers. This resistance is called the on-state resistance ($R_{ds,on}$) or on-resistance for short.

As can be seen in [26] there exist a lot of different power MOSFET structures which all fundamentally work via the same principle. All these structures have the same layers as the power VD-MOSFET structure, which is shown in Figure 9. The on-resistance is the total resistance of resistance of the device which causes a voltage drop across it. It can be obtained by the addition of all the resistances of the different layers through which current normally travels. How all these resistances are calculated is shown in [26]. Note that the structure the SiC MOSFETs used in the converter, only differs slightly from the VD-MOSFET structures shown in Figure 9. This difference has no real impact on the total $R_{ds,on}$. This is because the current passes through the same layers in both MOSFET structures.

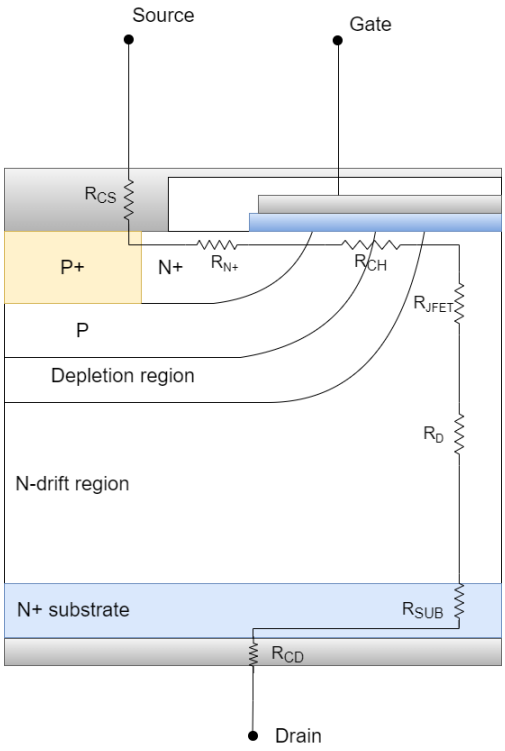

Figure 9: The typical VD-MOSFET structure with internal resistances for each of the layers where current passes through [13].

In [22], [25] the conduction losses for a single MOSFET are calculated as follows:

$$P_{cond,MOSFET} = I_{RMS,MOSFET}^2 \cdot R_{ds,on} \tag{2}$$

where R_{ds} is the on-resistance of the MOSFET and I_{RMS} is the RMS-value of the switch current. However, if the current ripple ratio is very small, the current is equal to

$$I_{RMS,MOSFET} \approx I_{DC} \cdot \sqrt{D} \tag{3}$$

where I_{DC} is equal to the average current flowing through the transformer and D is the duty cycle of the MOSFETs.

In [5][27] the conduction losses are calculated, taking into account the temperature dependency of the on-resistance, which usually can be found in the datasheet of the device. Furthermore, the RMS-value of the current in these papers is determined via more accurate but complex formula compared to (3).

The converter model created in this thesis will use neither of these methods to determine $I_{RMS,MOSFET}$. This will be explained in 3.3.

2.2.3 Copper Losses

According to [9], copper losses are one of the losses caused by magnetic devices. These losses are caused by the resistance of the wires at both the primary and secondary side of the high frequency transformer. According to [5], [6], [28] they are equal to:

$$P_{copper} = R_{wire,1} \cdot I_1^2 + R_{wire,2} \cdot {I_2}^2 \tag{4}$$

$$R_{wire} = \rho \frac{N \cdot l_{turn}}{A_{wire}} \tag{5}$$

with $R_{wire,1}$ the resistance of the primary winding, $R_{wire,2}$ the resistance of the secondary winding, ρ the resistivity of the wire material, l_{turn} the length of one turn around the core, N the amount of turns and A_{wire} the cross-section area of the wire.

Note that for AC signals, the RMS value of the current is used which means these losses can normally vary in time and are depended on the load [6].

Eddy current effects, which include skin effect and proximity effect can cause a non-uniform distribution of current across the section of the wire, increasing the copper losses. In [6], [29] the use of Litz wires is recommended to suppress the losses caused by these effects. In this thesis, the proximity losses are assumed to be negligible, since an improved winding geometry and use of Litz wires can reduce these losses by a great amount like stated in [30]. The skin effect can take place at high switching frequencies and causes current to concentrate on the side surface of a conductor. This causes R_{wire} to increase because the effective area A_{eff}, where the current really flows, becomes smaller than the total section of the wire A_{wire} [5], [31]. The use of Litz wires will reduce the skin effect by increasing A_{eff}. However, this reduction falls outside the scope of this thesis and is further discussed in [29], [31]. This thesis assumes the use of Litz wires causes $A_{eff} \approx A_{wire}$.

2.2.4 Iron Losses

These losses are better known as core losses and are caused by the changing magnetic field in the transformer core. They are dependent on the type of materials in the core and their magnetic properties. They consist of hysteresis and Eddy current losses.

Hysteresis losses are caused by the magnetizing flux constantly changing direction along with the current in the primary. This causes domains in the core material to reorientate so their magnetic field becomes parallel to the magnetic lines of the flux. This reorientation requires some work, which is known as hysteresis losses [6], [32]. According to [5], [6], [32]–[36], the hysteresis losses (P_{hys}) can be calculated with the Steinmetz equation:

$$P_{hys} = k_i \cdot f_s^{\alpha} \cdot B_{max}^{\beta} \cdot V_{core} \tag{6}$$

with k_i, α and β as Steinmetz coefficients, B_{max} the peak magnetic flux density in the core and V_{core} as the volume of the transformer core.

This equation is only valid if the magnetic flux in the core has a sinusoidal wave form, which will not be the case for the transformer in the converter. In [5], [6], [33], [35], [36] this formula is further modified to fit any waveform and it is shown how k_i is calculated.

This complicated formula is eventually simplified to accurately calculate the iron losses of the transformer present in the DAB converter:

$$P_{hys} = \frac{k_i}{T} \cdot |4B_{max}|^{\alpha} |2B_{max}|^{\beta-\alpha} \tag{7}$$

Eddy current losses are losses caused by the heat dissipation of small, locally circulating currents, also known as Eddy currents, in the core material or the metal encasing of the transformer. These currents originate from locally induced EMF in the core. They are calculated as follows [6], [37]:

$$P_{eddy} = k_e f_s^2 t_{core}^2 B_{max}^2 \tag{8}$$

where k_e is the Eddy current constant and t_{core} the thickness of the transformer core.

As these losses only make up around 10% of the total losses present in the converter, they will not be included in the model, as this thesis will focus more on the losses caused by the electronic components and not the transformer.

2.2.5 Switching Losses

2.2.5.1 Schottky Diode

MOSFETS are not the only components which provide switching losses. The SBD placed in anti-parallel also contributes to these losses. These losses are mainly caused by the capacitance of the device, or to be more specific, the capacitance of the depletion region between the metallic layer and the epilayer. This characteristic allows the following effect to take place during on and off switching:

When the SBD is turned on, the epilayer has to be filled with charge for a certain duration of time, which is called the forward recovery time t_{fr}. During this time, the voltage drop across the diode will be larger than in regime. The higher the blocking voltage of the device, the thicker the epilayer has to be and the larger the forward voltage drop will be. This voltage drop is also temperature dependent [38].

When switching the Schottky diode off, the abundant charges in the epilayer will not directly disappear, but take some time to evacuate. During this time, the diode will keep conducting while the current decreases with di_f/dt. This decrease is determined by the rest of the circuit. As soon as the current reaches zero, a part of these charges will recombine inside the diode. The other part, called the reverse recovery charge (Q_{rr}) will be evacuated thanks to the reverse bias. The time it takes to evacuate Q_{rr} is called the reverse recovery time (t_{rr}). During this time, a reverse current will flow through the diode until it reaches a maximum and rises back to zero. From the moment the maximum reverse current is reached, till the moment the current rises back to and reaches zero, the charge Q_{rr} is being evacuated. After this the diode is completely turned off and the voltage across the diode is equal to the reverse bias. Q_{rr} and t_{rr} often indicate the ability of a diode

to switch at high frequencies. However, due to the low capacitance of Schottky diodes, the Q_{rr} and t_{rr} are almost zero and negligible [13], [23], [38].

The losses caused by this effect are less complex to determine and can be calculated via

$$P_{sw,SBD_{prim}} = f_s \cdot V_{in}(I_{L1} \cdot t_{rr} + Q_{rr}) \tag{9}$$

$$P_{sw,SBD_{sec}} = f_s \cdot V_{out}(I_{L2} \cdot t_{rr} + Q_{rr}) \tag{10}$$

with V_{in} and V_{out} respectively the input and output voltage of the converter, I_{L1} and I_{L2} the maximum reverse current flowing through the diodes in primary and secondary respectively and t_{rr} the reverse recovery time of the device, which is almost zero for SBDs [5].

Like is said many times before, the converter used in this thesis does not employ SBD's as freewheeling diodes but uses the intrinsic body diode of the MOSFETs and synchronous rectification to deal with the reverse currents which occur when the other MOSFET in same leg of the bridge is turned off. As said earlier in this section, SBDs have smaller reverse recovery characteristics than the intrinsic body diode. This is the reason why these kind of diodes are chosen as the external freewheeling diodes for the MOSFETs in this application. Because of the smaller Q_{rr} and t_{rr}, they tend to switch on much faster than the body diode. This means the body diode has a much higher Q_{rr} and t_{rr} and their switching losses will be higher than those of SBDs. This will be taken into account when analyzing the experimental results.

2.2.5.2 MOSFET

Switching losses occur when the MOSFET is transitioning between the on-state to the off-state and vice versa. Logically this makes these losses frequency dependent and not duty cycle dependent. The prediction of switching losses in power converters is becoming more complex and necessary due to the increase of operating frequencies to minimize the size of passive components of the system, like for example the transformer [39]. A deeper understanding of MOSFET behavior during these transitioning stages is needed in order to accurately estimate these losses.

According to [5], [13], [26] the switching speed of a power MOSFET is limited by its parasitic capacitances, caused by the junctions formed between the internal layers. Three relevant capacitances can be determined between the connections of the device, as shown in Figure 10 and Figure 11.

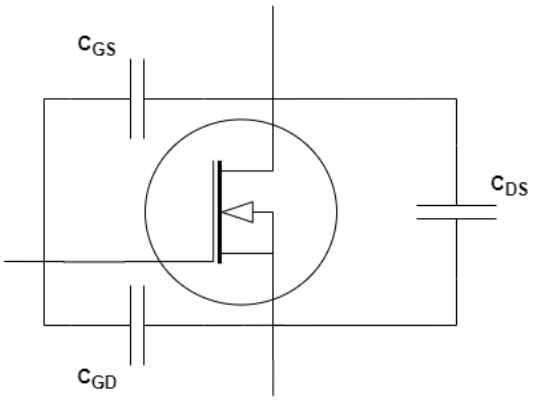

Figure 10: Parasitic capacitances between the three connections of a MOSFET.

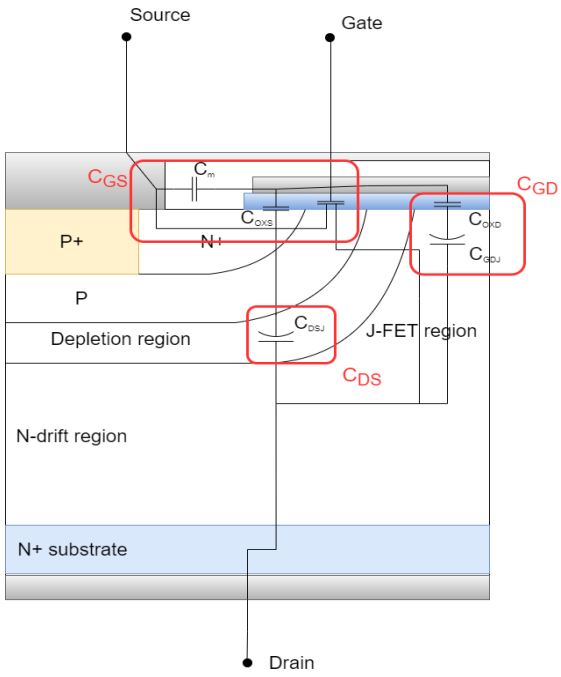

Figure 11: Parasitic capacitances between the different layers in a power MOSFET [13].

This is further supported by [17], which states how recent size reductions of the SiC MOSFET cause these device capacitances to shrink relative to the amount of current conducted, which in turn allow for a greater switching speed to be reached.

The capacitance C_{gd} consists of the capacitance of the gate oxide (C_{OX}) in series with the capacitance of the depletion region in the JFET region under the gate oxide (C_{GDJ}). The capacitance C_{ds} consists of the capacitance of the depletion region between the P-base and N-drift layers (C_{DSJ}). The final parasitic capacitance C_{gs} consist of the capacitances created due to the overlap of the gate metallization over the source and the P-base layers (C_m and C_{OXS}).

In [5], [25], [40]–[42] these three characteristic capacitances are combined as follows:

$$C_{iss} = C_{gs} + C_{gd} \tag{11}$$

$$C_{oss} = C_{ds} + C_{gd} \tag{12}$$

$$C_{rss} = C_{gd} \tag{13}$$

Most manufacturers only provide values for these three capacities in their datasheets. However, explaining the behavior of a MOSFET during the turn-on and turn-off processes is much simpler when only considering C_{gs}, C_{gd} and C_{ds}.

When considering the transients during turn-on and turn-of processes, C_{oss} appears to be the most important capacitance [43]–[46]. This is because C_{ds} discharges and charges when the device is turned on or off respectively. This will cause the current flowing through the channel of the MOSFET ($I_{channel}$) to be different than the current measured at the drain terminal (I_d) when the device is being turned on or off. As will be seen later, this will have an influence on the switching losses of the device. The capacitance C_{iss} is important when considering the switching speed of the device. Both C_{gd} and C_{gs} have to be charged or discharged by the gate driver circuit, which falls outside the scope of this thesis, before the MOSFET is fully turned on or off respectively [43], [44]. The capacitance C_{rss} is equal to C_{gd}. This capacitance is often called the Miller Capacitor and is mostly used to explain the behavior of V_{gs} during turn-on and turn-off processes.

According to [40], [41], [43]–[50], both C_{ds} and C_{gd} do not show a linear behaviour under different operating conditions. C_{ds} will show a non-linear behaviour when the drain-source voltage V_{ds} varies, especially at low voltages. For this reason, [44], [46] provide a way to model this non-linear behavior, using only datasheet parameters and curves. While [40], [50] try to model this behavior by only curve fitting the diagrams shown in the datasheet. C_{gd} is the most complex of the three characteristic capacitances to model and is attempted in [40], [42], [44], [45], [50].

In most models, C_{gs} is considered to be constant or at least have a linear value [41]–[50]. However in [40], it is attempted to model this capacitance more accurately, using a hyperbolic-tangent-based function to describe its behavior with varying gate to source voltage V_{gs}.

In [49], a model for C_{oss} is achieved by experimentally measuring the energy dissipated between the charging and discharging of the capacitance during operation.

Finally, to better understand the switching losses of a power MOSFET, a detailed understanding of the transients occurring during on and off switching of the device is required. These will be explained in the following paragraph and are visualized in Figure 12. Note that these are the normal transients occurring in a MOSFET without taking special switching modes like zero voltage switching (ZVS) or zero current switching (ZCS) into consideration. These switching modes and the difference between them will be discussed later on.

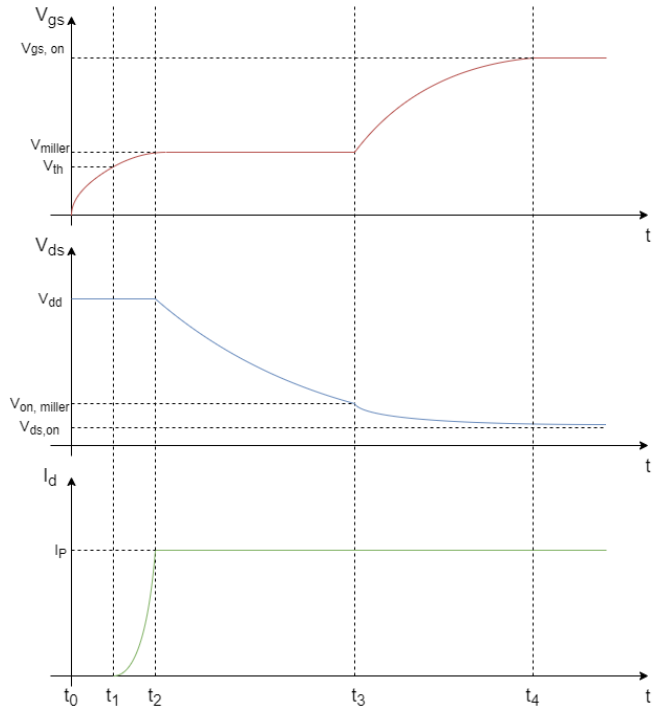

Figure 12: Ideal transition waveforms of the gate-source voltage, drain-source voltage and the drain current during on-switching of a Power MOSFET [5].

Initially, the MOSFET still remains in its off-state. This state can be recognized by the following conditions: $V_{gs} = 0, I_d = 0$ and $V_{ds} = V_{dd}$. Where V_{dd} is equal to the drain-source bias. When the gate driver circuit gives the signal to start the turn-on process, the gate voltage bias $V_{gs,on}$ will be applied to the gate electrode and begin to charge C_{iss}. This will cause V_{gs} to start rising. No current will be able to flow through the drain until V_{gs} reaches its threshold voltage (V_{th}), ending the first phase at time t_1. From the moment this voltage is reached, I_d will begin to rise exponentially until it becomes equal to the load current I_P, ending the second phase at time t_2. From this point on, V_{ds} will start to decrease towards its on-state value $V_{ds,on}$, while V_{gs} and I_d remain constant. During this time, all the gate current is used to charge the reverse transfer capacitance (C_{rss}). As soon as V_{ds} has reached the value $V_{on,miller}$ corresponding to the gate voltage at that time, phase three ends at time t_3. Finally V_{gs} will rise exponentially towards the gate voltage bias while V_{ds} decreases at the same rate towards the actual on-state voltage $V_{ds,on}$. As soon as these values are reached, phase four ends at time t_4 and the MOSFET is turned on [25].

After this the MOSFET can be turned off as soon as the duty cycle ends. V_{gs}, I_d and V_{ds} still have the same values as at the end of phase four (t_4). After de drive circuit gives the signal to start the turn-off process, the gate voltage bias is taken away and the gate electrode is connect to the source via a resistance. This will allow C_{iss} to be discharged. This will cause V_{gs} to decrease towards V_{miller}. Meanwhile I_d and V_{ds} still remain constant, as shown in Figure 13.

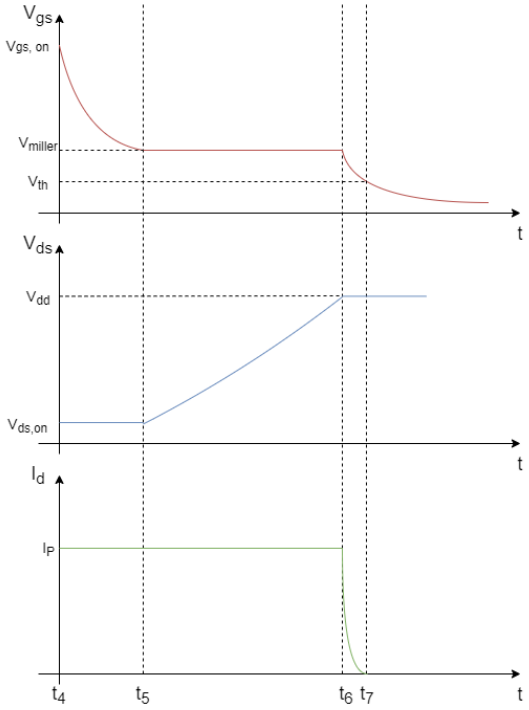

Figure 13: Ideal transition waveforms of the gate-source voltage, drain-source voltage and drain current during off-switching of a power MOSFET [5].

After V_{gs} reaches V_{miller}, it remains constant together with I_d while V_{ds} rises back to V_{dd}. As soon as V_{ds} reaches this value at time t_6, the drain current I_d decreases exponentially, often transferring the current in case of an inductive load to the freewheeling diode. As V_{ds} remains constant, so does C_{gd}. This will allow the current passing through the gate resistance to discharge C_{iss}, which causes V_{gs} to fall beneath V_{th} at time t_7. By this point I_d has also reached zero. However it still takes some time for V_{gs} to decrease exponentially to zero, depending on the value of C_{gd} [13][25].

As can be seen in both cases, an overlap is made between V_{ds} and I_d during both on- and off-switching. The area of this overlap indicates the amount of energy lost during switching. Estimating the amount of losses is a complex task and can be done by either experimentally measuring the switching transients or estimating it with the help of datasheet parameters. Of course the latter is more interesting since it doesn't require the construction of a prototype, but for completeness of the thesis, all methods will be shortly addressed. Because of the limited time of this thesis, existing models will be taken from earlier studies, and will be implemented in the Python models. These models will then be compared with experimental measurement, taken from the prototype DAB converter at EnergyVille.

Experimental Models

Experimental models try to simplify the calculation of the switching losses. They often require the measurement of fewer values, but in turn won't be as accurate as the usual method. The usual method of determining the experimental losses is done by measuring

$V_{ds}, I_{channel}$ and V_{gs} during both on- and off-transitions. Next, the following formula is used to calculate the switching losses:

$$P_{sw,MOSFET} = f_s \int_{t_e}^{t_b} V_{ds}(t) \cdot I_d(t)\, dt \tag{14}$$

with t_b signifying the beginning of the on- or off-transition and t_e the ending of the respective transition. According to [39], t_b is reached when V_{ds} starts to fall and t_e when V_{gs} has reached the gate bias $V_{gs,on}$. At turn-off, t_b is reached when V_{gs} starts to fall and t_e when V_{ds} has reached V_{dd}.

In [51] a calorimetric measurement of the switching losses of a full bridge is done. The heat generated by both conduction and switching losses are measured. If the RMS value of the drain current (I_d) is known, these conduction losses can be calculated and subtracted from the total losses to become the switching losses. Even though this method would directly give some interesting results like operating temperature, it will not be used in this paper, as it gives less insight in the current and voltage waveforms occurring during switching.

In [20] the switching losses are calculated by

$$P_{sw,MOSFET} = f_s E_{sw} \left(\frac{I_{avg,d}}{I_{ref}}\right)^{K_I} \left(\frac{V_{ds}}{V_{ref}}\right)^{K_V}) \tag{15}$$

where $I_{avg,d}$ is the average drain output current, I_{ref} and V_{ref} the respective current and voltage available in the datasheet of the MOSFET, obtained from earlier switching loss measurements and K_I and K_V are coefficients defined as exponents for respectively the current and voltage dependency of the switching losses. Often being $K_I \approx 1$ and $K_V \approx 1.3 - 1.4$, as stated in [52].

Simulation software Models

The next category of models uses a simulation software like LTSpice in which the DAB converter is built and where the software simulates the waveforms during on- and off-transitions. After this, the switching losses are calculated similarly to the experimental method. This is done to some degree in [53], [54]. A downside to using software like LTSpice is that the model of the MOSFET has to be present in its database. Some manufacturers don't allow models of their devices to be included in certain circuit simulators.

Datasheet Models

The final category of models contains the ones which will be used in this thesis. Not all models will be implemented in Python, as some model the losses in a very similar way. Also note that most models consider a different switching mode than the mode which is

used by the converter of this thesis. This will of course mean that some models will be more accurate than others when comparing their results with the experimental results from the converter. However, since there are not many models which consider the switching mode from the prototype converter at EnergyVille, it may be interesting to compare the estimated losses for different switching modes over the converters operating range. This difference will be the indicator of the effectiveness of the different switching modes which will also be discussed later on.

Model 1

The first analytical model proposed in [39] is based on an estimation the turn-off and turn-on voltage and current waveforms in the MOSFET observed during normal operation of a DC/DC-converter, meaning it switches in hard switching mode. This paper tries to model the ideal waveforms which were addressed above via a series of formulas and datasheet parameters. After these waveforms have been modeled for both on- and off-transitions, formula (14) is used with the same criteria to determine the values for t_b and t_e like was stated for the usual experimental method. The same methods and formulas were employed in [55], [56]. This is also true for [57], with the only exception that this model relies heavily on the curve fitting of a lot of datasheet parameters, making the model more complex.

Important to note in this model is the fact that for this model, the dynamic behavior of C_{oss} has somewhat been taken into account. When a certain voltage has been reached across the MOSFET, the value of C_{oss} drops significantly. This certain value is referred to as V_{FD} or the voltage V_{ds} reaches at the beginning of the Miller Plateau during turn-on or at the end of the Miller Plateau during switch off. Therefore, two new values for C_{oss} are determined, based on V_{ds}:

$$C_{oss} = \begin{cases} C_{oss,1} & V_{ds} < V_{FD} \\ C_{oss,2} & V_{ds} > V_{FD} \end{cases} \tag{16}$$

The same is done in [56].

In [55], the C_{oss} is also considered a non-linear capacitance dependent on V_{ds}. The paper models these capacitances as follows:

$$C_{gd}(V_{ds}) = \frac{k_1}{\left(1 + \frac{V_{ds}}{k_2}\right)^{\frac{1}{2}} + k_3} \tag{17}$$

$$C_{ds}(V_{ds}) = \frac{k_4}{\left(1 + \frac{V_{ds}}{k_5}\right)^{\frac{1}{2}}} \tag{18}$$

where $k_1 - k_7$ can be found via curve fitting of the plots given in the datasheet of the MOSFET.

C_{iss} and C_{rss} have proven to show a relatively linear gradient at common operating voltages. These capacitances are therefore often considered to be constant during both switching processes.

According to [55], some parasitic elements have an influence on the total switching losses of the MOSFET. These elements, and the effect they have on the switching transients and losses during hard switching are as follows:

- Gate-source capacitance C_{gs}:
  The only effect that an increase of C_{gs} has on the transients and losses, is that it slows down the increase and decrease of V_{gs}, ensuring that it crosses V_{th} after a longer time. This causes V_{ds} and I_d to start decreasing and increasing at a later time. This also means the switching losses will occur at a later time after applying or taking away the gate bias.

- Gate-drain capacitance C_{gd}:
  An increase in C_{gd} has minor effects on both V_{gs} and I_d. It does however cause V_{ds} to decrease at a slower speed at turn-on and V_{ds} to increase and I_d to decrease at a lower speed. This causes slightly more overlap between V_{ds} and I_d and thus a minor increase in switching losses.

- Drain-Source capacitance C_{ds}:
  An increase in C_{ds} affects neither V_{gs} or I_d. It only seems the amplitude of the oscillation of both V_{ds} and I_d at turn-off, which has minor effects on the switching losses.

- Source inductance L_s:
  An increase in the L_s has the most effect on the transients during turn-on. Even though I_d now rises at a slower rate, the delay until V_{ds} begins to increase cause a major increase in switching losses at turn-on. At turn-off, I_d decreases at a slower rate, causing more switching losses to occur at turn-off.

- Drain inductance L_d:
  An increase in L_d causes I_d to rise at a lower rate during turn-on and V_{ds} to have a much higher voltage drop at the beginning of its descend towards $V_{ds,on}$. This ensures a smaller overlap between V_{ds} and I_d at turn-on and decreases the switching losses accordingly. It has minor effects on the transients at turn-off, only causing the oscillations at the end of the transition to have a larger amplitude.

- Gate resistance R_g:
  An increase in this value mostly causes a delay because of the slower increase or decrease of V_{gs} at turn-on or turn-off respectively. This again causes the switching losses to be more delayed in time after applying or taking away the gate bias.

- Capacitance of the freewheeling diode C_f:
  An increase in this value has no real influence on the transients, except for a minor initial increase and decrease of I_d at turn-on and turn-off respectively.

Another interesting phenomenon discussed in both [39], [58] and proven in [53] is the current diversion where internally some current is displaced to charge or discharge the capacitances of the device. This can only occur during some periods when a fast turn-on and turn-off is attempted. This phenomenon is visualized in Figure 14. If the gate has a low external resistance ($R_{g,ext}$), a high current is needed to charge C_{oss} in a short amount of time. This causes I_d to split up in current needed to charge the output capacitance ($I_{C_{oss}}$) and $I_{channel}$. This takes place at the start of the Miller plateau, where the current in the channel can suddenly drop a bit during turn-off. The same phenomenon can occur with C_{iss} but the current needed to charge this capacitance is negligible.

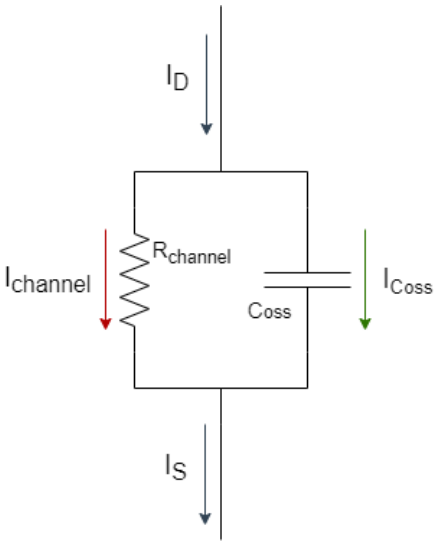

Figure 14: Visual representation of the current displacement phenomenon [39].

Model 2

In [5], [60]–[62] a commonly used formula to estimate hard switching losses in a power MOSFET is given:

$$P_{sw,MOSFET} = \frac{1}{2} I_d V_{ds} (t_{off} + t_{on}) f_s + \frac{1}{2} C_{oss} V_{ds}^2 f_s \tag{19}$$

However, this formula assumes a linear transition of the drain to source voltage and drain current. As can be seen in Figure 12 and Figure 13, this is not the case. The second term shows the losses caused by the output capacitance. These losses are caused by the discharging of the energy stored in C_{oss} during the turn-off sequence, dissipating in the

form of joule-heating during the turn-on sequence. The switching times t_{on} and t_{off} can be calculated with

$$t_{on} = t_{off} = Q_g / I_g \tag{20}$$

$$I_g = \frac{V_g - V_{GP}}{R_g} \tag{21}$$

where Q_g is the gate switch charge, I_g is the gate drive current, V_g the supply voltage of the gate control circuit and V_{GP} is the voltage level of the gate at the Miller plateau. In [5] the losses related to the charging of the gate of the MOSFET has also been accounted for:

$$P_{sw,MOSFET,gate} = V_g Q_g f_s \tag{22}$$

Model 3

The next model described in [58] is an analytical switching loss model for a half bridge. It is a fast calculation based on charge equivalent approximation of the MOSFET capacitances with only the datasheet parameters. During the analysis of the turn-off, the following equations for energy losses is obtained for a half bridge.

$$E_{T,off} = \frac{1}{2} t_{rv} V_{ds,on} \left(I_d - 2I_{C_{oss}}\right) + \frac{1}{2} t_{fi} (V_{ds,on} + V_{LD})(I_d - 2I_{C_{oss}}) \tag{23}$$

with t_{rv} the time where V_{gs} reaches V_{miller} at the Miller plateau, t_{fi} the time it takes for the current to reach zero while $V_{gs} < V_{miller}$, $I_{C_{oss}}$ the part of the drain current which charges C_{oss} and V_{LD} the voltage drop across the parasitic drain inductance (L_d)

$$E_{T,on} = \frac{1}{2} t_{ri} V_{ds,0} I_P + \frac{1}{2} t_{fv} V_{ds,0} \left(I_d - 2I_{C_{oss}}\right) + t_{rs} V_{ds,0} I_d) \tag{24}$$

with t_{ri} the time it takes for I_d to reach the current that flows when the MOSFET is completely turned on (I_P), t_{rs} the time it takes for I_d to reach its maximum value after reaching I_P and t_{fv} is the time it takes for V_{ds} to reach $V_{ds,on}$ after the maximum value for I_d is reached.

If the sum of these equations is multiplied by f_s, the total power losses for the MOSFET are obtained. The model suggests that with the energy losses from the MOSFET, the energy loss from the reverse recovery of the diode should also be considered. The model also presents an ideal current range for Zero-Voltage-Switching so that the losses are minimalized which will be discussed later on. The limitations of this model depend on the available information of the datasheet. With more information, the temperature dependence could be included. Nevertheless, the model can estimate the switching loss energies with a mean error of 10%.

In [63] a sensitivity analysis is made for the calculation of conduction and switching losses of a SiC power MOSFET. In this paper it is shown that the reverse recovery charge of the internal body diode does not have a large influence over the total switching losses of the device. However, this thesis will still take those losses into account.

2.2.6 Unknown Losses

As stated in section 2.2.1, the value of the unknown losses cannot be determined with one or even multiple formulas. However, this does not mean the origin of these losses is unknown. In [9] a list is given of four phenomena which contribute to these losses:

- Ohmic losses caused by the laminated DC-bus bars.
- Unaccounted Temperature-dependent conduction, switching and copper losses from the SiC modules and magnetic devices.
- Slightly increased copper losses of Litz wires in the magnetic devices due to skin and proximity effects.
- Power-losses from the equivalent resistance of the capacitors.

2.3. Operation of the Converter

2.3.1 Modulation

Because the converter covers a wide voltage and current range, modulation is mostly used to improve the converter efficiency and/or power density [64].

The phase shift modulations have been the most attractive modulation techniques for the DAB converter [65]. We can distinguish different types of phase shift modulation.

The first kind of phase shift modulation is the single-phase shift modulation method. This was first cited when the DAB converter was proposed in [66]. This shows that the output power can be controlled by the phase shift between the voltage at the input bridge and the output bridge. The phase shift ratio D is the ratio needed to multiply with $T_s/2$ so that the shift in time between two signals is obtained. T_s is the switching period. This is shown in Figure 15 together with the waveforms.

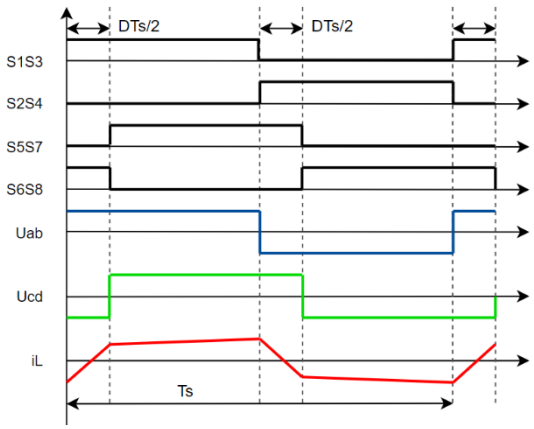

Figure 15: Waveforms of SPS modulation method [65].

We can achieve higher output power ratings when modulating in the soft switched area shown in Figure 16, where d is the DC-DC conversion ratio. This will be handled in the next chapter about ZVS. The maximum power that can be transferred according to [67], [68] at a phase shift of 90° is:

$$P_{max} = \frac{n \cdot V_{in} \cdot V_{out}}{8 \cdot f_s \cdot L} \tag{25}$$

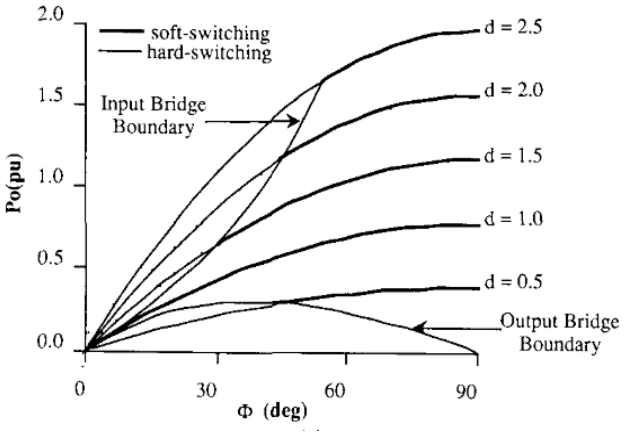

Figure 16: Output power vs. φ of a DAB converter [66].

The power characteristics of the DAB converter under single phase shifting are acceptable with less device and component stress, smaller filter components, reduced switching losses, bidirectional power flows, buck boost operation and low sensitivity to parasitic parameters [69]–[71]. However, the DAB converter achieves good efficiency when both sides operate under the same voltage during single phase shift modulation. When the voltages applied to both sides do not match there is always going to be high circulating power and limited zero voltage switching. This has a negative effect on the efficiency [65]. To overcome these challenges and increase the efficiency, modulations have been added in recent years. These include dual phase shift modulation (DPS), extended phase shift modulation (EPS) and triple phase shift modulation (TPS).

The next kind of modulation is dual phase shift modulation. This method orders two phase shift ratios in the DAB converter, the inner phase shift ratio (D1) and the outer phase shift ratio (D2). D2 is the phase shift ratio for the gating signal for every two MOSFETs on both sides of the bridges, for example MOSFET 1 on the input and MOSFET 5 on the output. The meaning of D2 is identical to the meaning of the single-phase shift ratio D. D1 refers to the phase shift between two MOSFETs in the primary bridge between the two bridge legs, for example MOSFET 1 and MOSFET 4 of the input bridge and is located on both bridges. The MOSFETs are shown in Figure 1. In this modulation we can distinguish two conditions, when D2 is smaller than D1 and both are located between 0 and 1, shown in Figure 17(a). Or when D2 is greater dan D1 and also both located between 0 and 1, shown in Figure 17(b).

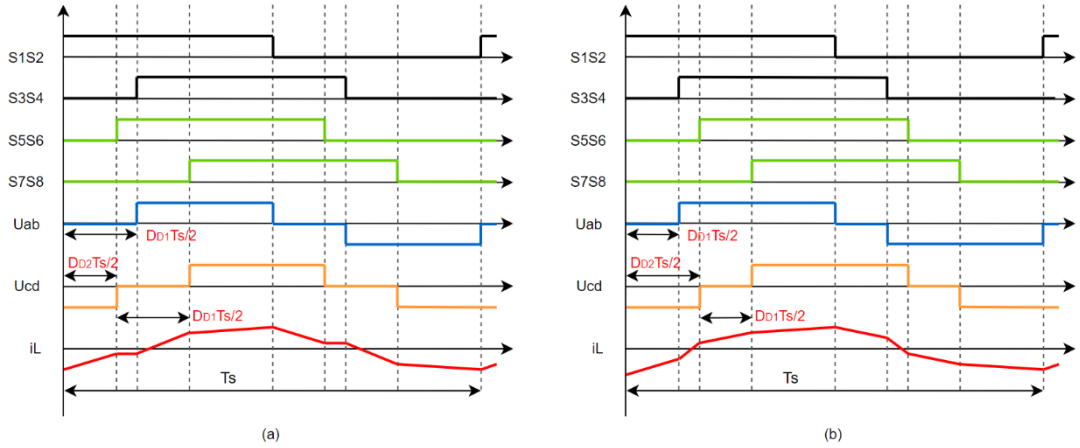

Figure 17: Waveforms of the DPS modulation method [65].

Next is the extended phase shift modulation. The difference with the DPS is that the inner phase shift ratio is located at the input H bridge or the output H bridge [72]. As a result there are also two conditions, namely if the phase shift takes place in the first H-bridge, shown in Figure 18(a), or if the phase shift takes place in the second H bridge, shown in Figure 18(b). Resembling to the DPS modulation it creates less current stress, the ZVS region expands and the reactive power decreases. Different with the DPS, when switching between buck and boost, it must be ensured that the inner phase shift ratio of the EPS modulation must be located at the side of high voltage. This to ensure the increase of efficiency properly [65].

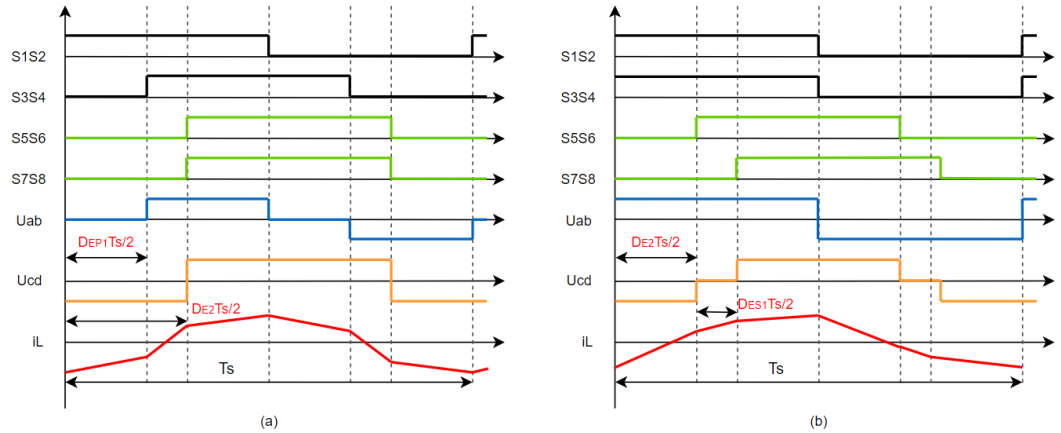

Figure 18: Waveforms of the EPS modulation method [65].

Lastly there is the triple phase shift modulation method, this one does not differ that much from the DPS modulation. There is still an outer phase shift ratio and two inner phase shift ratios like in the DPS modulation. The big difference with DPS is that the two inner phase shift ratios are allowed to be different. This achieves minimum current stress, minimum conducting losses, minimum power losses and an increase of ZVS soft-switching range [68], [73], [74]. According to [68] the TPS modulation is most used for applications with an high power demand. The Waveforms and ratios are shown in Figure 19.

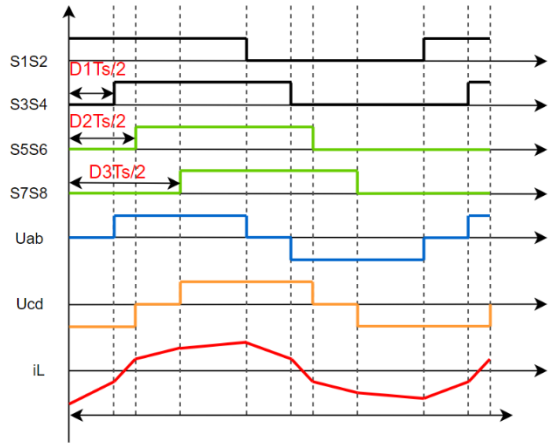

Figure 19: Waveforms of the TPS modulation method [65].

Outside of the phase shift modulation we can also use the variable frequency modulation method. This method is mostly used when large power ranges are required [65]. The variable frequency modulation ensures that ZVS is possible for a large power range with low reactive power and minimal circulation currents [75]. If the selected switching frequency range does not affect the converter filter or the component choices, it can be used to extend the power range and to improve the power quality in converter systems [65].

Although the EPS modulation and the DPS modulation are proposes for boosting the efficiency of the DAB converter, the TPS modulation can always provide the best efficiency [76], [77]. The transferred power can be obtained directly by the phase shift ratios. There are generally only three possible phase shift ratios for an DAB converter i.e. D1, D2, and D3 [65]. In Figure 20 below, the relation between the different phase shift modulations and the three possible phase shift ratios are shown. All the modulations start from the TPS. If D1 is equal to 0 or if D2 and D3 are equal to each other, the result is EPS. If D1 is equal to the difference of D3 and D2, the outcome is DPS. Lastly if D1 is equal to the difference of D3 and D2 and this is equal to zero, the result is SPS. From this we can deduce that TPS always has the largest efficiency. In [65] the formulas for the calculation of the transferred power, the output current and the boundary inductance current for TPS are displayed.

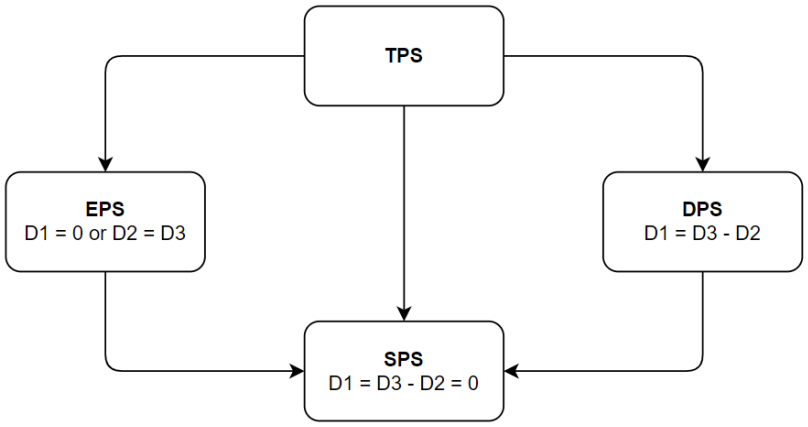

Figure 20: Correlation diagram of typical phase shift modulation methods [65].

2.3.2 Switching Modes

As was mentioned in the previous sections, there are several ways to switch the switching devices in the converter. In this thesis, two categories will be discussed. These are hard switching and zero voltage switching (ZVS), also called soft switching. Additionally, the concept of synchronous rectification and the use of the intrinsic body diode of the MOSFETs will be explained in detail, since this will also be the case for the converter used in this thesis. There also exists a third category called zero current switching (ZCS). However, since this switching mode is almost only used in combination with insulated gate bipolar transistors (IGBTs), it will not be discussed in this thesis. More about this switching mode can be read in [5], [78].

2.3.2.1 Hard Switching

Hard switching can be viewed as the most normal switching mode of a switching device. In short, it switches the device without regard for the voltage across the device of the current flowing through it. In case of the DAB converter, this causes relatively high turn-on losses because of the overlap between V_{ds} and I_d, as is shown in Figure 21 [27], [79].

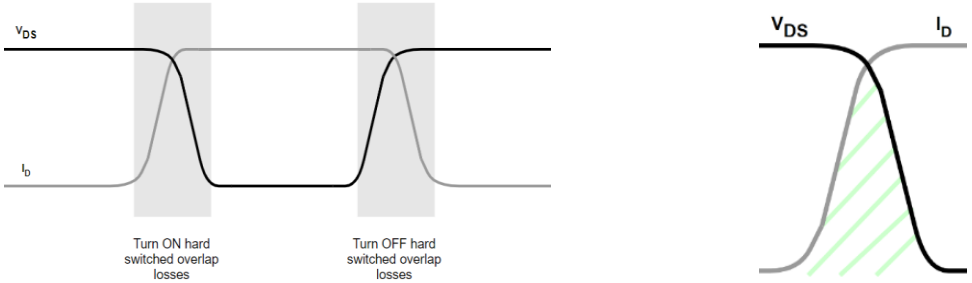

Figure 21: Transients of drain-source voltage, drain current and their overlap during hard on- and off-switching of a power MOSFET [27].

Figure 22 and Figure 23 show the flow of operating and reverse current before and after the off-switching of S_1 and S_4.

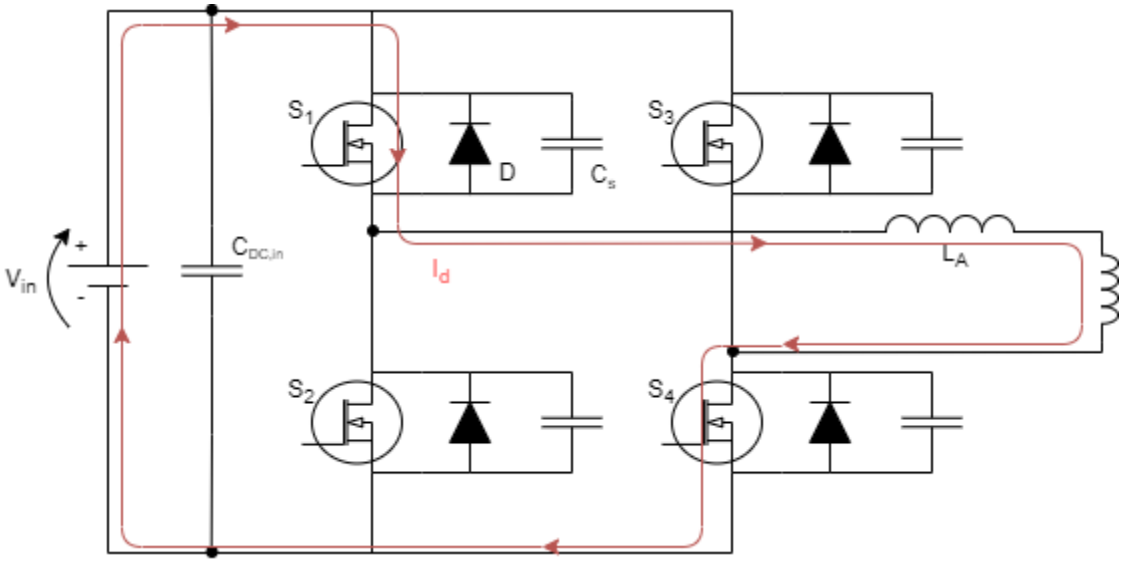

Figure 22: Operating state where S_1 and S_4 are switched on [5].

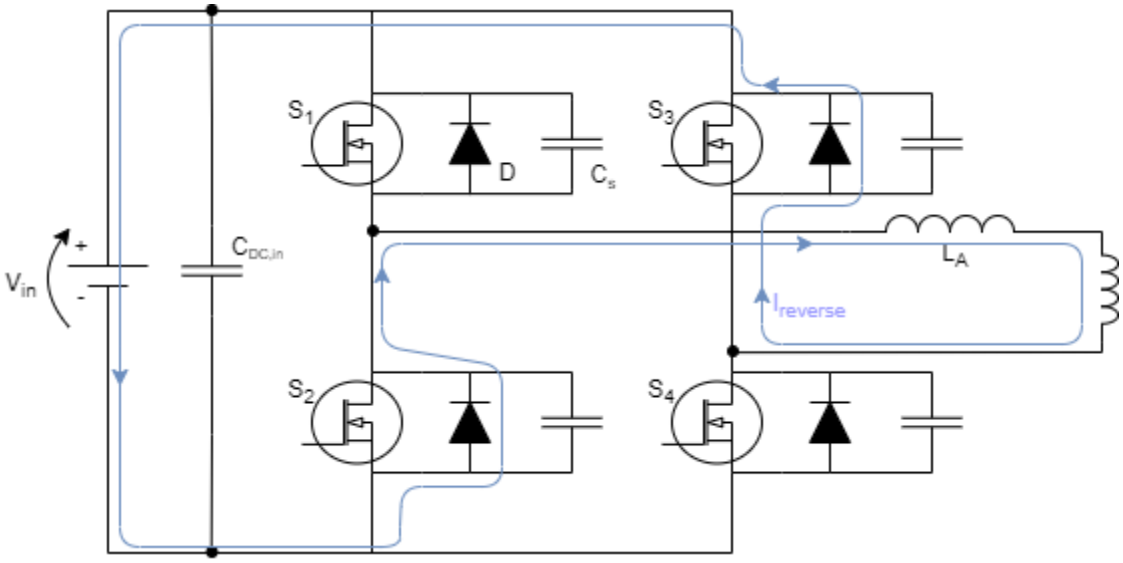

Figure 23: Operating state during the dead time after switching off S_1 and S_4 [5].

As can be seen in Figure 23, a very short dead time (t_{dead}) has been implemented after a pair of MOSFETs has been turned off. This is done to ensure that all four MOSFETs can't conduct at the same time and prevent short circuits of V_{in} [5]. However, since the converter used in this thesis is mostly supposed to work in soft switching mode, this mode will not be discussed any further.

2.3.2.2 Zero Voltage Soft Switching

Soft switching improves upon the hard switching mode and drastically reduces the turn-on losses caused by the previous switching mode. This is done by ensuring that V_{ds} decreases earlier than usual which causes the overlap between V_{ds} and I_d to be much smaller, like is shown in Figure 24.

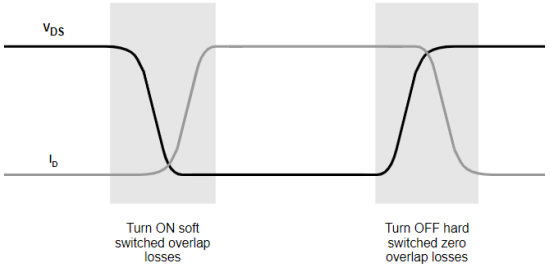

Figure 24: transients of drain-source voltage, drain current and their overlap during soft on- and hard-off switching of a power MOSFET [27].

This is done by discharging C_{ds} before the device is turned on. This can be done by implementing enough dead time (t_{dead}) before transitioning to the next operating stages, which were shown in the previous section. This allows a reverse current to flow through the freewheeling diodes of the MOSFETs which will be turned on in the next operating state. This reverse current causes C_{ds}, along with the snubber capacitor (C_s) to discharge, which lowers the voltage across the MOSFET before it is turned on and current is forced to flow through it [27], [79], [80]. The use of snubber capacitors placed across the switching devices, like C_s, allows more for energy to be stored in the converter itself. It does however mean, that a longer t_{dead} is required to due to the slower charging rate.

Initially, S_1 and S_4 are conducting for the duration of their entire duty cycle. This is shown in Figure 25.

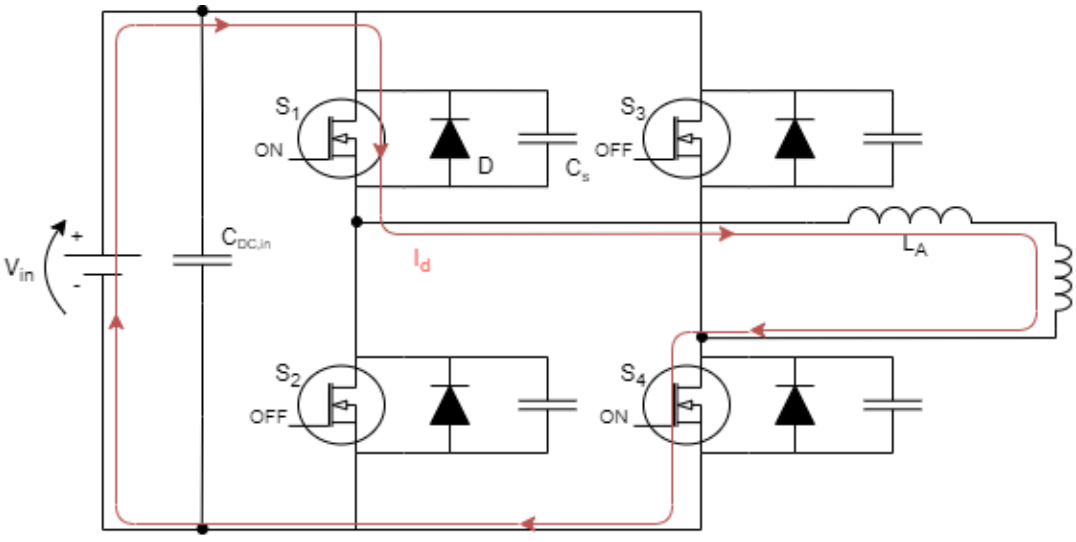

Figure 25: Operating where S_1 and S_4 are switched on [5].

At the end of the duty cycle, S_4 is turned off first, causing a reverse current ($I_{reverse}$) to flow through S_1 and the anti-parallel diode across S_3. This is shown in Figure 26. This current causes the C_{oss} and C_s of S_3 to discharge, while those of S_4 are being charged. In this process, energy is taken from the C_{oss} and C_s of S_3 and to charge the C_{oss} and C_s of S_4. This means the energy stored in the capacitances of S_3 does not get lost. This also helps in reducing the turn-on losses.

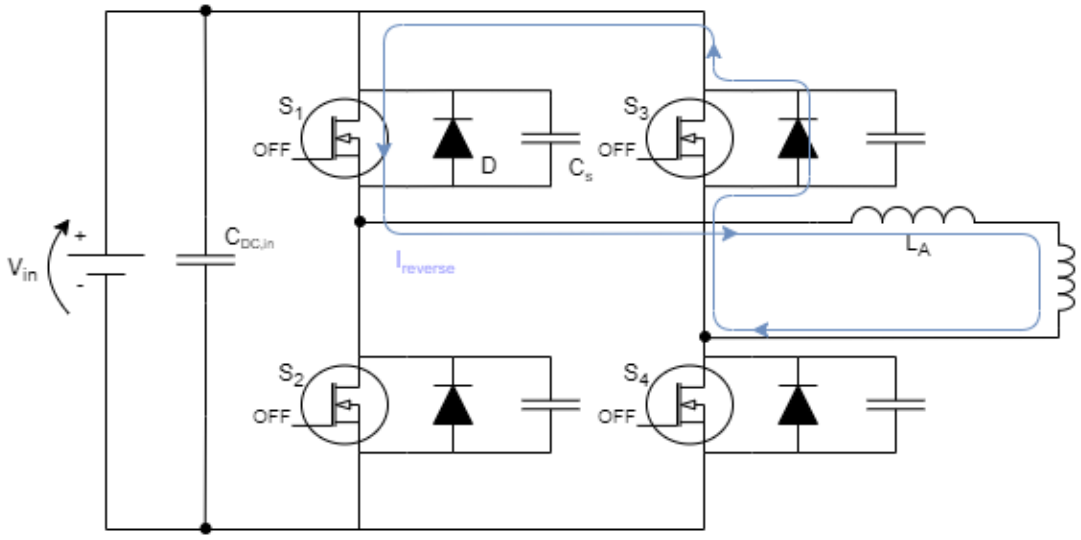

Figure 26: Operating state where S_1 is switched on and S_4 is switched off [5].

Next, S_1 is switched off. Now reverse current will flow through the anti-parallel diodes of S_2 and S_3. Afterwards the C_{oss} and C_s of both S_2 and S_3 discharge, while the C_{oss} and C_s of both S_1 and S_4 charge. This is shown in Figure 27.

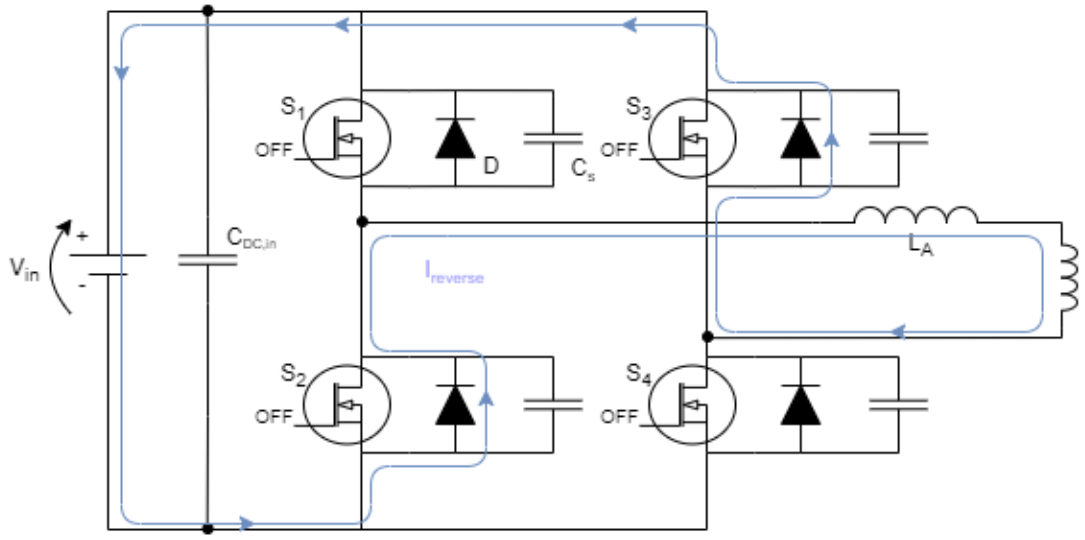

Figure 27: Operating state where both S_1 and S_4 are switched off [5].

Finally, after the C_{oss} and C_s of both S_2 and S_3 have completely discharged, the voltage across these MOSFETs will equal to $V_{ds,on}$. This means that they can both be turned on with significantly reduced switching losses [5]. Their on-state operation is illustrated in Figure 28.

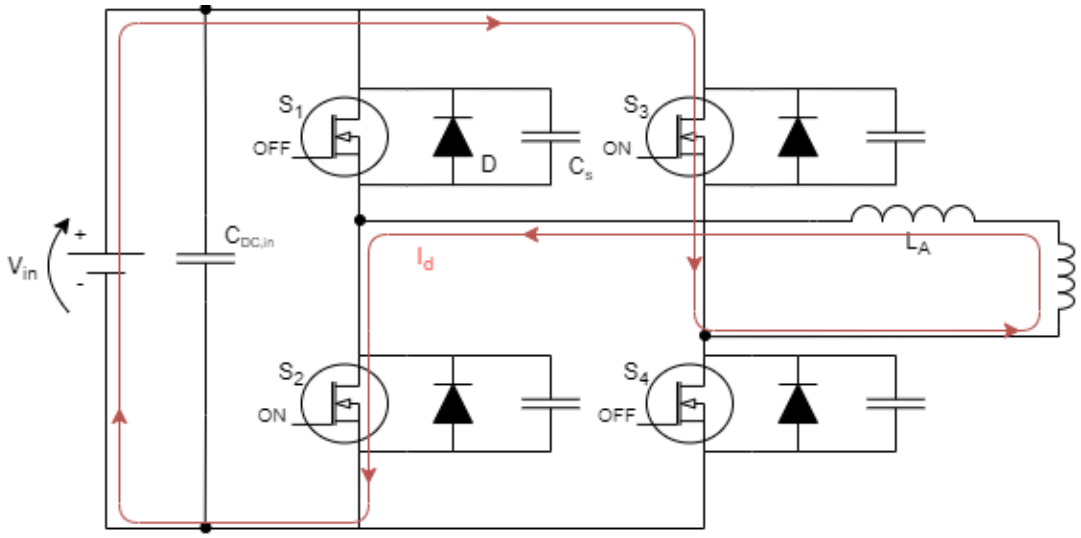

Figure 28: Operating state where both S_1 and S_4 are switched off, while S_2 and S_3 are turned on [5].

The optimal t_{dead} which is needed to let the capacitances charge and discharge, depends on whether the converter is working in buck or boost mode and can be calculated as follows [5][81]:

$$t_{dead,buck} = \frac{V_{in} + nV_{out}(2d-1)}{4f_s[V_{in} + nV_{out}]} \tag{26}$$

$$t_{dead,boost} = \frac{V_{in}(2d-1) + nV_{out}}{4f_s[V_{in} + nV_{out}]} \tag{27}$$

$$d = \frac{V_{out}}{V_{in}} \tag{28}$$

with n the winding ratio of the high-frequency transformer and d the voltage gain of the output compared to the input of the converter.

2.3.2.3 Synchronous Rectification

In most cases, SiC SBDs are used as freewheeling diodes to minimize switching losses as much as possible. However, like has been mentioned before, the converter used for this thesis utilizes the intrinsic body diode of the MOSFETs as a freewheeling diode. These diodes have slightly higher switching losses than SiC SBDs, but still show a decent

performance even at high frequencies. For this reason, the use of SiC SBDs can be avoided in order to lower costs and minimize the chip count of the converter [14], [16].

However, a method called synchronous rectification can be employed to reduce the conduction losses which occur while the body diode of the MOSFET returns. According to [16], the MOSFET of which the antiparallel diode is conducting a reverse current, switches on near the end of t_{dead}. This will cause the conductive channel to form underneath the gate oxide. Since this channel has a lower voltage drop than the body diode, $I_{reverse}$ commutates from the body diode to the channel. Note that the channel of a MOSFET can conduct current in both directions when a positive gate bias is applied. This is shown in Figure 29.

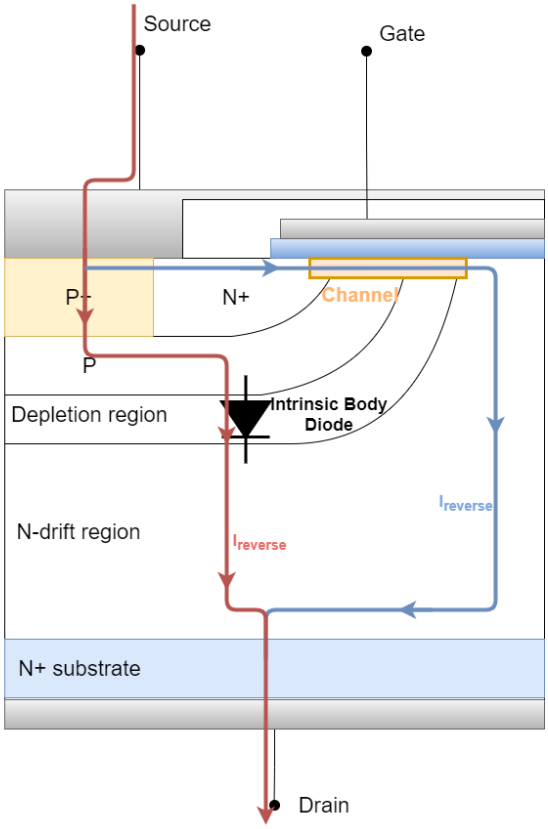

Figure 29: Transition of the reverse current flowing through the intrinsic body diode (red), to the channel of the MOSFET (blue) [16].

This dynamic will be used to lower the conduction losses occurring during t_{dead}. In [16], it was concluded that the use of SR instead of external SiC SBDs even increases the efficiency. However, when t_{dead} is made too long, SR will use its efficiency advantage as the body diode will conduct too long. This will cause the conduction losses to exceed the conduction losses caused by the use of SBDs.

2.3.3 ZVS Regions

As shown in previous section, to achieve ZVS for all the eight MOSFETs in the converter, the anti-parallel freewheeling diodes should conduct prior to the switches turn-on.

Accordingly, the absolute values of inductor current at times t_0, t_1, t_2 and t_3 found in Figure 30 must be higher than the reference current I_0, represented by formula (29).

$$I_{0-min} = \max(V_1, nV_2)\sqrt{\frac{2C_{oss}}{L}} \tag{29}$$

The minimum value of the reference current depends on the resonant circuit formed by the inductor L and the parasitic capacitance C_{oss} of the MOSFETs [68]. To achieve ZVS for, e.g. S1 in Figure 1, the anti-parallel diode of S1 must conduct before switch S4 turns on. This means the inductor current at t_0 should be higher than the resonant current to discharge all the energy within the parasitic capacitance of the MOSFET. When the inductor current is larger than the absolute value of I_0, the inductor current is large enough to transfer the charge between two MOSFETs parasitic capacitances C_{oss}, so that the ancillary switch is turned on at ZVS conditions [68].

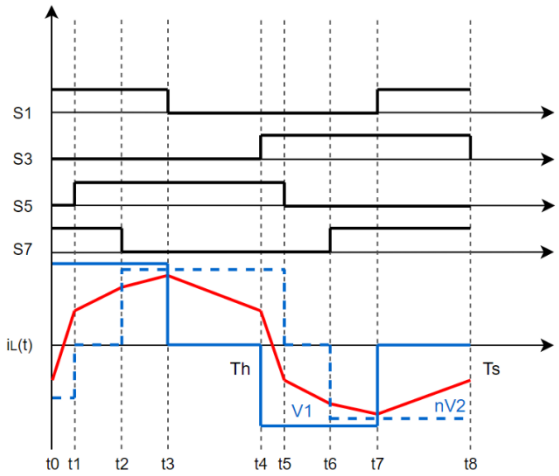

Figure 30: Timing diagram of TPS control in DAB converter of buck operating mode [68].

The DAB converter is used for its soft switched turn on capability for all its semiconductor devices. It improves efficiency by eliminating the turn on losses, however the ideal operating range where zero voltage switching turn on is achieved, is limited by system parameters and its operating conditions. The understanding of the boundaries of the region where ZVS turn on is achieved, is necessary [66]. The regions of ZVS differ from the type of phase shift modulation to type of phase shift modulation. In this thesis only the ZVS regions for single phase shift modulation will be discussed. According to [82] the ZVS regions and boundaries can be calculated using the following equations:

$$I_{S1}, I_{S7} \leq 0 \tag{30}$$

$$I_{S3}, I_{S5} \geq 0 \tag{31}$$

The designation of the switches follows from Figure 1. For more complex equations for the solution to the boundaries of ZVS regions for each converter leg can be found in [82]. In Figure 31 the ZVS regions and boundaries are shown for single phase shift modulation.

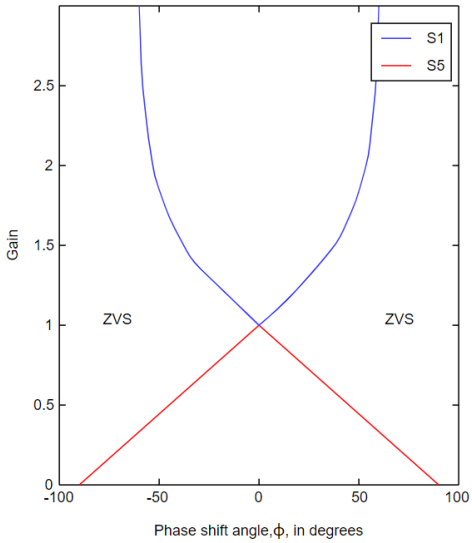

Figure 31: ZVS regions and boundaries for phase shift modulation [82].

This figure is with the duty cycles from both bridges at a value of 0,5. As illustrated in the figure, the ZVS region is the largest at a gain of 1, which is the gain for the DAB converter for the application processed. When the DAB converter has a larger or smaller gain, the ZVS region narrows.

2.4. Multimodule Operation

In order to ensure that a charging station can work at its optimal efficiency and have a certain level of redundancy, a modular power system architecture is recommended [83]–[85]. This means that, instead of only comprising of one singular DAB converter, the charger consists of many smaller DAB converters. These smaller converters are referred to as modules. These modules can be built with components which withstand relatively lower voltages and power flows. According to [86], [87], when considering only two modules, four possible combinations can be made when considering the input-output connections. These combinations are shown in Figure 32.

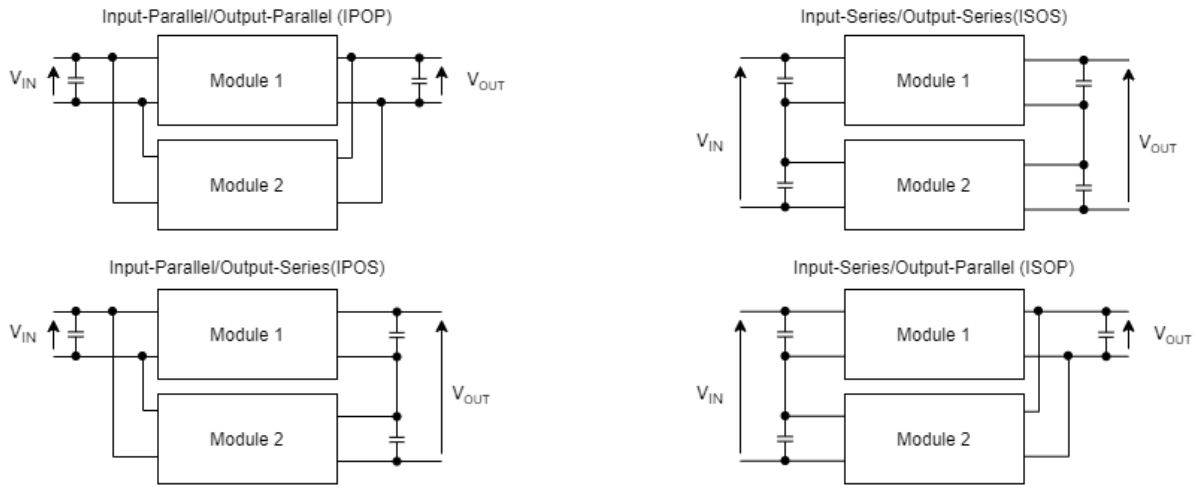

Figure 32: Schematic representation of four possible combinations to connect modules.

According to [86]–[89] when having a parallel connection at the input, the input power is distributed between the two modules by dividing the current flowing through them. This also means all modules work at the same voltage. In order to ensure an equal sharing of load current, the difference in the component parameters between the two modules need to be minimal. The control parameters also cannot differ too much in order for the converter to reach a steady state [2], [86]–[88]. The parallel connection at the input allows the converter to be used in applications where high currents and low voltages might occur at the input of the converter. The same conditions apply when having a parallel output connection. This architecture allows the modules to use semiconductor devices which have a lower current rating. In turn, this allows the semiconductor devices to be smaller in size and achieve a higher switching frequency. The downside of this connection is that a special controller needs to ensure the equal Input Current Sharing (ICS) or Output Current Sharing (OCS).

A series connection at the input or output of the modules distributes power by sharing the voltage over the equally modules, while the same current flows through them. Like the parallel connection, differences in component and control parameters between the modules cannot be too great. This architecture also allows the use of components with smaller voltage rating. This allows the use of MOSFETs with a smaller $R_{ds,ON}$, which lower the conduction losses caused by these devices. The series connection is often used in high-voltage application and also needs a controller to ensure Input Voltage Sharing (IVS) or Output Voltage Sharing (OVS) [2], [86], [88], [90], [91].

Like stated in [2], [7], [86], [88], [90], the ISOP configuration is a well-studied configuration which is used in a lot of applications because it is able to withstand a high input current, while its output is able to work in a wide voltage region.

In order to construct a reliable 350 kW fast charger with a certain level of redundancy and modularity, which is able to work in a voltage region from 200V-900V and charges with up to 500A, a combination of both connections is desired at the output. The connections made on the input largely depend on which voltage level of the utility grid the converter

is connected to. In this case, the charger will be connected to the low voltage grid with a line voltage of 400V

According to [7], a IPOP converter with all of its modules working has a lower efficiency when working at light-load conditions. A higher efficiency can be achieved by simply turning off one module, which is done by setting zero signals at that modules' switches. This means a clear analysis has to be made of the losses when working with multiple modules. By defining the number of modules which need to be active at a certain load, a controller can make sure the charger is always working at its optimal efficiency during the entire charging process, all this while making sure the charger works in its predefined current and voltage regions. This makes it an efficient, reliable and universal charger which fits any EV [2].

3. Models

Before a complete model that estimates the total losses and efficiency of a DAB converter over its entire operating range based on datasheet parameters can be made, different switching loss models from earlier studies will be implemented in Python and Matlab. As soon as this is done, a model which estimates all the different losses, mentioned in 2.2., can also be implemented. These models will only require datasheet parameters, voltages and currents at the in- or output and switching frequency. Note that for all models, a duty cycle of 0.5 is assumed.

3.1. Reading-in the capacitances

As was mentioned in 2.2.5.2, the parasitic capacitances of the MOSFETs show a non-linear behavior for a varying V_{ds}. This behaviour can be found in figure 18 in the datasheets for the MOSFETs used in the primary of the converter, the CREE C3M0030090K, and for the MOSFETs used in the secondary, the CREE C3M0016120K, in appendix A and B respectively.

Each of the switching loss models uses its own technique to model these capacitances so they can be used for calculations. Since reading the values on these graphs is a long and tedious task, there is a need for a faster, more automated way to load these values into Python or Matlab.

In [92], the tool *Engauge Digitizer* is used to recognize and extract data from graphs of the manufacturer datasheet. This program automatically determines the points needed to recreate a certain curve trough linear interpolation. These points can then be outputted as a csv-file, which can be read in in both Python and Matlab. An example of this process can be seen in Figure 33.

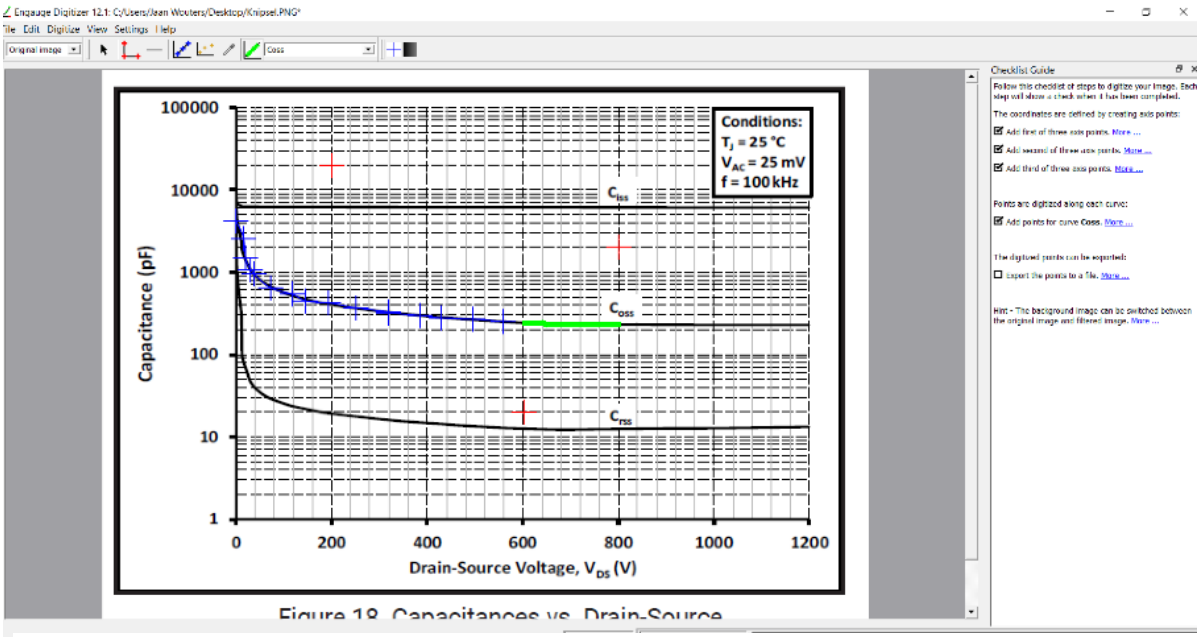

Figure 33: Example of the extraction of points of C_{oss} for the secondary MOSFETs via Engauge Digitizer.

After these points are read into Python or Matlab, they are linearly interpolated to derive the value of the parasitic capacities for each integer value of V_{ds}. This method of linearization will be implemented in all switching loss models and is given in Appendix C. It will output arrays for V_{ds}, C_{iss}, C_{oss} and C_{rss}. These four arrays will always serve as the starting point for each method to model the parasitic capacitances. The Python and Matlab code for this procedure can be found in appendix C. Figure 34 shows the results from this procedure.

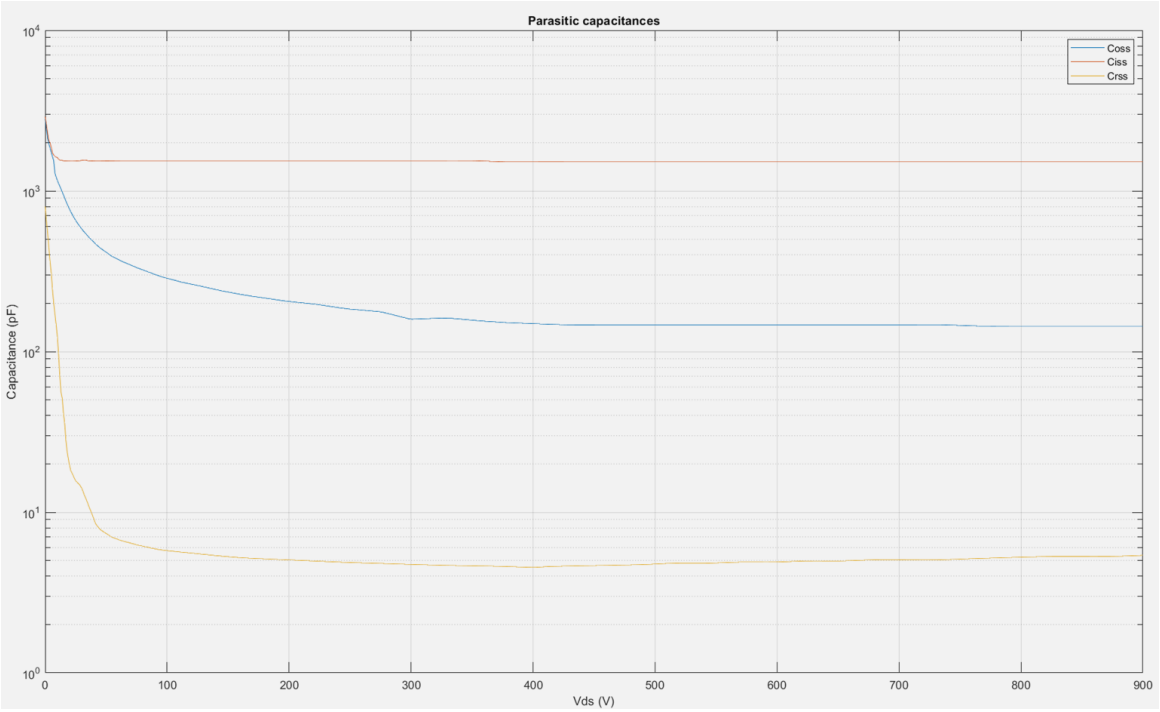

Figure 34: Read-in and linearized values for the parasitic capacitances of C3M0030090K in Matlab.

3.2. MOSFET Switching Loss Models

3.2.1 Model 1

This is the simplest model to be implemented into Python. It is based on [60], [62] and already discussed in 2.2.5.2, but a few changes were made so the model could be verified by the experimental setup. The input values of the model are the operating voltage, the operating current and the switching frequency. Hereby the values of the capacitances can be found for every value of the output voltage. In the model in [62] the phase shift between the two bridges are assumed constant. In the constructed model, this value is calculated with formula (32).

$$P_{out} = \frac{V_{in} \cdot \frac{V_{out}}{n} \cdot \varphi \cdot (\pi - \varphi)}{2\pi \cdot f_s \cdot L \cdot \pi} \tag{32}$$

Where L is the leak inductance, $\frac{V_o}{n}$ the voltage on the secondary side of the leak inductance and φ the phase-shift between the two bridges. The phase shift is limited to a value of $\frac{\pi}{2}$ as seen in 2.3.2. However, if the phase shift is greater than $\frac{\pi}{2}$, the output power would exceed the maximum power of the converter in the experimental setup. Therefore, if the equation cannot be solved within the limits, the phase shift is set to $\frac{\pi}{2}$ and the corresponding output power is calculated with (32). The current through the leak inductance is used to calculate the switching losses in the primary bridge. In the secondary bridge, the transformer ratio has to be taken into account. The rest of the method in [62] remains the same. The parasitic capacitances are converted into a single value by taking the mean of their values in the interval of V_{ds} at which the MOSFET works.

3.2.2 Model 2

Model 2 is more comprehensive than model 1. It divides the turn-on and turn-off events into different intervals to predict the switching losses more accurate. Here the input parameters are also the operating voltage, the operating current and the switching frequency. Other than the model described in [39], the $I_{rr\text{-}max}$ known as the peak reverse recovery current of the body diode of the MOSFET, is taken constant at a value of 35 A. This is the value given in the datasheet in Appendix A. It simplifies the model a bit because the reverse recovery current does not differ that much. Further, the parasitic capacitances are read in as described in 3.1. Because the model in [39] does not describe the turn-off losses properly, another similar paper is used for the turn-off losses. The model in [55] uses the same method as [39] but the turn-off losses are better described. To calculate the VFD another self-found method is used. VFD is defined as the voltage where the C_{rss} goes up, when looked in a reverse way. This is coded in the Python code by comparing the next value of C_{rss} with the current value. When the difference between the two values is bigger than 0,1%, VFD is defined at the current voltage. After this, VFD is used to model the non-linear behavior of the parasitic capacitances by defining two discrete values for each of these elements. VFD defines at which value of V_{ds}, the model has to switch from the first discrete value to the second or vice versa.

3.2.3 Model 3

This model is the most comprehensive model of the three. It is based on [58] and the theoretic background is explained in 2.2.5.2. The input parameters are the operating voltage, the operating current and the switching frequency. All the datasheet parameters can be found in Appendix A for the MOSFET in the input bridge and in Appendix B for the MOSFET in the output bridge. First the values of the capacitances obtained in 3.1 are interpolated so these can be used for every value of the operating voltage. After this, the capacitances are converted into a single value in the same way as is done in model 1. Now all the parameters are acquired for formulas (23) and (24) to determine the switching losses for turn-on and turn-off according to [58]. The only difference between turn-on and turn-off is besides the formulas, the used MOSFETs. This differs for input bridge and

output bridge. It is important to know that the reverse capacitances are also modeled like the output capacitances.

3.3. Converter Model

A model that estimates the total losses of the converter has also been made. This includes the losses estimated by the previously implemented switching loss models of the MOSFETs, the conduction losses of the MOSFETs, and conduction losses of the transformer. A code has also been implemented which allows the estimation of the iron losses of the transformer, but these losses will not be estimated and verified in this thesis because of lacking details about the HF-transformer of the studied converter. This code has been added so all significant losses of the converter are considered. Additionally, an estimation has been made of the temperatures which occur in the MOSFETs and the additional heat sinks, based on the losses provided by the model. Again, due to the shortage of time, these estimated temperatures will not be verified with experimental results.

In this section, a brief explanation will be given about the content of this code, which is added in appendix D. The most important implemented formulas will be described. In addition, another code has been implemented that can determine the losses over the entire operating area of the converter. A brief explanation about the utilization of this code is provided at the end of this section.

Note that these two pieces of code could only be implemented in Python, as the Sympy-engine in Matlab took too long to solve some values form equations in both the converter and switching loss models. For this reason, the scipy.optimize-library available in Python was used.

First, the model of the converter requires 8 input parameters: the first four parameters are the names of the switching loss models which need to be used to calculate the turn-on losses of the primary MOSFETs, the turn-on losses of the secondary MOSFETs, the turn-off losses of the primary MOSFETs and the turn-off losses of the secondary MOSFETs respectively. The fifth parameter prints all information about the losses if set to 'True', this parameter will be set to 'False' when the converter model is used in the code to estimate the losses over the entire operating area. The sixth and seventh parameter are the values of the output voltage in volts, and the output power in Watts. The eighth and final parameter is also a value which is best set to 'True'. Just like the fifth parameter, it will be set to 'False' when the converter model is used in the code of the operating area.

What follows next are the specific datasheet parameter input of all the components of the converter. These values normally only change when something is physically adjusted to the converter, like the replacing of a component.

Next, the output current is estimated. If the eight input parameter of the model is set to 'True', the output power will be checked and limited if it exceeds the maximum output power. This also limits the output current of the model.

Thereafter, the needed phase shift angle to reach the output power is calculated. As was shown in section 2.3.1, this angle needs to have a value between 0 and $\frac{\pi}{2}$. It is calculated by solving φ from formula (32). Normally this value will also have to be checked and limited to $\frac{\pi}{2}$, but this is no longer needed, as the output power will normally be limited to the maximum power.

Next, the effective currents which occur after turn-on (I_p) and before turn-off (I_L) of the MOSFETs will be estimated for both primary and secondary. This is done with the following formulas:

$$I_P = \frac{2 \cdot V_{in} \cdot \varphi + (\frac{V_{out}}{n} - V_{in})}{2 \cdot \omega_s \cdot L_A} \tag{33}$$

$$I_L = \frac{(V_{in} - \frac{V_{out}}{n}) \cdot (\pi - \varphi)}{\omega_s \cdot L_A} + I_P \tag{34}$$

After this, the RMS-current in the primary windings of the HF-transformer is calculated This can be done with the following, self-obtained formula:

$$I_{RMS} = \frac{V_{in}}{2\,\pi f_s} \cdot \sqrt{\frac{1}{3\pi} \cdot \left(\frac{\pi^3 d^2}{4} - 2d \cdot \varphi + 3\pi \cdot d \cdot \varphi^3 - \frac{\pi^3 d}{2} + \frac{\pi^3}{4}\right)} \tag{35}$$

with d the ratio of the output voltage over the rated output voltage ($V_{out,nom}$).

Next, with this value, the actual RMS-currents through the MOSFETs on both primary and secondary are estimated:

$$I_{RMS,MOSFET,Prim} = \frac{I_{RMS}}{\sqrt{2}} \tag{36}$$

$$I_{RMS,MOSFET,Sec} = \frac{I_{RMS}}{n \cdot \sqrt{2}} \tag{37}$$

With these two values, the conduction losses of all the MOSFETs can be estimated with formula (2) for both the primary and secondary. Note that this formula only estimates the conduction losses for one MOSFET, which mean these values have to be multiplied by four. After this, the iron and conduction losses of the transformer are estimated. As said before, the part of the code which models the latter will not be used in this thesis. The transformer conduction losses will be estimated by using formula (4). Note that only the resistance of the primary wire has to be measured.

The switching losses of the converter will be estimated as last. For this purpose, the possibility of operation of the converter in ZVS mode will be taken into account. First, the turn-off losses of both primary and secondary switches will be estimated with the switching model which was specified at the parameter input. Then, the conditions for zero voltage switching will be checked:

- When $I_{P,prim} > 0$ and $I_{L,prim} > 0$, ZVS will occur in both bridges.
- When $I_{P,prim} < 0$ and $I_{L,prim} > 0$, ZVS will only occur at the primary bridge.
- When $I_{P,prim} > 0$ and $I_{L,prim} < 0$, ZVS will only occur at the secondary bridge.

with $I_{P,prim}$ the maximum value of current after turning on the switching device and $I_{L,prim}$ the peak current occurring through the switching device just before turn-off.

When ZVS does not occur in one or both of the bridges, the switching loss models will be used to calculate the hard switching losses in that bridge. When ZVS does occur, the turn-on losses in that bridge will be assumed to be zero, like is stated in [9]. This is arguably one of the most important statements that need to be verified.

Finally, the input power can be estimated by adding all the before mentioned losses to the output power. With the input power known, the efficiency can also be calculated.

The converter model can be used to calculate the losses and efficiency of the converter over its entire operating range. This is done with the Python code provided in Appendix E. In this code, a few voltage levels which define the output voltage range of the converter are defined. This is done by creating a list with several values of d, which has the same meaning as in equation (35) . Then, a number of output currents are defined which represent the range of the output current. All these voltage and current levels can be freely adjusted until the desired operating range is obtained. All the estimated losses and efficiencies will be shown in 3D plots and exported to CSV-files. In these CSV-files, each row represents a different output voltage level and each column a different output current level. Both are listed in the same order as defined in the Python-code.

4. Experimental Verification

4.1. Verification of Switching Loss Models

All of the switching loss models are compared to losses calculated from experimentally measured operating points. This is done by measuring V_{gs}, V_{ds} and I_d of a MOSFET in one of the legs on the primary side of the converter with an oscilloscope. Above is achieved for 10 operating points which were scattered evenly throughout the operating range. Sadly, no points could be measured for voltages under 400V. This is because high currents occurred at these voltage levels, which would trip the current protections of the circuit. Additionally, the limit of the current probe, which was used, would have been exceeded, as it could only withstand up to 50A. The cause of this seems to be the relatively high demand of Q for the HF-transformer at low output power.

4.1.1 Description of the analyzing code

For each operating point, 20 periods were measured. Since the switching frequency of the converter was kept at a constant of 50 kHz, this so that a single measurement had a duration of around 400 µs. The three values of the MOSFETs were measured every 4 ns. This means that the CSV-files for each operating point contained around 4 million measurements of either time, V_{gs}, V_{ds} or I_d. Since it would be a long and tedious task to distinguish all the turn-on and turn-off switching from these measurements, a Python code was created to analyze these files automatically. This code can be found in appendix F.

First, this code automatically clears the DC-offset of I_d, caused by the Rogowski coil which was used to measure this current. To do this, $I_{RMS,transfo}$ also had to be measured by the oscilloscope. This current could be measured with a more accurate probe. The constant value of the DC-offset could then be found by comparing I_d with $I_{RMS,transfo}$. After this, the value for the offset could be subtracted from I_d, in order to let I_d match with $I_{RMS,transfo}$ while the MOSFET is switched on. This is done with all 1 million values of I_d in a single CSV-file.

After this, the switching events are distinguished. In order to do this, it must first be verified if the MOSFET is conducting at the start of the measurement or not. This can be done by looking at the value of V_{gs}. For this reason, the on- and off-values for V_{gs} are asked at the parameter input at the beginning of the file. As soon as this is known, turn-on events can be found by verifying if the value of V_{ds} becomes negative while the MOSFET is turned off, and turn-off events can be found by checking V_{gs} in the same manner as is done in the beginning to verify if the MOSFET is turned off, when the MOSFET is turned on.

As soon as a turn-on or turn-off event is found, the code retraces back to the point where the start criteria of the event are met. These criteria are directly taken from [39]. For a turn-on event, this point can be found by checking if V_{ds} begins to decrease towards zero or the intrinsic body diode of the MOSFET begins to conduct the reverse current and I_d

rises. It is also verified whether or not ZVS-conditions are met. This can be done by checking if the MOSFET is not yet conducting at this point, meaning that V_{gs} has to be lower than V_{th}.

Since the MOSFET is not directly turned on at this point, switching losses are not being generated yet if ZVS-conditions were met. The only losses at this point are the conduction losses of the body diode. The body diode keeps conducting until V_{gs} rises above V_{th} and the MOSFET channel becomes active. This causes the reverse current to commutate to the channel and shut off the body diode, causing it to generate reverse recovery losses. Note that these losses are only an estimation based on formulas (9) and (10) and largely rely on datasheet parameters, only using the $I_{rr,max}$ which is measured at the beginning of the turn-on event. From this point on, only the MOSFET conducts meaning the only losses during this stage are the conduction losses generated from the reverse current flowing through the channel. These losses are not directly calculated, as this reverse current will be taken into account when calculating the RMS-value of the current flowing through the MOSFET. Finally, the MOSFET will start conducting forward current, and the switching event will end as soon as V_{gs} has reached its on-state value. This can be seen in Figure 35.

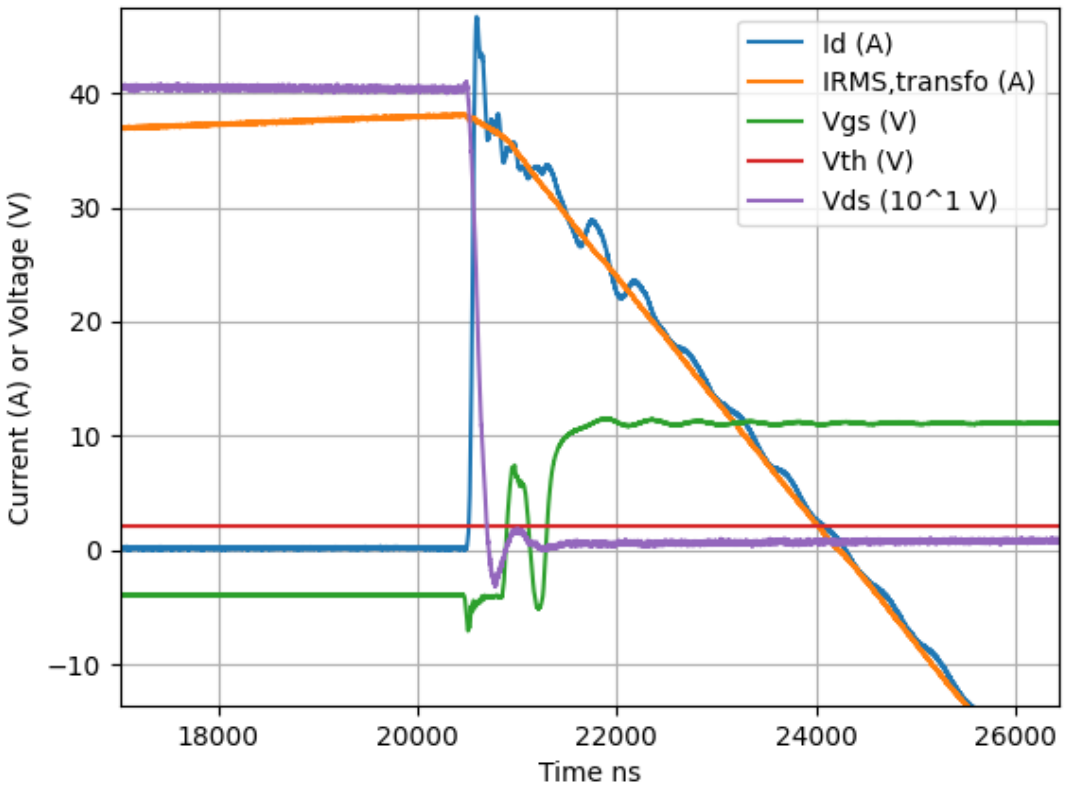

Figure 35: Detail of a turn-on of a MOSFET in the primary bridge of the converter with operating point with 800V and 11.96A.

If ZVS-conditions were not met, the same process will be followed. The only differences are the much shorter t_{dead} where the body diode conducts and the fact that because of this, V_{ds} will not yet reach zero when the MOSFET is turned on, causing high switching losses to be generated.

If a turn-off event is found, as is the case for a turn-on event, steps will be taken back until a point where all starting criteria are met. For a turn-off, this is the case when V_{gs} start to decrease towards its off-state value. From this point on, switching losses will be generated. The turn-off event will end as soon as V_{ds} approaches its on-state value.

4.1.2 Results and comparison with models

The results from all the experimental measurements and the estimations for these values given by all the different switching loss models are shown in appendix G. Note that these values represent the total losses of the four switching devices in the primary bridge of the converter. This could be done by simply multiplying the losses measured from the single MOSFET by a factor of 4. Another important remark is that two operating points with the highest output current at 900V would exceed the maximum output power of the converter. For this reason, the current has to be limited and will not be equal to the one specified in the table.

The modelled turn-on losses are equal to zero for most of the operating points of the converter. Note that the ZVS conditions of the model could not be fulfilled when working at low power at 900V. Sadly, it could not be experimentally verified if this is true because these points could not be accurately measured. However, it can be verified that for all points that were measured, ZVS conditions were indeed met, as was stated each time by the analyzing code. Based on the experimental losses, it can be concluded that even though ZVS is applied, still up to 0.14% of the input power is lost to turn-on losses.

The reverse recovery losses from the body diode are also determined by the experimental results. They remain quasi constant in the hole operating range. This causes the losses to take up to 5.37% of the total input power when the converter is operating at light loads. This can be seen in Table 1. When ZVS occurs, the reverse recovery losses are neglected together with the switching losses. Only when there is no ZVS, model 3 can calculate these losses.

Table 1: Experimentally calculated total reverse recovery losses of the body diodes as a percentage of the input power of the converter.

Experimental Primary Body Diode Reverse Recovery Losses vs Input Power		Current (A)									
		1.33	1.53	1.7	5.94	7.79	7.93	8.81	10.97	11.46	11.96
Voltage (V)	200										
	300										
	400		5.37%				1.28%				
	500										
	600				1.24%				0.65%		
	700			3.34%				0.71%		0.53%	
	800	3.75%				0.69%					0.46%
	900										

The experimentally calculated turn-off losses seem to decrease as the output current and the output voltage increase. They seem to take up to 3.5% of the input power and this percentage decreases as output power increases. This can be seen in Table 2.

Table 2: Experimentally calculated total primary turn-off losses as a percentage of the input power of the converter.

Experimental Primary Turn-Off Losses vs Input Power		Current (A)									
		1.33	1.53	1.7	5.94	7.79	7.93	8.81	10.97	11.46	11.96
Voltage (V)	200										
	300										
	400		3.34%				0.89%				
	500										
	600				0.70%				0.29%		
	700			1.36%				0.30%		0.25%	
	800	1.38%				0.29%					0.22%
	900										

The switching losses estimated by all switching loss models seem to show the same behavior as the experimental switching losses. However, model 3 seems to represent the most accurate switching loss model. Model 1 seems to overestimate both turn-on and turn-off losses. The turn-off losses of model 1 are for example two to six times larger than the experimentally calculated ones. This is probably due to the fact that the non-linear behavior of the capacitance is not taken into account. The model oversimplifies the overlap area between V_{ds} and I_d at turn off. It also expects a constant current to flow through the gate circuit during t_{off}, which also causes an error. However, the model does appear to become more accurate in the low power region at high voltages, as is shown in Table 3.

Table 3: The modeled turn-off losses of model 1 as a percentage of the experimentally measured turn-off losses.

Modeled turn-off losses as a percentage of the experimental turn-off losses.		Current (A)									
		1.33	1.53	1.7	5.94	7.79	7.93	8.81	10.97	11.46	11.96
Voltage (V)	200										
	300										
	400		621%				651%				
	500										
	600				496%				867%		
	700			373%				670%		744%	
	800	186%				475%					617%
	900										

Model 2 on the other hand seems to do the exact opposite and grossly underestimates the turn-off losses, as seen in Table 4. In the high voltage and low power region, the modelled losses of model 2 even turn negative. This is probably caused by the fact that VFD could not be calculated as was stated in [59]. This would require an accurate estimation of the charge present in C_{rss} during a variation of V_{ds}, which is difficult to implement as C_{rss} shows a non-linear behavior during the variation of V_{ds}. Also, the description of the turn-off model in [59] was complete, with a few important parameters missing. For this reason, it was completed with formulas found in [55]. This could eventually be the cause of the negative values for the turn-off losses in the low power, high voltage region.

Table 4: The modeled turn-off losses of model 2 as a percentage of the experimentally measured turn-off losses.

Modeled turn-off losses as a percentage of the experimental turn-off losses.		Current (A)									
		1.33	1.53	1.7	5.94	7.79	7.93	8.81	10.97	11.46	11.96
Voltage (V)	200										
	300										
	400		11.1%				11.3%				
	500										
	600				8.9%				15.4%		
	700			5.0%				12.1%		13.4%	
	800					7.8%					11.1%
	900										

For this reason, model 3 is recommended to use when trying to accurately model the losses in a high power, DAB converter. However, it is important to note that this model is also not perfect. It seems to underestimate the turn-off losses when the converter is operating at light load and high output voltage, as shown in Table 5. It can be noted that aside from the low power and high voltage region, the turn-off losses estimated by this model appear to be more relatively accurate. The underestimating of losses at high voltage and low power can be caused by the fact that just like model 1, the non-linear behavior of the MOSFET is not taken into account sufficiently. Table 6 shows the percentage of the input power of the converter which is taken up by the turn-off losses of the 4 switches on the primary side of the converter. Similar conclusions could be made for this table and Table 2. Both show similar behavior: these losses are relatively negligible at higher power levels and become more important at lower power levels.

The 3D graphs with absolute values for the switching losses of model 3 for the total operating range are given in Figure 36, Figure 37 and Figure 38.

Table 5: The modeled turn-off losses of model 2 as a percentage of the experimentally measured turn-off losses.

Modeled turn-off losses as a percentage of the experimental turn-off losses.		Current (A)									
		1.33	1.53	1.7	5.94	7.79	7.93	8.81	10.97	11.46	11.96
Voltage (V)	200										
	300										
	400		109.2%				110.0%				
	500										
	600				94.9%				99.1%		
	700			54.5%				97.9%		97.3%	
	800	35.6%				97.5%					96.2%
	900										

Table 6: Modelled primary turn-off losses for model 3 as a percentage of the input power of the converter.

Modeled Primary Turn-off Losses vs Input Power		Current (A)									
		1.33	1.53	1.7	5.94	7.79	7.93	8.81	10.97	11.46	11.96
Voltage (V)	200										
	300										
	400		3.3%				1.1%				
	500										
	600				0.4%				0.4%		
	700			0.0%				0.2%		0.2%	
	800	0.0%				0.1%					0.2%
	900										

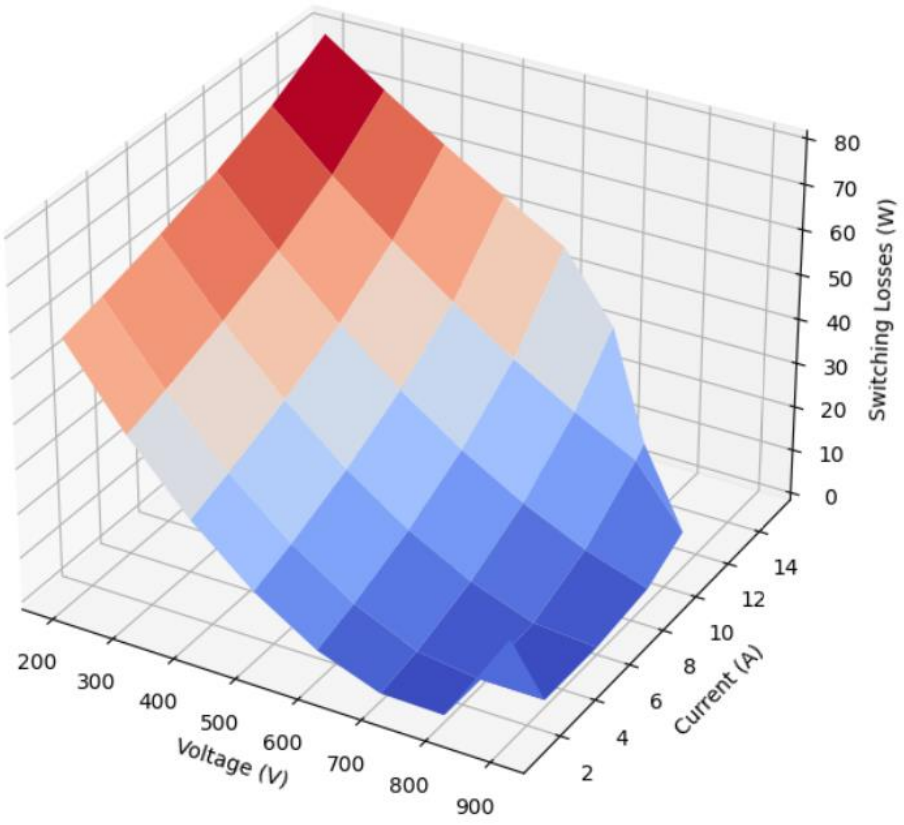

Figure 36: Total Switching losses of the 4 switches on the primary side (model 3).

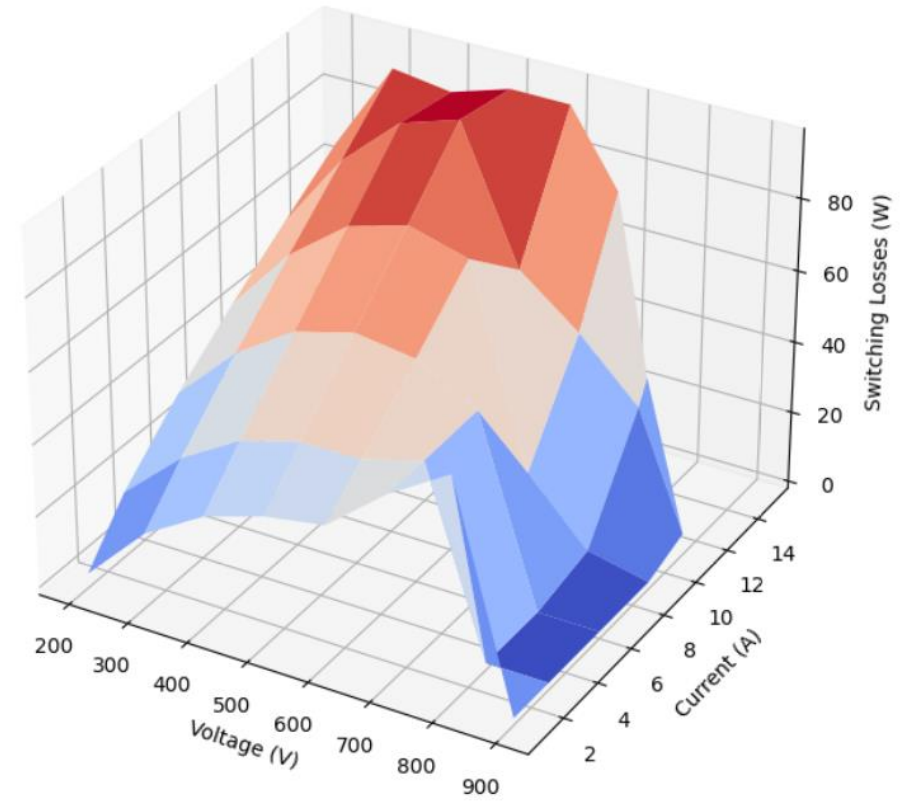

Figure 37: Total Switching losses of the 4 switches on the secondary side (model 3).

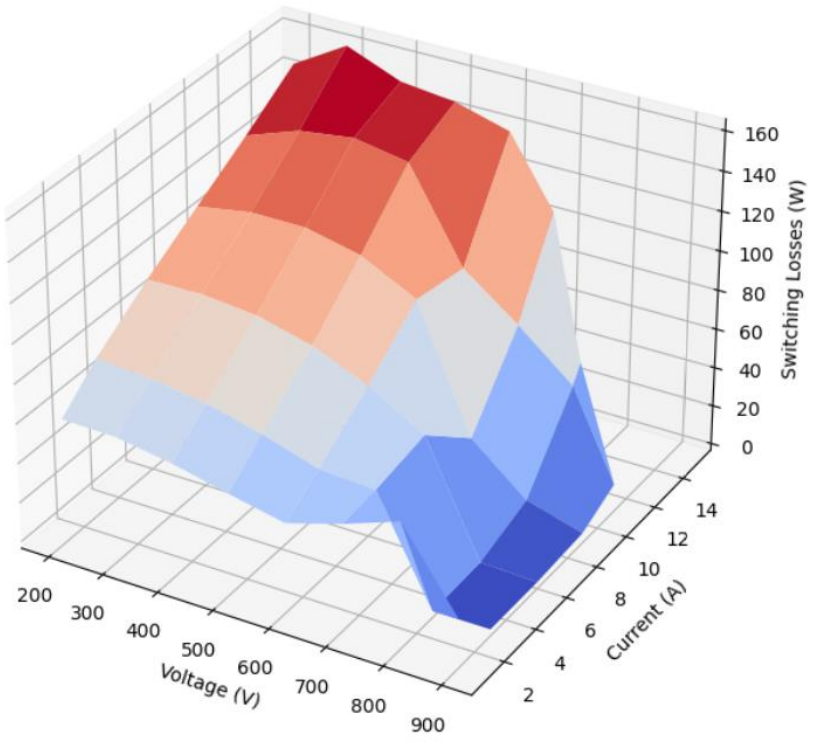

Figure 38: Total Switching losses of all the switches of the converter (model 3).

There is a great trend that the largest switching losses of the converter take place at low voltages and large currents. This can also be seen in Table 17, however it must be noted that the largest switching losses occur when turning off. This is because the converter achieves ZVS in turn on for most of the tests.

4.2. Verification Converter Model

In order to also verify the converter model, additional measurements were taken of P_{in}, P_{out} and $I_{RMS,transfo}$ while measuring the 10 operating points which were mentioned in the previous section. This allowed for a quick calculation of the efficiency, the MOSFET conduction losses and the transformer conduction losses. The experimental and modelled results are given in appendix H.

Since model 3 modeled the switching losses the most accurately, only the results from the converter model which uses model 3 to estimate switching losses will be compared with the experimental results. It is important to mention that the modeled conduction losses are the same for each model. This is because a set of formulas is used to calculate these and are not dependable on the switching model.

4.2.1 MOSFET Conduction Losses

First the MOSFET conduction losses are discussed. As seen in Table 19, Table 21, Table 24 and Table 27, the conduction losses are higher for high load and high voltage. This makes sense as the conduction losses are given by formula (2) and are directly proportional with the output current.

The ratio of MOSFET conduction losses to input power are given in Table 7 and Table 8. Because the output power is a lot larger with higher current and higher voltage, the ratio of the conduction losses is smaller.

Table 7: Experimentally calculated total primary conduction losses as a percentage of the input power of the converter.

Experimental Primary Conduction Losses vs input power		Current (A)									
		1,33	1,53	1,7	5,94	7,79	7,93	8,81	10,97	11,46	11,96
Voltage (V)	200										
	300										
	400		3,50%				1,10%				
	500										
	600				0,45%				0,36%		
	700			0,36%				0,24%		0,33%	
	800	0,12%				0,32%					0,57%
	900										

For lower voltages, the model overestimates the conduction losses of the MOSFET, this can be seen in the line of 400V. In the higher voltage area, the line of 800V, the model underestimates the conduction losses of the MOSFET.

Table 8: Modelled primary conduction losses as a percentage of the input power of the converter.

Modelled Primary Conduction Losses vs input power		Current (A)									
		1,33	1,53	1,7	5,94	7,79	7,93	8,81	10,97	11,46	11,96
Voltage (V)	200										
	300										
	400		3,83%				1,21%				
	500										
	600				0,43%				0,59%		
	700			0,20%				0,39%		0,54%	
	800	0,04%				0,31%					0,54%
	900										

4.2.2 Transformer Conduction Losses

The experimentally determined values of the transformer conduction losses are given in Table 19, Table 22, Table 25 and Table 28. The link between the MOSFET conduction losses and the transformer conduction losses is the same. The transformer conduction losses are also larger with higher power levels and higher voltage, they are however smaller than the MOSEFT conduction losses. Note that for all the models, the transformer conduction losses are the same, this is because it is used in the converter model and not in the switching losses models. The focus of this thesis lies with the switching losses.

The ratio of Transformer conduction losses and input power of the converter are given in Table 9 and Table 10. We can see that the model overestimates the conduction losses for all measured values except one. The 3D graph for the total conduction losses for model 3 is given by Figure 39 and is for the total operating range.

Table 9: Experimentally calculated Transformer Conduction Losses as a percentage of the input power of the converter.

Experimental Transformer Conduction losses vs input power		Current (A)									
		1,33	1,53	1,7	5,94	7,79	7,93	8,81	10,97	11,46	11,96
Voltage (V)	200										
	300										
	400		2,16%				0,67%				
	500										
	600				0,28%				0,36%		
	700			0,23%				0,24%		0,33%	
	800	0,07%				0,19%					0,34%
	900										

Table 10: Modeled Transformer Conduction Losses as a percentage of the input power.

Modeled Transformer Conduction losses vs input power		Current (A)									
		1,33	1,53	1,7	5,94	7,79	7,93	8,81	10,97	11,46	11,96
Voltage (V)	200										
	300										
	400		4,46%				1,41%				
	500										
	600				0,50%				0,69%		
	700			0,23%				0,46%		0,62%	
	800	0,05%				0,38%					0,63%
	900										

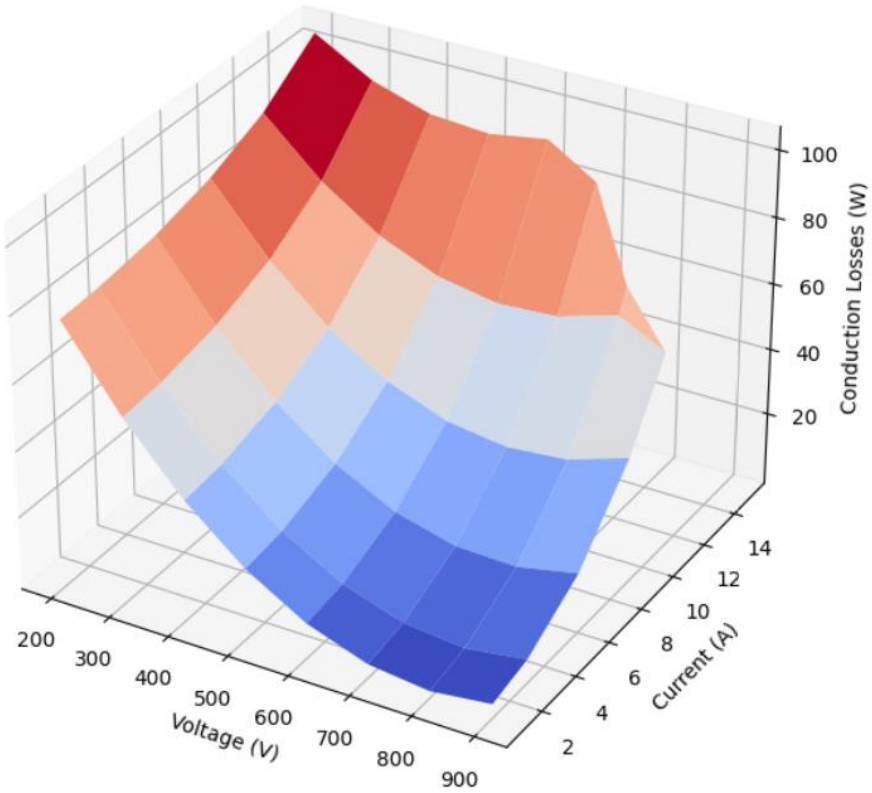

Figure 39: Total Conduction losses of all the MOSFETs in the converter for Model 3.

As seen in Figure 39, the conduction losses are the highest for low voltages and high currents. These values were hard to measure due to limitations of the set-up, so could not be experimentally verified.

4.2.3 Efficiency

For the efficiency, the values can be seen in Table 18, Table 20, Table 23 and Table 26. The trend of the efficiency is that with higher voltages and therefore higher powers, comes higher efficiencies. In the high voltage range, the efficiency is the highest with the middle currents. This is because the conduction losses are a lot higher with higher current levels and are lower with high voltages and lower currents. In Table 11, the difference between the efficiencies is given in percentage points. For lower currents, the difference between the experimental and the modeled efficiency is larger. This is because for lower currents, the phase shift between the two bridges has to be small to achieve the desired output power. A small variation in the phase shift results in large variations of the output power. Because the phase shift is hard to keep at a constant value, the variations need to be taken with a pinch of salt. For larger output power, the variations of the phase shift are negligible.

Table 11: Differences of the efficiency in percentage points for modeled and experimental values.

Modeled - Experimental Efficiency		Current (A)									
		1,33	1,53	1,7	5,94	7,79	7,93	8,81	10,97	11,46	11,96
Voltage (V)	200										
	300										
	400		7%				1%				
	500										
	600				2%				1%		
	700			6%				1%		1%	
	800	6%				1%					2%
	900										

In Figure 40 the total efficiency of the converter is given. As stated before, the efficiency increases when the output power increases. For low voltages and low currents, the DAB converter is not efficient at all.

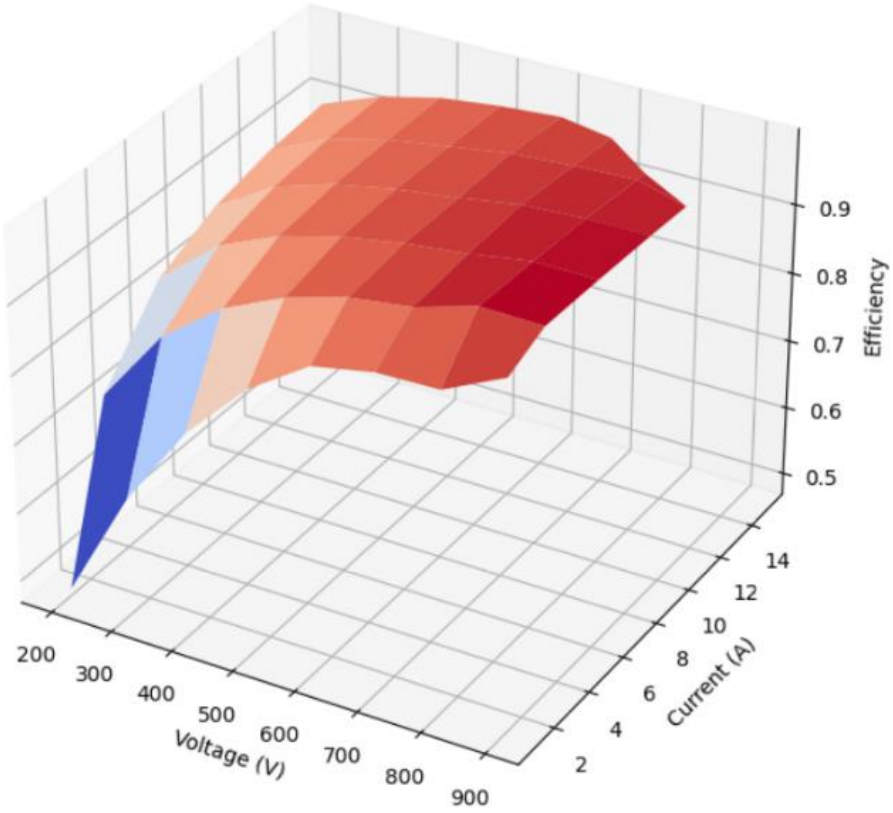

Figure 40: Total Efficiency of the converter for Model 3.

5. Conclusion

From the results given in section 4, it can be concluded that ZVS-conditions are met for almost the entire operating range of the converter. Only the high output voltage, low power operating point does not seem to achieve ZVS. Furthermore, it can also be concluded that the turn-on losses that occur while ZVS mode is active, increase if the power increases. However, since these losses take up a very small percentage of the input power, they can be considered negligible. It also verifies that the ZVS-conditions of the converter model are to some degree correct, as measuring the points where ZVS was not possible according to the model, was not possible either.

What must be taken into account is that the reverse recovery losses of the intrinsic body diode of the MOSFET still generate relatively significant losses, especially at operating points of low power. These losses are not taken into account in the converter model when ZVS is acquired. This could be done relatively simple by implementing equations (9) and (10) for the bridges where ZVS occurs, instead of assuming the losses to be zero.

Furthermore, it seems that the switching loss model 3 is a more accurate model, although it is the most complex one. However, it is still not perfect as it underestimates the turn-off losses at operating points with low power and high output voltages. This is especially important as although the turn-off losses decrease considerably at higher output voltages and lower power, these losses still make up an important percentage of the input power at these operating points. For this reason, this error cannot be neglected and a correction is needed. Consequently, a hybrid model could be used. It may be advised to use model 1 in this voltage range, as it overestimates the losses at these points by up to 80%, which is at least better than underestimating them by at least 70% as it done with model 3. The use of model 2 to estimate the turn-off losses is not recommended, as it massively underestimates the losses by about 90% over the entire operating range and does not even return valid results in the low power, high voltage region of the operating range.

Both the conduction losses of the MOSFETs and the transformer seem to be estimated in a correct way as there is only a slight difference with the experimentally measured losses. Nevertheless, it is unfortunate that the iron losses could not be modelled and experimentally verified, as specifications for the HF-transformer could not be obtained.

Finally, the efficiency seems to be modelled in a correct manner, as it shows the same behavior as the measured efficiency in the known operating points. As expected, the efficiency generally seems to rise when the output power rises. The slight difference in efficiency could be caused by the iron losses and reverse recovery losses of the body diodes, which were not taken into account by the converter model. The slight difference in turn-off losses can also cause an insignificant increase in the efficiency estimated by the model. Despite all this, the converter model seems to only overestimate the efficiency of the converter by 2% or less when the converter is operating at high power, but as expected, overestimates the efficiency by 7% or more when the converter is operating at low power. This does not directly pose a problem, because the converter will most likely only be used at operating points with a higher power output. This could also be deduced from the

experimentally measured efficiency. The converter will operate at a significantly lower efficiency at these more inaccurate points.

6. Future work

A model that could estimate the total losses of the isolated DAB DC-DC converter with variable output voltage and current was constructed. This model allowed for the efficiency of a high-power converter to estimate based on only datasheet parameters. With this, the next step is to decide the ideal number of modules and the maximum power of these modules which will eventually form a modular, 350 kW DC fast charger. The information given in section 2.4 could be used as a starting point.

Based on the number of modules and their efficiency at different operating points, an optimal control algorithm can be developed, which decides the operating point for each module depending on the load of the charger. This is of course also largely dependent on the connection made between the modules. This also means that further research needs to be done about the ideal number of parallel and/or series connections at the input or output of the DAB modules. These works would represent major steps forward in the building of a real modular, and above all future-proof fast-charger.

Alternatively, the converter model could also be further improved. This could for example be done by implementing a switching loss model which takes both ZVS and SR into account and by adding reverse recovery losses of the intrinsic body diode into the model for each ZVS turn-on.

Bibliography

[1] C. Suarez and W. Martinez, “Fast and Ultra-Fast Charging for Battery Electric Vehicles - A Review,” *2019 IEEE Energy Convers. Congr. Expo. ECCE 2019*, pp. 569–575, 2019.

[2] M. Elmenshawy and A. Massoud, “Hybrid Multimodule DC-DC Converters for Ultrafast Electric Vehicle Chargers,” 2020.

[3] Y. C. Wang, Y. C. Wu, and T. L. Lee, “Design and implementation of a bidirectional isolated dual-active-bridge- based DC/DC converter with dual-phase-shift control for electric vehicle battery,” *2013 IEEE Energy Convers. Congr. Expo. ECCE 2013*, pp. 5468–5475, 2013.

[4] S. Saeed, “Design and construction of a DAB Converter for integration of energy storage systems in Power Electronic applications,” *2015 6th Int. Conf. Power Electron. Syst. Appl. Electr. Transp. - Automotive, Vessel Aircraft, PESA 2015*, 2016.

[5] L. Boets and M. Desmet, “Detailed Power Loss Analysis of a Dual Active Bridge DC / DC Power Converter [thesis],” 2020.

[6] R. Everaerts and N. Martin, *Thesis Transformer Design [thesis]*. Diepenbeek: Gezamenlijke opleiding Industriële Ingenieurswetenschappen UHasselt & KU Leuven, 2020.

[7] M. Rolak, C. Sobol, M. Malinowski, and S. Stynski, “Efficiency Optimization of Two Dual Active Bridge Converters Operating in Parallel,” *IEEE Trans. Power Electron.*, vol. 35, no. 6, pp. 6523–6532, 2020.

[8] G. G. Oggier and M. Ordonez, “High-efficiency DAB converter using switching sequences and burst mode,” *IEEE Trans. Power Electron.*, vol. 31, no. 3, pp. 2069–2082, 2016.

[9] H. Akagi, T. Yamagishi, N. M. L. Tan, Y. Miyazaki, S. I. Kinouchi, and M. Koyama, “Power-loss breakdown of a 750-V 100-kW 20-kHz bidirectional isolated DC-DC converter using SiC-MOSFET/SBD dual modules,” *IEEE Trans. Ind. Appl.*, vol. 51, no. 1, pp. 420–428, 2015.

[10] R. Thoelen, *Analoge Elektronica*. Hasselt: Pearson Education Limited, 2014.

[11] N. Mohan, T. M. Undeland, and W. P. Robbins, *Power Electronics: Converters, Applications and Design*, Third. John Wiley & Sons, Inc., 2003.

[12] C. Based, S. S. Diode, H. Mirzaee, S. Member, A. De, and S. Member, “Design Comparison of High-Power Medium-Voltage Converters Based on a 6.5-kV Si-IGBT/Si-PiN Diode, a 6.5-kV Si-IGBT/SiC-JBS Diode, and a 10-kV SiC-MOSFET/SiC-JBS Diode,” vol. 50, no. 4, pp. 2728–2740, 2014.

[13] L. Vinet and A. Zhedanov, *Fundamental of Power Semiconductor Devices*, vol. 44, no. 8. 2011.

[14] D. Martin, P. Killeen, W. A. Curbow, B. Sparkman, L. E. Kegley, and T. Mcnutt, “Comparing the Switching Performance of SiC MOSFET Intrinsic Body Diode to Additional SiC Schottky Diodes in SiC Power Modules,” pp. 242–246, 2016.

[15] T. Funaki, M. Matsushita, M. Sasagawa, T. Kimoto, and T. Hikihara, “A study on SiC devices in synchronous rectification of DC-DC converter,” *Conf. Proc. - IEEE Appl. Power Electron. Conf. Expo. - APEC*, pp. 339–344, 2007.

[16] S. Yin, Y. Liu, Y. Liu, K. Jet Tseng, J. Pou, and R. Simanjorang, “Comparison of SiC voltage source inverters using synchronous rectification and freewheeling diode,” *IEEE Trans. Ind. Electron.*,

vol. 65, no. 2, pp. 1051–1061, 2017.

[17] X. Li, L. Zhang, S. Guo, Y. Lei, A. Q. Huang, and B. Zhang, “Understanding switching losses in SiC MOSFET: Toward lossless switching,” in *WiPDA 2015 - 3rd IEEE Workshop on Wide Bandgap Power Devices and Applications*, 2015, vol. 5, pp. 257–262.

[18] E. Platania *et al.*, “A physics-based model for a SiC JFET device accounting for the mobility dependence on temperature and electric field,” *Conf. Rec. - IAS Annu. Meet. (IEEE Ind. Appl. Soc.*, pp. 1–8, 2008.

[19] F. Chimento, S. Musumeci, A. Raciti, M. Melito, and G. Sorrentino, “Super-junction MOSFET and SiC diode application for the efficiency improvement in a boost PFC converter,” *IECON Proc. (Industrial Electron. Conf.*, pp. 2067–2072, 2006.

[20] J. Loncarski and V. G. Monopoli, “Converters for EV Chargers : Approach for Efficiency Comparison with Minimum Switching Losses Based on Complete Parasitic Modeling,” 2020.

[21] M. J. Heathcote, “Transformer theory,” *J P Transform. B.*, pp. 1–13, 2007.

[22] N. Yamashita, N. Murakami, and T. Yachi, “Conduction power loss in MOSFET synchronous rectifier with parallel-connected Schottky barrier diode,” *IEEE Trans. Power Electron.*, vol. 13, no. 4, pp. 667–673, 1998.

[23] B. Ozpineci and L. M. Tolbert, “Characterization of SiC Schottky diodes at different temperatures,” *IEEE Power Electron. Lett.*, vol. 1, no. 2, pp. 54–57, 2003.

[24] T. Instruments, “Bi-Directional , Dual Active Bridge Reference Design for Level 3 Electric Vehicle Charging Stations,” *Texas Instruments*, no. June, pp. 1–51, 2019.

[25] S. Maniktala, “Conduction and Switching Losses,” *Power Sources Supplies World Cl. Des.*, pp. 247–278, 2008.

[26] E. Sugawara and H. Nikaido, *Advanced Power MOSFET Concepts*, vol. 58, no. 12. 2014.

[27] P. Zuk and S. Havanur, “Zero-Voltage Switching Full-Bridge Converter: Operation, FOM, and Guidelines for MOSFET Selection,” pp. 1–6, 2014.

[28] V. C. Valchev, A. Van Den Bossche, and P. V. Yankov, “High frequency power loss measurement platform,” *Int. J. Electron. Lett.*, vol. 8, no. 1, pp. 28–37, 2020.

[29] X. Liu, Y. Wang, J. Zhu, Y. Guo, G. Lei, and C. Liu, “Calculation of core loss and copper loss in amorphous/nanocrystalline core-based high-frequency transformer,” *AIP Adv.*, vol. 6, no. 5, 2016.

[30] M. Spang and M. Albach, “Optimized winding layout for minimized proximity losses in coils with rod cores,” *IEEE Trans. Magn.*, vol. 44, no. 7, pp. 1815–1821, 2008.

[31] R. Everaerts and N. Martin, “Transformer design [thesis],” 2020.

[32] J. Reinert, A. Brockmeyer, and R. W. A. A. De Doncker, “Calculation of losses in ferro- and ferrimagnetic materials based on the modified Steinmetz equation,” *IEEE Trans. Ind. Appl.*, vol. 37, no. 4, pp. 1055–1061, 2001.

[33] S. Yue, Q. Yang, Y. Li, and C. Zhang, “Core loss calculation for magnetic materials employed in SMPS under rectangular voltage excitations,” *AIP Adv.*, vol. 8, no. 5, 2018.

[34] J. Mühlethaler, J. Biela, J. W. Kolar, and A. Ecklebe, “Improved core-loss calculation for magnetic components employed in power electronic systems,” *IEEE Trans. Power Electron.*, vol. 27, no. 2, pp. 964–973, 2012.

[35] M. Mu and F. C. Lee, “A new core loss model for rectangular AC voltages,” *2014 IEEE Energy Convers. Congr. Expo. ECCE 2014*, pp. 5214–5220, 2014.

[36] H. Matsumori, T. Shimizu, T. Kosaka, and N. Matsui, “Core loss calculation for power electronics converter excitation from a sinusoidal excited core loss data,” *AIP Adv.*, vol. 10, no. 4, 2020.

[37] K. Yamazaki, Y. Fukushima, and M. Sato, “Loss analysis of permanent-magnet motors with concentrated windings - Variation of magnet eddy-current loss due to stator and rotor shapes,” *IEEE Trans. Ind. Appl.*, vol. 45, no. 4, pp. 1334–1342, 2009.

[38] J. Pollefliet, *Elektronische Vermogencontrole*, Ninth., vol. 1, no. Schakelaars en Convertoren. Uitgeverij Academia Press, 2018.

[39] I. Castro *et al.*, “Analytical switching loss model for superjunction MOSFET with capacitive nonlinearities and displacement currents for DC-DC power converters,” *IEEE Trans. Power Electron.*, vol. 31, no. 3, pp. 2485–2495, 2016.

[40] Z. Duan, T. Fan, X. Wen, and D. Zhang, “Improved SiC Power MOSFET Model Considering Nonlinear Junction Capacitances,” *IEEE Trans. Power Electron.*, vol. 33, no. 3, pp. 2509–2517, 2018.

[41] G. Chindris, O. Pop, G. Alin, and F. Hurgoi, “New PSPICE model for power MOSFET devices,” *Proc. Int. Spring Semin. Electron. Technol.*, vol. 2001-Janua, pp. 158–162, 2001.

[42] M. Mudholkar *et al.*, “MOSFET Model,” vol. 29, no. 5, pp. 2220–2228, 2014.

[43] R. Ahmed, R. Todd, S. Member, A. J. Forsyth, and S. Member, “Predicting SiC MOSFET Behavior Under Turn-On Conditions,” vol. 64, no. 11, pp. 9001–9011, 2017.

[44] H. Li, X. Liao, Y. Hu, Z. Huang, and K. Wang, “Analysis of Voltage Variation in Silicon Carbide MOSFETs during Turn-On and Turn-Off,” 2017.

[45] J. Wang *et al.*, “Application of 10-kV SiC MOSFET,” vol. 55, no. 8, pp. 1798–1806, 2008.

[46] K. Chen *et al.*, “The Impact of Nonlinear Junction Capacitance on Switching Transient and Its Modeling for SiC MOSFET,” vol. 62, no. 2, pp. 333–338, 2015.

[47] I. H. Holger, “Nonlinear Parasitic Capacitance Modelling of High Voltage Power MOSFETs in Partial Nonlinear Parasitic Capacitance Modelling of High Voltage Power MOSFETs in Partial SOI Process,” 2016.

[48] C. Angelo, R. Angelo, S. Rosario, and S. Alfio, “Determination of the Power Losses Due to the Nonlinear Coss Capacitance of SJ MOSFETs Submittet to Voltage Transients in ZVS Applications.”

[49] M. Escudero, M. Kutschak, N. Fontana, N. Rodriguez, and D. P. Morales, “Non-Linear Capacitance of Si SJ MOSFETs in Resonant Zero Voltage Switching Applications,” pp. 116117–116131, 2020.

[50] S. Yin *et al.*, “An Accurate Subcircuit Model of SiC Half-Bridge Module for Switching-Loss Optimization,” *IEEE Trans. Ind. Appl.*, vol. 53, no. 4, pp. 3840–3848, 2017.

[51] J. A. Anderson, C. Gammeter, L. Schrittwieser, and J. W. Kolar, “Accurate Calorimetric Switching Loss Measurement for 900 v 10 m Ω SiC mosfets,” *IEEE Trans. Power Electron.*, vol. 32, no. 12, pp. 8963–8968, 2017.

[52] SEMIKRON, *Application Manual Power Semiconductors*. 2015.

[53] V. Höch, J. Petzoldt, A. Schlögl, H. Jacobs, and G. Deboy, “Determination of transient transistor

capacitances of high voltage mosfets from dynamic measurements," *Proc. Int. Symp. Power Semicond. Devices ICs*, pp. 148–151, 2009.

[54] W. Zhang, Z. Y. Zhang, F. Wang, L. M. Tolbert, D. Costinett, and B. Blalock, "Characterization and modeling of a SiC MOSFET's turn-off overvoltage," *Mater. Sci. Forum*, vol. 924 MSF, pp. 827–831, 2018.

[55] J. Wang, H. S. H. Chung, and R. T. H. Li, "Characterization and experimental assessment of the effects of parasitic elements on the MOSFET switching performance," *IEEE Trans. Power Electron.*, vol. 28, no. 1, pp. 573–590, 2013.

[56] M. Liang, T. Q. Zheng, and Y. Li, "An improved analytical model for predicting the switching performance of SiC MOSFETs," *J. Power Electron.*, vol. 16, no. 1, pp. 374–387, Jan. 2016.

[57] S. K. Roy and K. Basu, "Analytical estimation of turn on switching loss of sic mosfet and schottky diode pair from datasheet parameters," *IEEE Trans. Power Electron.*, vol. 34, no. 9, pp. 9118–9130, 2019.

[58] D. Christen and J. Biela, "Analytical Switching Loss Modeling Based on Datasheet Parameters for mosfets in a Half-Bridge," *IEEE Trans. Power Electron.*, vol. 34, no. 4, pp. 3700–3710, 2019.

[59] I. Castro *et al.*, "Analytical switching loss model for superjunction MOSFET with capacitive nonlinearities and displacement currents for DC-DC power converters," *IEEE Trans. Power Electron.*, vol. 31, no. 3, pp. 2485–2495, 2016.

[60] Y. Xiong, S. Sun, H. Jia, P. Shea, and Z. John Shen, "New physical insights on power MOSFET switching losses," *IEEE Trans. Power Electron.*, vol. 24, no. 2, pp. 525–531, 2009.

[61] J. Fu, Z. Zhang, Y. F. Liu, and P. C. Sen, "MOSFET switching loss model and optimal design of a current source driver considering the current diversion problem," *IEEE Trans. Power Electron.*, vol. 27, no. 2, pp. 998–1012, 2012.

[62] Y. H. Abraham, H. Wen, W. Xiao, and V. Khadkikar, "Estimating power losses in Dual Active Bridge DC-DC converter," *2011 2nd Int. Conf. Electr. Power Energy Convers. Syst. EPECS 2011*, pp. 1–5, 2011.

[63] J. Müting and U. Grossner, "Simulation-based sensitivity analysis of conduction and switching losses for silicon carbide power MOSFETs," *Mater. Sci. Forum*, vol. 924 MSF, pp. 693–696, 2018.

[64] J. Everts, F. Krismer, J. Van Den Keybus, J. Driesen, and J. W. Kolar, "Optimal zvs modulation of single-phase single-stage bidirectional dab ac-dc converters," *IEEE Trans. Power Electron.*, vol. 29, no. 8, pp. 3954–3970, 2014.

[65] N. Hou and Y. W. Li, "Overview and Comparison of Modulation and Control Strategies for a Nonresonant Single-Phase Dual-Active-Bridge DC-DC Converter," *IEEE Trans. Power Electron.*, vol. 35, no. 3, pp. 3148–3172, 2020.

[66] W. A. A. De Doncker and D. M. Divan, "A Three-phase Soft-Switched high-power-density dc/dc converter for high-power Applications," vol. 27, no. 1, 1991.

[67] A. Garcia-Bediaga, I. Villar, A. Rujas, and L. Mir, "DAB modulation schema with extended ZVS region for applications with wide input/output voltage," *IET Power Electron.*, vol. 11, no. 13, 2018.

[68] N. A. Dung, H. J. Chiu, J. Y. Lin, Y. C. Hsieh, and Y. C. Liu, "Efficiency optimisation of ZVS isolated bidirectional DAB converters," *IET Power Electron.*, vol. 11, no. 8, pp. 1–8, 2018.

[69] S. Inoue and H. Akagi, "A bidirectional isolated DC/DC converter as a core circuit of the next-

generation medium-voltage power conversion system," *PESC Rec. - IEEE Annu. Power Electron. Spec. Conf.*, vol. 22, no. 2, pp. 535–542, 2006.

[70] W. P. Siriwongpairat and K. J. R. Liu, "Performance Characterization of a high-power dual active bridge dc-to-dc converter," *Ultra-Wideband Commun. Syst.*, vol. 28, no. 6, pp. 97–120, 2007.

[71] S. Inoue and H. Akagi, "A bidirectional DC – DC Converter for an Energy storage system with galvanic isolation," *IEEE Trans. Power Electron.*, vol. 22, no. 6, pp. 2299–2306, 2007.

[72] F. An, W. S. Song, and K. X. Yang, "Optimised power control with extended phase shift in dual-active-bridge DC-DC converters," *Electron. Lett.*, vol. 54, no. 10, pp. 651–653, 2018.

[73] S. S. Muthuraj, V. K. Kanakesh, P. Das, and S. K. Panda, "Triple Phase Shift Control of an LLL Tank Based Bidirectional Dual Active Bridge Converter," *IEEE Trans. Power Electron.*, vol. 32, no. 10, pp. 8035–8053, 2017.

[74] A. Tong, L. Hang, G. Li, X. Jiang, and S. Gao, "Modeling and Analysis of a Dual-Active-Bridge-Isolated Bidirectional DC/DC Converter to Minimize RMS Current with Whole Operating Range," *IEEE Trans. Power Electron.*, vol. 33, no. 6, pp. 5302–5316, 2018.

[75] J. Hiltunen, V. Vaisanen, R. Juntunen, and P. Silventoinen, "Variable-Frequency Phase Shift Modulation of a Dual Active Bridge Converter," *IEEE Trans. Power Electron.*, vol. 30, no. 12, pp. 7138–7148, 2015.

[76] N. Hou, W. Song, and M. Wu, "Minimum-Current-Stress Scheme of Dual Active Bridge DC-DC Converter with Unified Phase-Shift Control," *IEEE Trans. Power Electron.*, vol. 31, no. 12, pp. 8552–8561, 2016.

[77] J. Huang, Y. Wang, Z. Li, and W. Lei, "Unified Triple-Phase-Shift Control to Minimize Current Stress and Achieve Full Soft-Switching of Isolated Bidirectional DC-DC Converter," *IEEE Trans. Ind. Electron.*, vol. 63, no. 7, pp. 4169–4179, 2016.

[78] M. Trivedi and K. Shenai, "Internal dynamics of igbt under zerovoltage and zerocurrent switching conditions," *IEEE Trans. Electron Devices*, vol. 46, no. 6, p. 12741282, 1999.

[79] M. R. Ahmed, R. Todd, and A. J. Forsyth, "Predicting SiC MOSFET Behavior under Hard-Switching, Soft-Switching, and False Turn-On Conditions," *IEEE Trans. Ind. Electron.*, vol. 64, no. 11, pp. 9001–9011, 2017.

[80] A. P. Camacho, V. Sala, H. Ghorbani, and J. L. R. Martinez, "A Novel Active Gate Driver for Improving SiC MOSFET Switching Trajectory," *IEEE Trans. Ind. Electron.*, vol. 64, no. 11, pp. 9032–9042, 2017.

[81] W. JING, "The Bidirectional Dual Active Bridge DC / DC Converter for Photovoltaic Application," *Xi'an Jiaotong-Liverpool Univ.*, no. July 2012, 2012.

[82] S. S. Shah, V. M. Iyer, and S. Bhattacharya, "Exact Solution of ZVS Boundaries and AC-Port Currents in Dual Active Bridge Type DC-DC Converters," *IEEE Trans. Power Electron.*, vol. 34, no. 6, pp. 5043–5047, 2019.

[83] D. J. Perreault, R. L. Selders, and J. G. Kassakian, "Frequency-based current-sharing techniques for paralleled power converters," *IEEE Trans. Power Electron.*, vol. 13, no. 4, pp. 626–634, 1998.

[84] R. T. Sataloff, M. M. Johns, and K. M. Kost, "Reliability Analysis of a Direct Parallel Connected n+1 Redundant Power System Based On Highly Reliable DC/DC Modules."

[85] R. T. Sataloff, M. M. Johns, and K. M. Kost, "Reliability Improvement in Parallel Connected Converter Systems."

[86] R. Ayyanar, R. Giri, and N. Mohan, “Active input-voltage and load-current sharing in input-series and output-parallel connected modular dc-dc converters using dynamic input-voltage reference scheme,” *IEEE Trans. Power Electron.*, vol. 19, no. 6, pp. 1462–1473, 2004.

[87] E. Mena, “Modular Isolated DC-DC Converters for Ultra-Fast,” 2020.

[88] P. Zumel, L. Ortega, A. Lazaro, C. Fernandez, and A. Barrado, “Control strategy for modular dual active bridge input series output parallel,” *2013 IEEE 14th Work. Control Model. Power Electron. COMPEL 2013*, 2013.

[89] W. M. Dos Santos, H. R. E. Mamede, and D. C. Martins, “Paralleling of dab converter using the gyrator theory,” *2014 IEEE 5th Int. Symp. Power Electron. Distrib. Gener. Syst. PEDG 2014*, 2014.

[90] Y. Lian, G. Adam, D. Holliday, and S. Finney, “Modular input-parallel output-series DC/DC converter control with fault detection and redundancy,” *IET Gener. Transm. Distrib.*, vol. 10, no. 6, pp. 1361–1369, 2016.

[91] M. Elmenshawy and A. Massoud, “Multimodule DC-DC Converters for High-Voltage High-Power Renewable Energy Sources,” *2nd Int. Conf. Smart Grid Renew. Energy, SGRE 2019 - Proc.*, 2019.

[92] S. Saeed, J. Garcia, M. S. Perdigao, V. S. Costa, B. Baptista, and A. M. S. Mendes, “Improved Inductance Calculation in Variable Power Inductors by Adjustment of the Reluctance Model through Magnetic Path Analysis,” *IEEE Trans. Ind. Appl.*, vol. 57, no. 2, pp. 1572–1587, 2021.

[93] CREE, “C3M0030090K Silicon Carbide Power MOSFET,” no. 1, pp. 1–10, 2017.

[94] CREE, “C3M0016120K Silicon Carbide Power MOSFET,” no. 1, pp. 1–10, 2017.

Appendices

Appendix A [93]

CREE

C3M0030090K

Silicon Carbide Power MOSFET
C3M™ MOSFET Technology

N-Channel Enhancement Mode

V_{DS}	900 V
$I_{D\ @\ 25°C}$	73 A
$R_{DS(on)}$	30 mΩ

Features

- C3M™ SiC MOSFET technology
- Optimized package with separate driver source pin
- 8mm of creepage distance between drain and source
- High blocking voltage with low on-resistance
- High-speed switching with low capacitances
- Fast intrinsic diode with low reverse recovery (Q_{rr})
- Halogen free, RoHS compliant

Benefits

- Reduce switching losses and minimize gate ringing
- Higher system efficiency
- Reduce cooling requirements
- Increase power density
- Increase system switching frequency

Applications

- Solar inverters
- EV battery chargers
- High voltage DC/DC converters
- Switch Mode Power Supplies

Package

Halogen-Free

RoHS

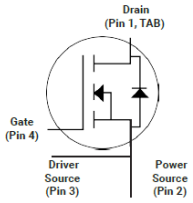

Part Number	Package	Marking
C3M0030090K	TO 247-4	C3M0030090K

Maximum Ratings (T_C = 25 °C unless otherwise specified)

Symbol	Parameter	Value	Unit	Test Conditions	Note
V_{DSmax}	Drain - Source Voltage	900	V	V_{GS} = 0 V, I_D = 100 µA	
V_{GSmax}	Gate - Source Voltage (dynamic)	-8/+19	V	AC (f >1 Hz)	Note: 1
V_{GSop}	Gate - Source Voltage (static)	-4/+15	V	Static	Note: 2
I_D	Continuous Drain Current	73	A	V_{GS} = 15 V, T_C = 25°C	Fig. 19
		48		V_{GS} = 15 V, T_C = 100°C	
$I_{D(pulse)}$	Pulsed Drain Current	200	A	Pulse width t_P limited by T_{jmax}	Fig. 22
P_D	Power Dissipation	240	W	T_C=25°C, T_J = 150 °C	Fig. 20
T_J , T_{stg}	Operating Junction and Storage Temperature	-40 to +150	°C		
T_L	Solder Temperature	260	°C	1.6mm (0.063") from case for 10s	
M_d	Mounting Torque, (M3 or 6-32 screw)	1 8.8	Nm lbf-in		

Note (1): When using MOSFET Body Diode V_{GSmax} = -4V/+19V
Note (2): MOSFET can also safely operate at 0/+15 V

CREE

Electrical Characteristics (T_C = 25˚C unless otherwise specified)

Symbol	Parameter	Min.	Typ.	Max.	Unit	Test Conditions	Note
$V_{(BR)DSS}$	Drain-Source Breakdown Voltage	900			V	V_{GS} = 0 V, I_D = 100 µA	
$V_{GS(th)}$	Gate Threshold Voltage	1.7	2.4	3.5	V	V_{DS} = V_{GS}, I_D = 11 mA	Fig. 11
			2.1		V	V_{DS} = V_{GS}, I_D = 11 mA, T_J = 150°C	
I_{DSS}	Zero Gate Voltage Drain Current		1	100	µA	V_{DS} = 900 V, V_{GS} = 0 V	
I_{GSS}	Gate-Source Leakage Current		10	250	nA	V_{GS} = 15 V, V_{DS} = 0 V	
$R_{DS(on)}$	Drain-Source On-State Resistance		30	39	mΩ	V_{GS} = 15 V, I_D = 35 A	Fig. 4, 5, 6
			41			V_{GS} = 15 V, I_D = 35 A, T_J = 150°C	
g_{fs}	Transconductance		23		S	V_{DS}= 20 V, I_{DS}= 35 A	Fig. 7
			22			V_{DS}= 20 V, I_{DS}= 35 A, T_J = 150°C	
C_{iss}	Input Capacitance		1503		pF	V_{GS} = 0 V, V_{DS} = 600 V f = 1 MHz V_{AC} = 25 mV	Fig. 17, 18
C_{oss}	Output Capacitance		144				
C_{rss}	Reverse Transfer Capacitance		5				
E_{oss}	C_{oss} Stored Energy		30		µJ		Fig. 16
E_{ON}	Turn-On Switching Energy (SiC Diode FWD)		133		µJ	V_{DS} = 600 V, V_{GS} = -4 V/15 V, I_D = 35 A, $R_{G(ext)}$ = 2.5Ω, L= 59 µH, T_J = 150°C	Fig. 26, 29b
E_{OFF}	Turn Off Switching Energy (SiC Diode FWD)		111				
E_{ON}	Turn-On Switching Energy (Body Diode FWD)		246		µJ	V_{DS} = 600 V, V_{GS} = -4 V/15 V, I_D = 35 A, $R_{G(ext)}$ = 2.5Ω, L= 59 µH, T_J = 150°C	Fig. 26, 29a
E_{OFF}	Turn Off Switching Energy (Body Diode FWD)		99				
$t_{d(on)}$	Turn-On Delay Time		9		ns	V_{DD} = 600 V, V_{GS} = -4 V/15 V I_D = 35 A, $R_{G(ext)}$ = 2.5 Ω, Timing relative to V_{DS} Inductive load	Fig. 27
t_r	Rise Time		15				
$t_{d(off)}$	Turn-Off Delay Time		24				
t_f	Fall Time		9				
$R_{G(int)}$	Internal Gate Resistance		3		Ω	f = 1 MHz, V_{AC} = 25 mV	
Q_{gs}	Gate to Source Charge		20		nC	V_{DS} = 600 V, V_{GS} = -4 V/15 V I_D = 35 A Per IEC60747-8-4 pg 21	Fig. 12
Q_{gd}	Gate to Drain Charge		26				
Q_g	Total Gate Charge		74				

Reverse Diode Characteristics (T_C = 25˚C unless otherwise specified)

Symbol	Parameter	Typ.	Max.	Unit	Test Conditions	Note
V_{SD}	Diode Forward Voltage	4.5		V	V_{GS} = -4 V, I_{SD} = 17.5 A	Fig. 8, 9, 10
		4.0		V	V_{GS} = -4 V, I_{SD} = 17.5 A, T_J = 150 °C	
I_S	Continuous Diode Forward Current		48	A	V_{GS} = -4 V, T_C = 25 °C	Note 1
$I_{S, pulse}$	Diode pulse Current		200	A	V_{GS} = -4 V, pulse width t_P limited by T_{jmax}	Note 1
t_{rr}	Reverse Recover time	24		ns	V_{GS} = -4 V, I_{SD} = 35 A, V_R = 600 V dif/dt = 3075 A/µs, T_J = 150 °C	Note 1
Q_{rr}	Reverse Recovery Charge	536		nC		
I_{rrm}	Peak Reverse Recovery Current	35		A		

Thermal Characteristics

Symbol	Parameter	Typ.	Max.	Unit	Test Conditions	Note
$R_{\theta JC}$	Thermal Resistance from Junction to Case	0.48	0.52	°C/W		Fig. 21
$R_{\theta JA}$	Thermal Resistance From Junction to Ambient		40			

Typical Performance

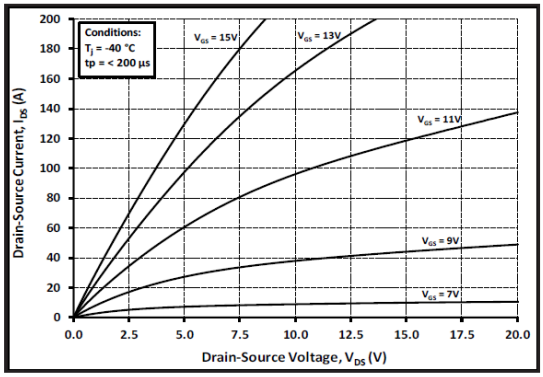

Figure 1. Output Characteristics T_J = -40 °C

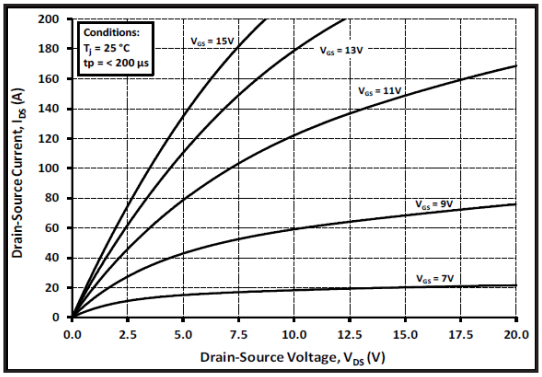

Figure 2. Output Characteristics T_J = 25 °C

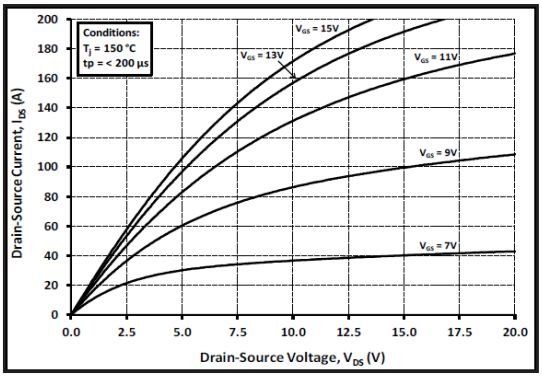

Figure 3. Output Characteristics T_J = 150 °C

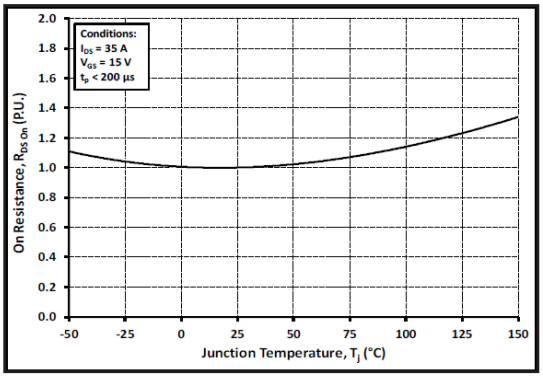

Figure 4. Normalized On-Resistance vs. Temperature

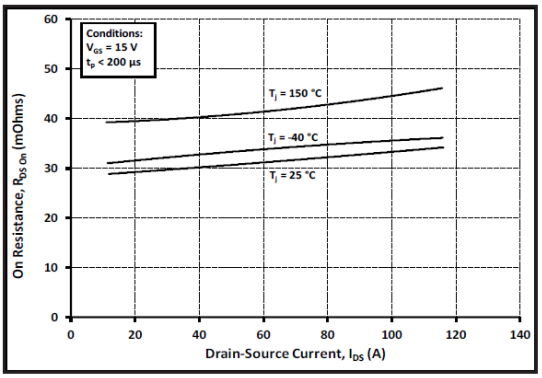

Figure 5. On-Resistance vs. Drain Current
For Various Temperatures

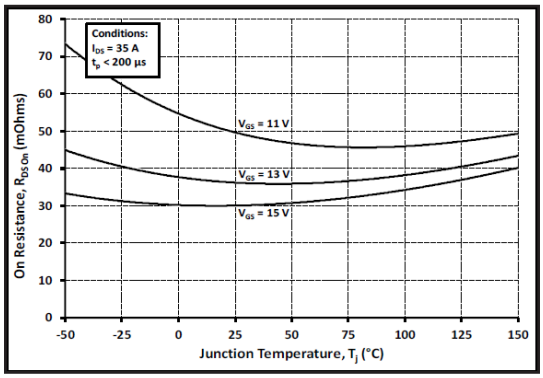

Figure 6. On-Resistance vs. Temperature
For Various Gate Voltage

Typical Performance

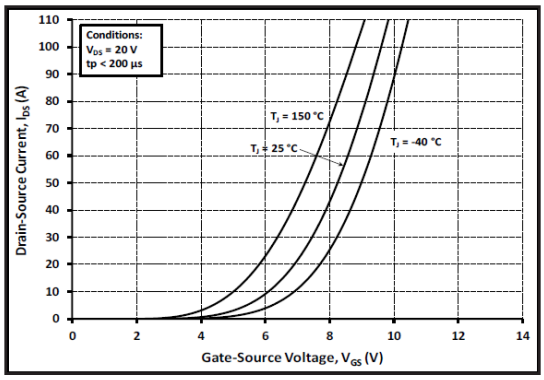

Figure 7. Transfer Characteristic for Various Junction Temperatures

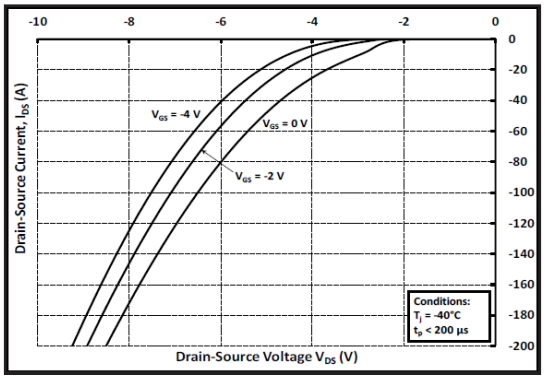

Figure 8. Body Diode Characteristic at -40 °C

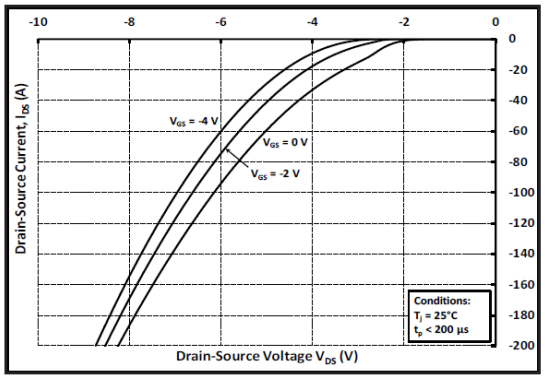

Figure 9. Body Diode Characteristic at 25 °C

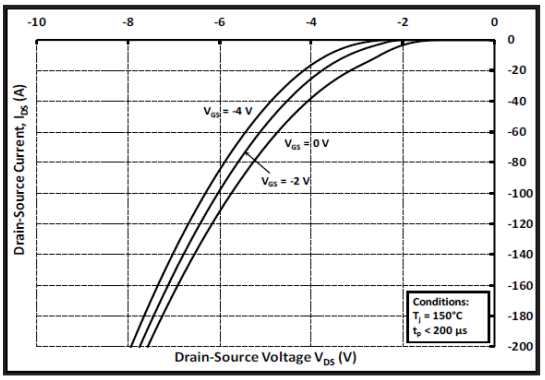

Figure 10. Body Diode Characteristic at 150 °C

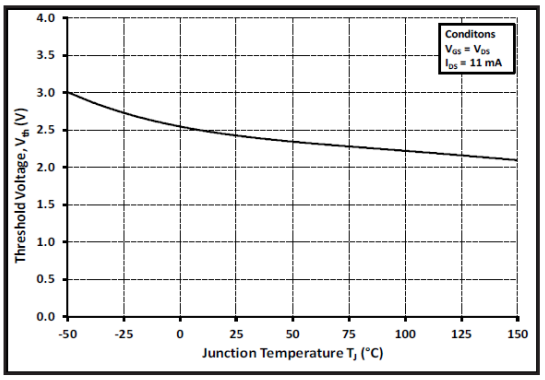

Figure 11. Threshold Voltage vs. Temperature

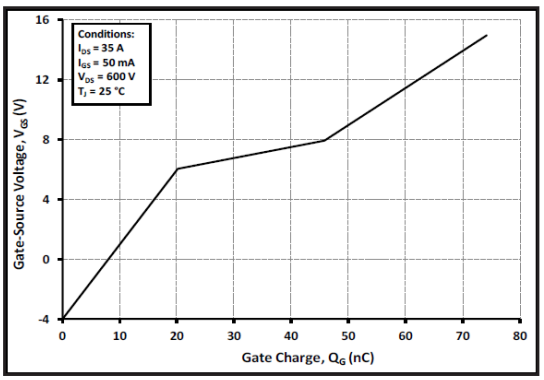

Figure 12. Gate Charge Characteristics

Typical Performance

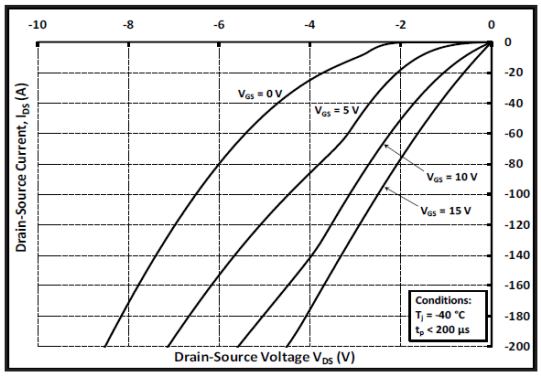

Figure 13. 3rd Quadrant Characteristic at -40 °C

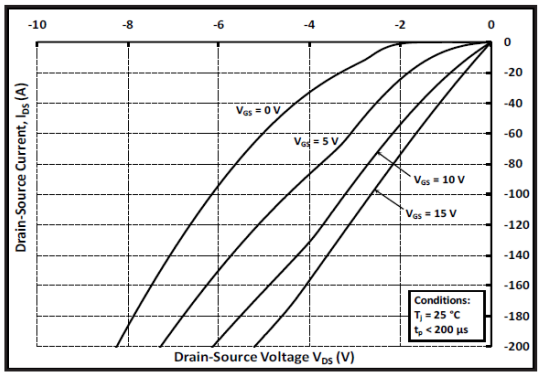

Figure 14. 3rd Quadrant Characteristic at 25 °C

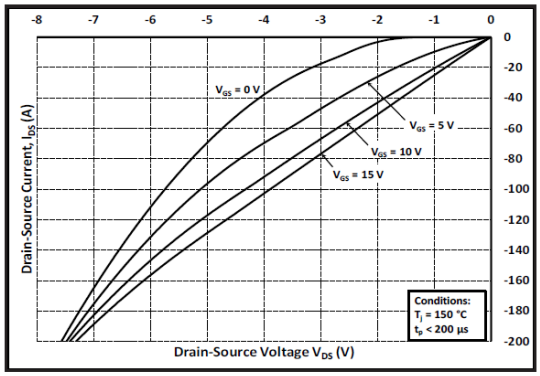

Figure 15. 3rd Quadrant Characteristic at 150 °C

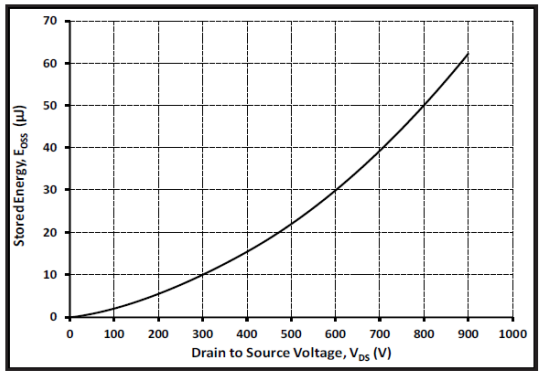

Figure 16. Output Capacitor Stored Energy

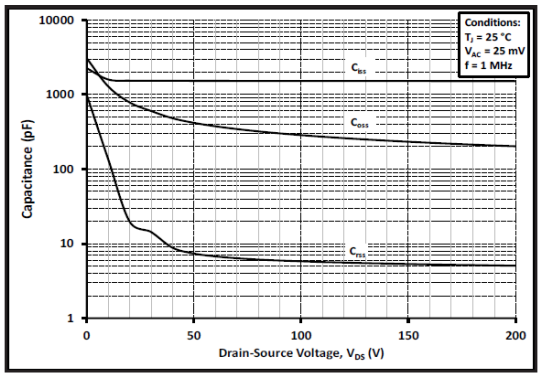

Figure 17. Capacitances vs. Drain-Source Voltage (0 - 200V)

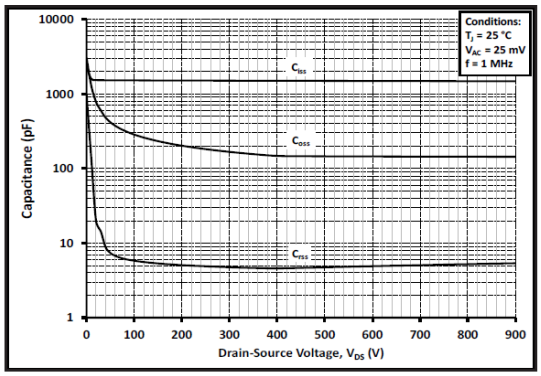

Figure 18. Capacitances vs. Drain-Source Voltage (0 - 900V)

Typical Performance

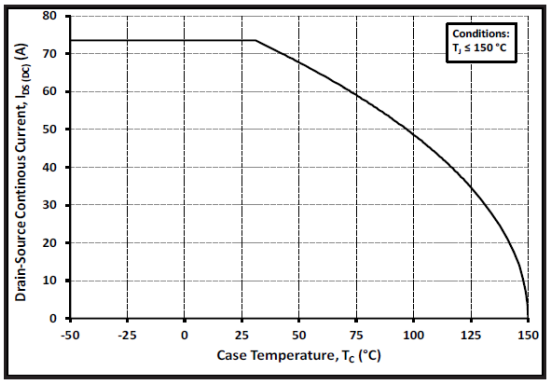

Figure 19. Continuous Drain Current Derating vs. Case Temperature

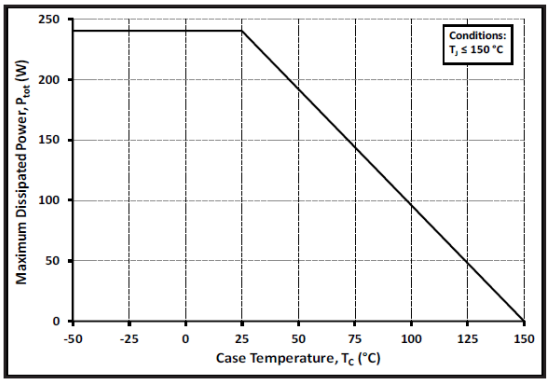

Figure 20. Maximum Power Dissipation Derating vs. Case Temperature

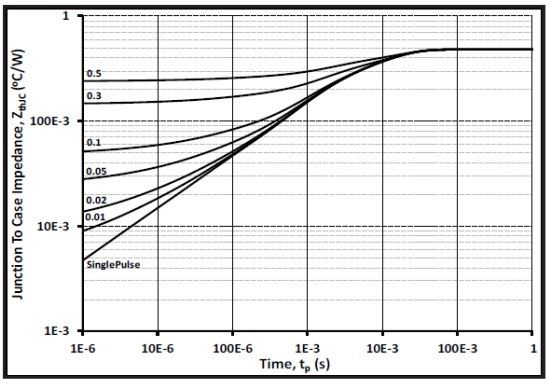

Figure 21. Transient Thermal Impedance (Junction - Case)

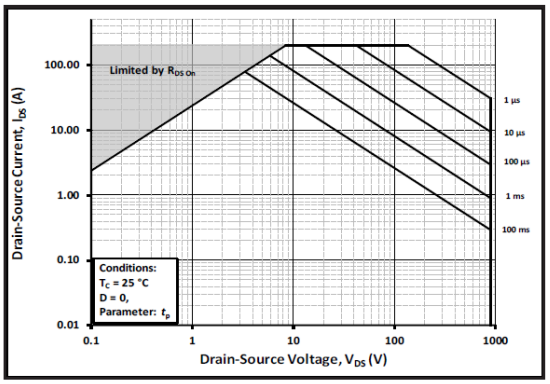

Figure 22. Safe Operating Area

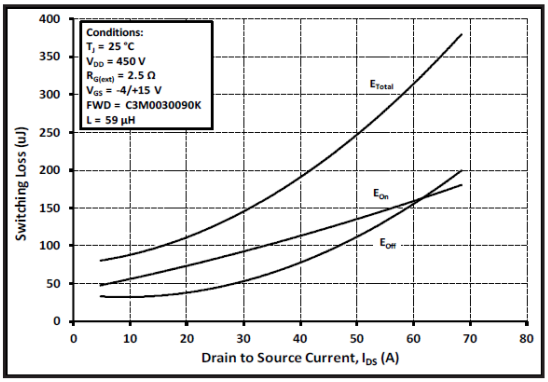

Figure 23. Clamped Inductive Switching Energy vs. Drain Current (V_{DD} = 450V)

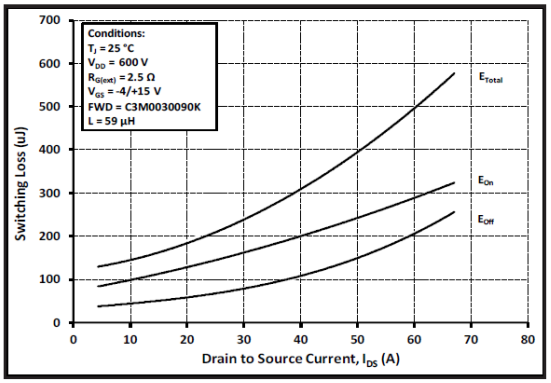

Figure 24. Clamped Inductive Switching Energy vs. Drain Current (V_{DD} = 600V)

Typical Performance

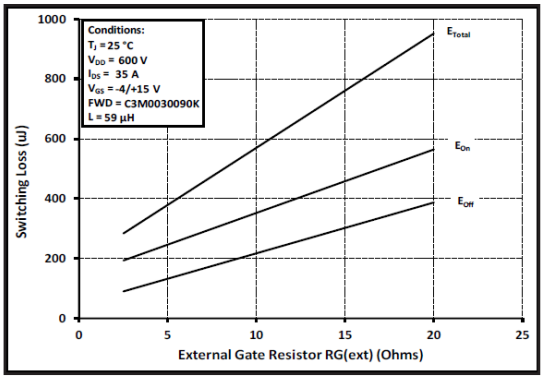

Figure 25. Clamped Inductive Switching Energy vs. $R_{G(ext)}$

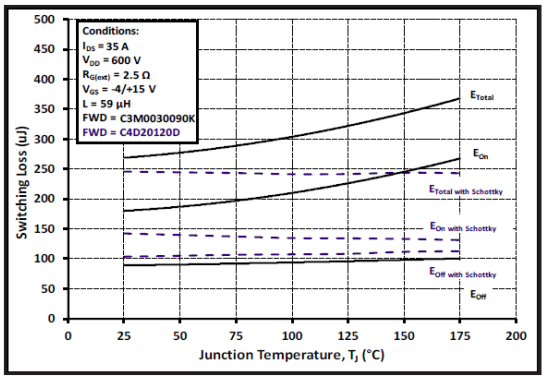

Figure 26. Clamped Inductive Switching Energy vs. Temperature

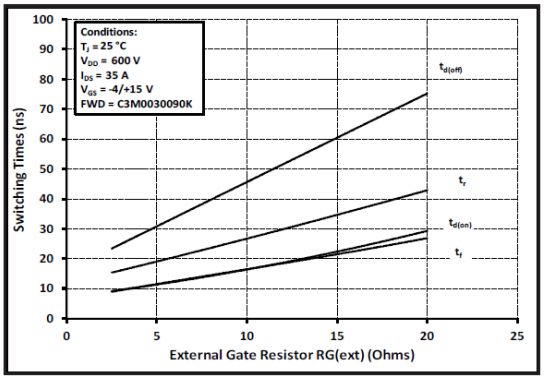

Figure 27. Switching Times vs. $R_{G(ext)}$

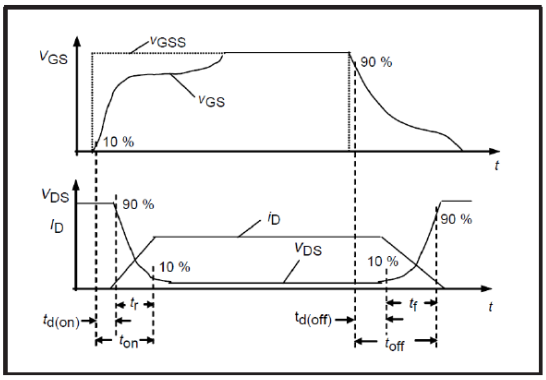

Figure 28. Switching Times Definition

Appendix B [94]

CREE

C3M0016120K

Silicon Carbide Power MOSFET
C3M™ MOSFET Technology

N-Channel Enhancement Mode

V_{DS}	1200 V
$I_{D\ @\ 25^{\circ}C}$	115 A
$R_{DS(on)}$	16 mΩ

Features

- 3rd generation SiC MOSFET technology
- Optimized package with separate driver source pin
- 8mm of creepage distance between drain and source
- High blocking voltage with low on-resistance
- High-speed switching with low capacitances
- Fast intrinsic diode with low reverse recovery (Q_{rr})
- Halogen free, RoHS compliant

Benefits

- Reduce switching losses and minimize gate ringing
- Higher system efficiency
- Reduce cooling requirements
- Increase power density
- Increase system switching frequency

Applications

- Solar inverters
- EV motor drive
- High voltage DC/DC converters
- Switched mode power supplies
- Load switch

Package

Halogen-Free

RoHS

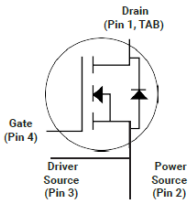

Part Number	Package	Marking
C3M0016120K	TO 247-4	C3M0016120K

Maximum Ratings (T_C = 25 °C unless otherwise specified)

Symbol	Parameter	Value	Unit	Test Conditions	Note
V_{DSmax}	Drain - Source Voltage	1200	V	V_{GS} = 0 V, I_D = 100 µA	
V_{GSmax}	Gate - Source Voltage (dynamic)	-8/+19	V	AC (f >1 Hz)	Note 1
V_{GSop}	Gate - Source Voltage (static)	-4/+15	V	Static	Note 2
I_D	Continuous Drain Current	115	A	V_{GS} = 15 V, T_C = 25°C	Fig. 19
		85		V_{GS} = 15 V, T_C = 100°C	
$I_{D(pulse)}$	Pulsed Drain Current	250	A	Pulse width t_P limited by T_{jmax}	
P_D	Power Dissipation	556	W	T_C=25°C, T_J = 175 °C	Fig. 20
T_J , T_{stg}	Operating Junction and Storage Temperature	-40 to +175	°C		
T_L	Solder Temperature	260	°C	1.6mm (0.063") from case for 10s	

Note (1): When using MOSFET Body Diode V_{GSmax} = -4V/+19V
Note (2): MOSFET can also safely operate at 0/+15 V

CREE

Electrical Characteristics (T_C = 25˚C unless otherwise specified)

Symbol	Parameter	Min.	Typ.	Max.	Unit	Test Conditions	Note
$V_{(BR)DSS}$	Drain-Source Breakdown Voltage	1200			V	V_{GS} = 0 V, I_D = 100 µA	
$V_{GS(th)}$	Gate Threshold Voltage	1.8	2.5	3.6	V	V_{DS} = V_{GS}, I_D = 23 mA	Fig. 11
			2.0		V	V_{DS} = V_{GS}, I_D = 23 mA, T_J = 175ºC	
I_{DSS}	Zero Gate Voltage Drain Current		1	50	µA	V_{DS} = 1200 V, V_{GS} = 0 V	
I_{GSS}	Gate-Source Leakage Current		10	250	nA	V_{GS} = 15 V, V_{DS} = 0 V	
$R_{DS(on)}$	Drain-Source On-State Resistance	11.2	16	22.3	mΩ	V_{GS} = 15 V, I_D = 75 A	Fig. 4, 5, 6
			28.8			V_{GS} = 15 V, I_D = 75 A, T_J = 175ºC	
g_{fs}	Transconductance		53		S	V_{DS}= 20 V, I_{DS}= 75 A	Fig. 7
			47			V_{DS}= 20 V, I_{DS}= 75 A, T_J = 175ºC	
C_{iss}	Input Capacitance		6085		pF	V_{GS} = 0 V, V_{DS} = 1000 V f = 1 MHz V_{AC} = 25 mV	Fig. 17, 18
C_{oss}	Output Capacitance		230				
C_{rss}	Reverse Transfer Capacitance		13				
E_{oss}	C_{oss} Stored Energy		130		µJ		Fig. 16
E_{ON}	Turn-On Switching Energy (SiC Diode FWD)		1.1		mJ	V_{DS} = 800 V, V_{GS} = -4 V/+15 V, I_D = 75 A, $R_{G(ext)}$ = 2.5Ω, L= 65.7 µH, Tj = 175ºC	Fig. 26
E_{OFF}	Turn Off Switching Energy (SiC Diode FWD)		0.8				
E_{ON}	Turn-On Switching Energy (Body Diode FWD)		2.3		mJ	V_{DS} = 800 V, V_{GS} = -4 V/+15 V, I_D = 75 A, $R_{G(ext)}$ = 2.5Ω, L= 65.7 µH, Tj = 175ºC	Fig. 26
E_{OFF}	Turn Off Switching Energy (Body Diode FWD)		0.6				
$t_{d(on)}$	Turn-On Delay Time		34		ns	V_{DD} = 800 V, V_{GS} = -4 V/15 V $R_{G(ext)}$ = 2.5 Ω, I_D = 75 A, L= 65.7 Timing relative to V_{DS}, Inductive load	Fig. 27
t_r	Rise Time		33				
$t_{d(off)}$	Turn-Off Delay Time		65				
t_f	Fall Time		13				
$R_{G(int)}$	Internal Gate Resistance		2.6		Ω	f = 1 MHz, V_{AC} = 25 mV	
Q_{gs}	Gate to Source Charge		67		nC	V_{DS} = 800 V, V_{GS} = -4 V/15 V I_D = 75 A Per IEC60747-8-4 pg 21	Fig. 12
Q_{gd}	Gate to Drain Charge		61				
Q_g	Total Gate Charge		211				

CREE

Reverse Diode Characteristics (T_C = 25˚C unless otherwise specified)

Symbol	Parameter	Typ.	Max.	Unit	Test Conditions	Note
V_{SD}	Diode Forward Voltage	4.6		V	V_{GS} = -4 V, I_{SD} = 37.5 A, T_J = 25 °C	Fig. 8, 9, 10
		4.2		V	V_{GS} = -4 V, I_{SD} = 37.5 A, T_J = 175 °C	
I_S	Continuous Diode Forward Current		112	A	V_{GS} = -4 V, T_C = 25˚C	Note 1
$I_{S,pulse}$	Diode pulse Current		250	A	V_{GS} = -4 V, pulse width t_P limited by T_{jmax}	Note 1
t_{rr}	Reverse Recover time	30		ns	V_{GS} = -4 V, I_{SD} = 75 A, V_R = 800 V dif/dt = 4000 A/µs, T_J = 175 °C	Note 1
Q_{rr}	Reverse Recovery Charge	1238		nC		
I_{rrm}	Peak Reverse Recovery Current	64		A		
t_{rr}	Reverse Recover time	27		ns	V_{GS} = -4 V, I_{SD} = 75 A, V_R = 800 V dif/dt = 5500 A/µs, T_J = 175 °C	Note 1
Q_{rr}	Reverse Recovery Charge	1261		nC		
I_{rrm}	Peak Reverse Recovery Current	77		A		

Thermal Characteristics

Symbol	Parameter	Typ.	Unit	Test Conditions	Note
$R_{\theta JC}$	Thermal Resistance from Junction to Case	0.27	°C/W		Fig. 21
$R_{\theta JA}$	Thermal Resistance From Junction to Ambient	40			

Typical Performance

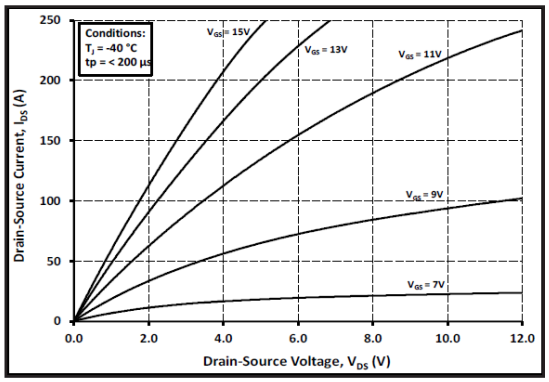

Figure 1. Output Characteristics T_J = -40 °C

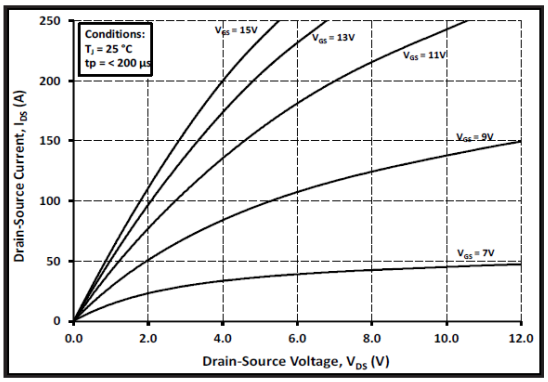

Figure 2. Output Characteristics T_J = 25 °C

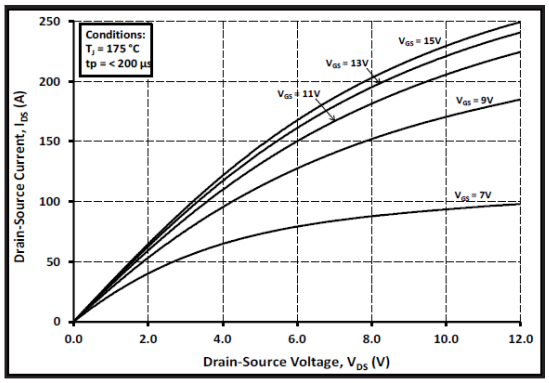

Figure 3. Output Characteristics T_J = 175 °C

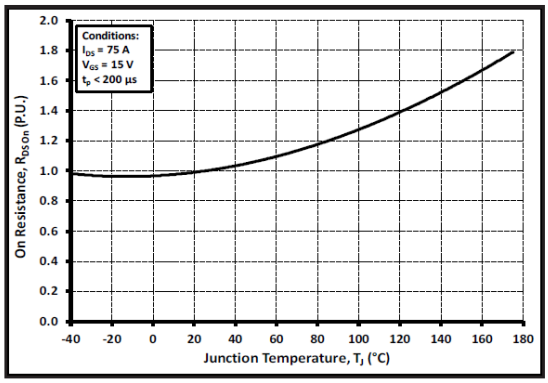

Figure 4. Normalized On-Resistance vs. Temperature

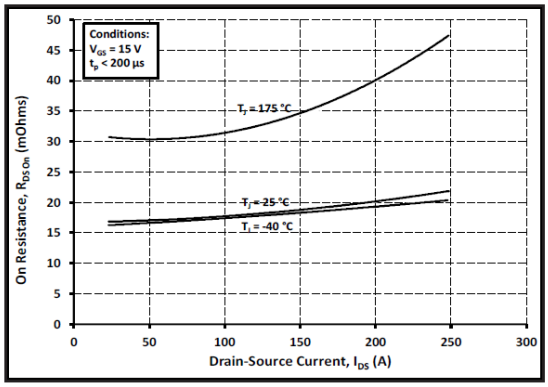

Figure 5. On-Resistance vs. Drain Current
For Various Temperatures

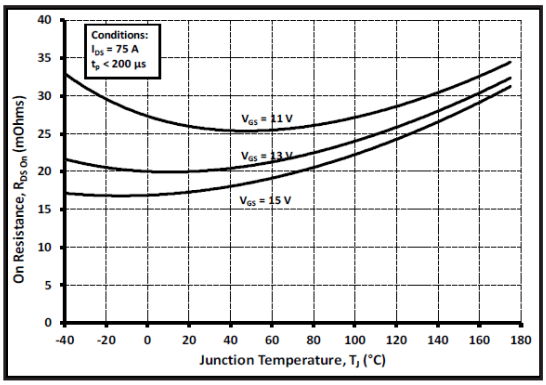

Figure 6. On-Resistance vs. Temperature
For Various Gate Voltage

Typical Performance

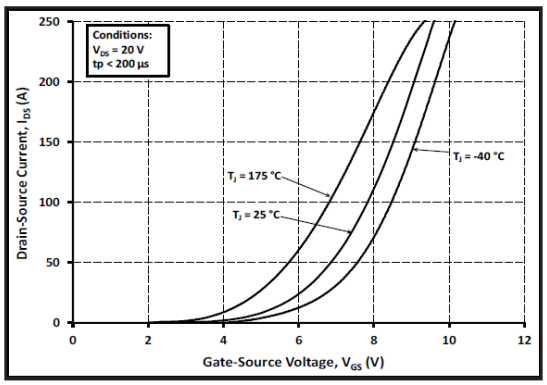

Figure 7. Transfer Characteristic for Various Junction Temperatures

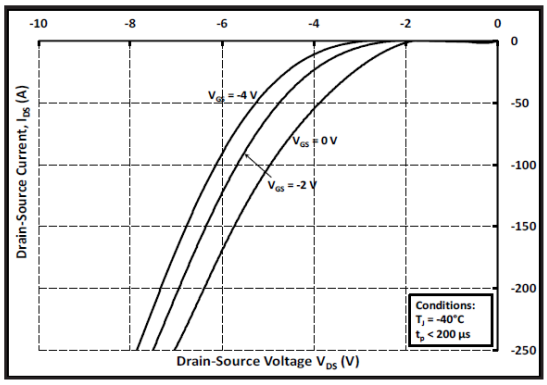

Figure 8. Body Diode Characteristic at -40 °C

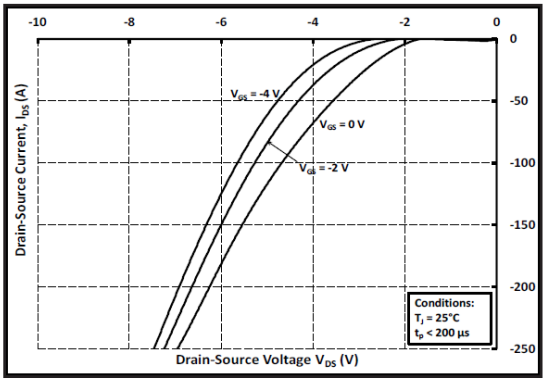

Figure 9. Body Diode Characteristic at 25 °C

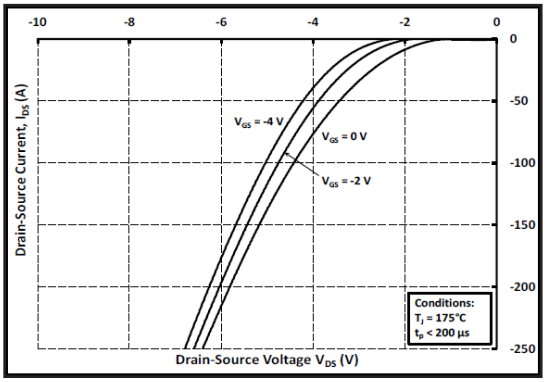

Figure 10. Body Diode Characteristic at 175 °C

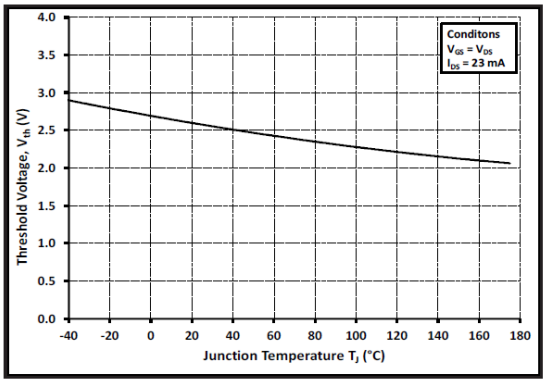

Figure 11. Threshold Voltage vs. Temperature

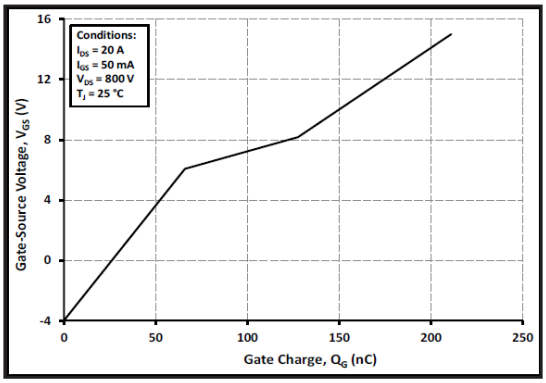

Figure 12. Gate Charge Characteristics

Typical Performance

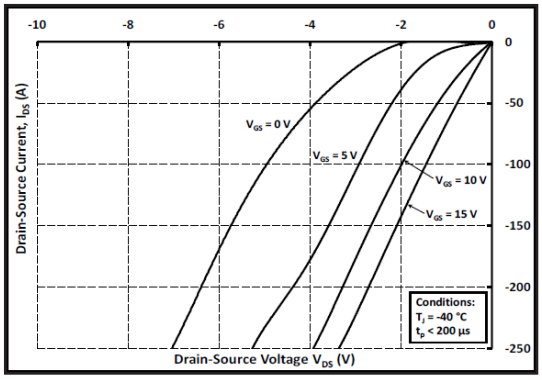

Figure 13. 3rd Quadrant Characteristic at -40 °C

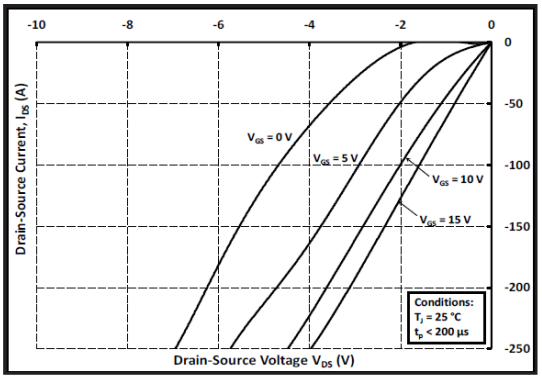

Figure 14. 3rd Quadrant Characteristic at 25 °C

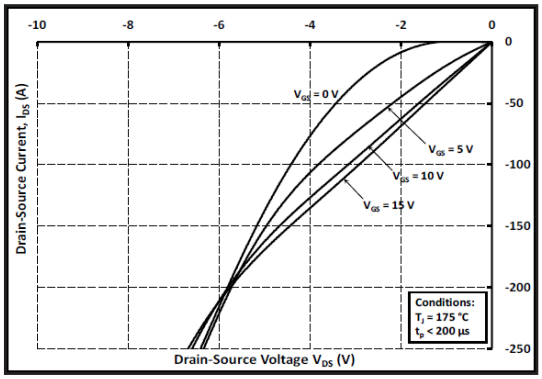

Figure 15. 3rd Quadrant Characteristic at 175 °C

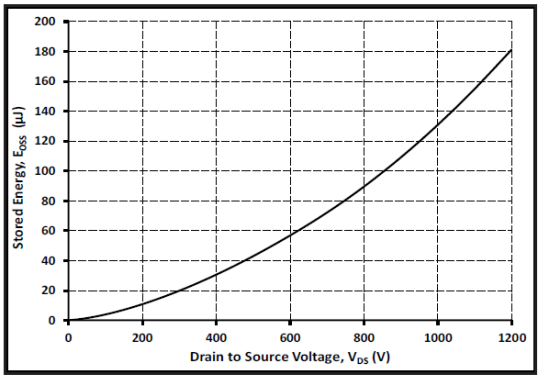

Figure 16. Output Capacitor Stored Energy

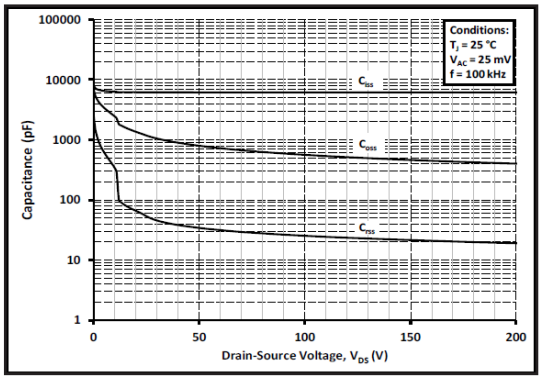

Figure 17. Capacitances vs. Drain-Source Voltage (0 - 200V)

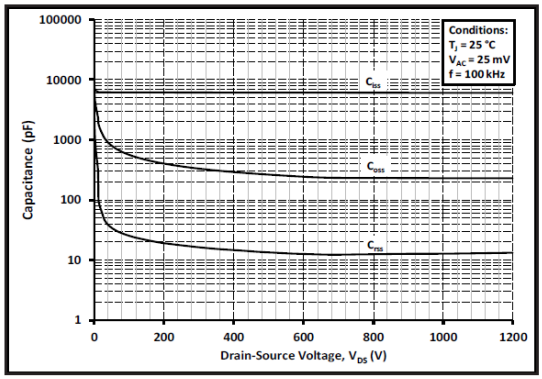

Figure 18. Capacitances vs. Drain-Source Voltage (0 - 1200V)

Typical Performance

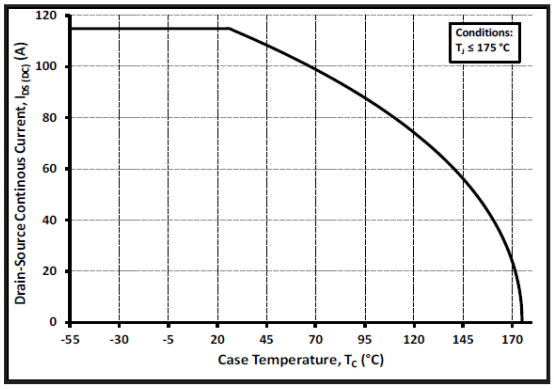

Figure 19. Continuous Drain Current Derating vs. Case Temperature

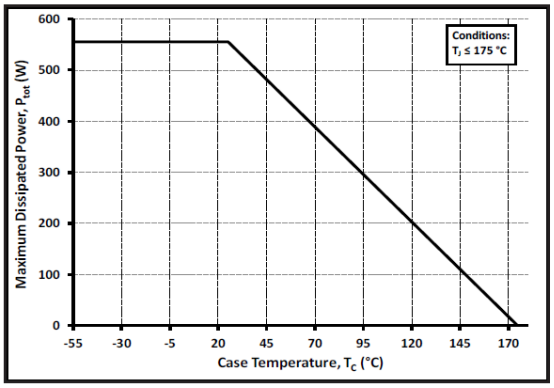

Figure 20. Maximum Power Dissipation Derating vs. Case Temperature

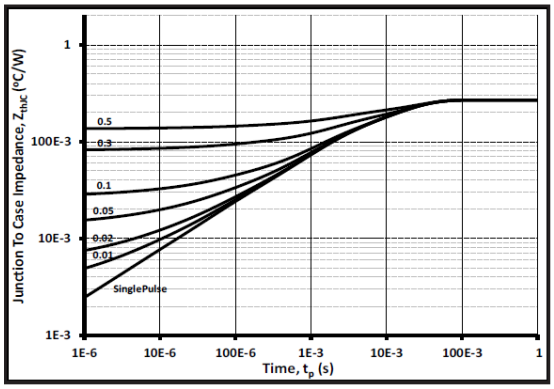

Figure 21. Transient Thermal Impedance (Junction - Case)

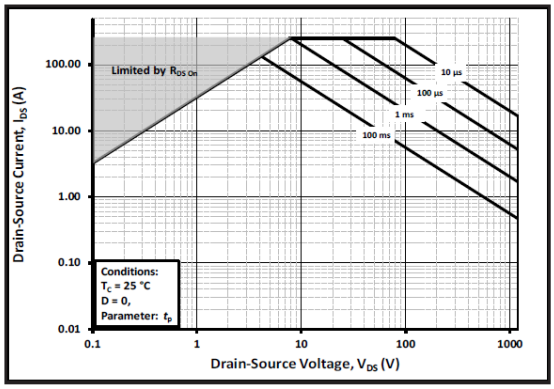

Figure 22. Safe Operating Area

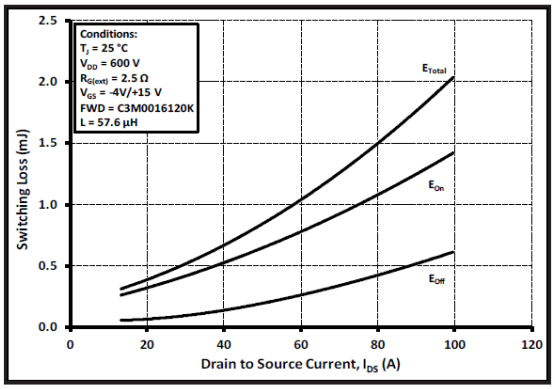

Figure 23. Clamped Inductive Switching Energy vs. Drain Current (V_{DD} = 600V)

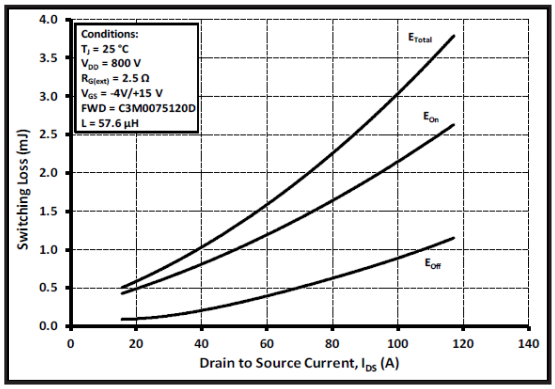

Figure 24. Clamped Inductive Switching Energy vs. Drain Current (V_{DD} = 800V)

Typical Performance

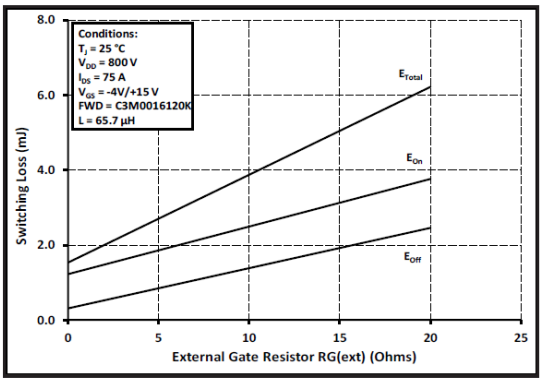

Figure 25. Clamped Inductive Switching Energy vs. $R_{G(ext)}$

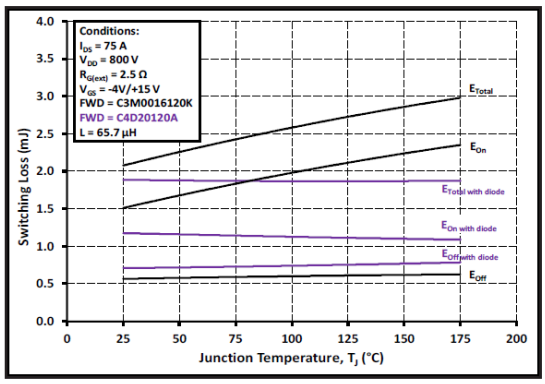

Figure 26. Clamped Inductive Switching Energy vs. Temperature

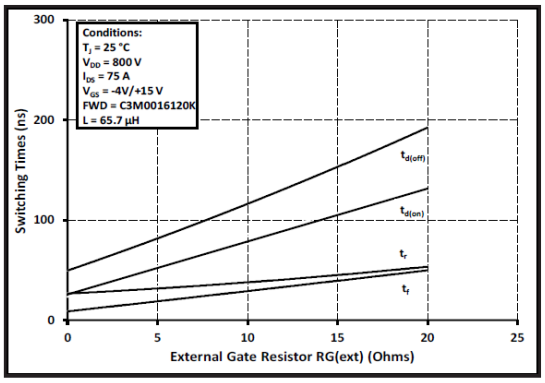

Figure 27. Switching Times vs. $R_{G(ext)}$

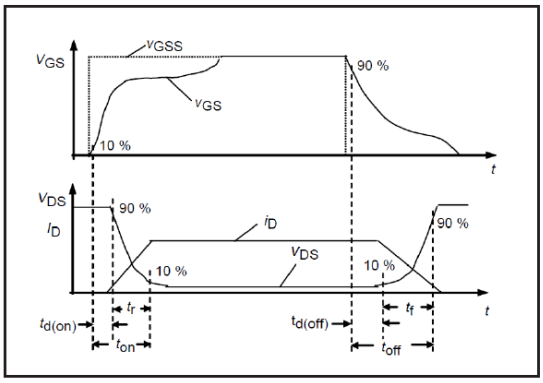

Figure 28. Switching Times Definition

Appendix C

Python: Reading in of switching device capacitances

```
Vo = round(Vo) # Maximum drain-source voltage, interpolation stops here
df = pd.read_csv("Capacitances C3M0090K.csv", encoding="utf-8") # Reading-
in CSV-file from Digitizer tool
V = df["x"]
Ciss = (df["Ciss"] * 10 ** -12).to_numpy() # Adding CSV-values into arrays
Coss = (df["Coss"] * 10 ** -12).to_numpy()
Crss = (df["Crss"] * 10 ** -12).to_numpy()

v1 = list(range(0, Vo + 1, 1)) # Create a voltage range for interpolation
Crss_ip = list()
Coss_ip = list()
Ciss_ip = list()

for i in v1: # Interpolation of values of all CSV files
    Crss_ip.append(np.interp(i, V, Crss))
    Coss_ip.append(np.interp(i, V, Coss))
    Ciss_ip.append(np.interp(i, V, Ciss))
```

Matlab: Reading in of switching device capacitances

```
% Trasistor Capacitance parameters
Vop=round(Vop);
a = csvread('Capacitances C3M0090K.csv',1,0); %Ignores the   header
splita = mat2cell(a,147,1*ones(1,4)); %Splits colums of Matrix into 4
matrices and puts them in 'splita'
V = splita{1,1};
Ciss = splita{1,2}*10^-12;
Coss = splita{1,3}*10^-12;
Crss = splita{1,4}*10^-12;

%% Curve from interporlation
Vds=0:1:Vop;

for i=1:Vop %points calculated every 1V
   Crss_ip(i)=interp1(V,Crss,i-1);
   Coss_ip(i)=interp1(V,Coss,i-1);
   Ciss_ip(i)=interp1(V,Ciss,i-1);
end
```

Appendix D

Python: the converter model

```
import math
from turnOnLosses_model1 import turnOnLossesC3M0090K_model1 ,
turnOnLossesC3M001620KK_model1
from turnOffLosses_model1 import turnOffLossesC3M0090K_model1,
turnOffLossesC3M001620KK_model1
from turnOnLosses_model3 import turnOnLossesC3M0090K_model3_Prim,
turnOnLossesC3M001620KK_model3_Sec, turnOnLossesC3M0090K_model3_Sec
from turnOffLosses_model3 import turnOffLossesC3M0090K_model3_Prim,
turnOffLossesC3M001620KK_model3_Sec, turnOffLossesC3M0090K_model3_Sec
from turnOffLosses_model2 import turnOffLossesC3M0090K_model2,
turnOffLossesC3M001620KK_model2
from turnOnLosses_model2 import turnOnLossesC3M0090K_model2,
turnOnLossesC3M001620KK_model2
import scipy.optimize
import scipy.integrate

'''
-------------------------------------------------------
Code to simulate switching losses in an isolated DAB converter
-------------------------------------------------------
'''

def ModelConverter(turnOnModelPrimary, turnOnModelSecondary ,
turnOffModelPrimary, turnOffModelSecondary, printlosses, v_out, p_out,
checkOutput):

    '''
    :param turnOnModelPrimary: Name of model which determines switching
losses of primary switches during turn-on.
    :param turnOnModelSecondary: Name of model which determines switching
losses of primary switches during turn-on.
    :param turnOffModelPrimary: Name of model which determines switching
losses of primary switches during turn-on.
    :param turnOffModelSecondary: Name of model which determines switching
losses of primary switches during turn-on.
    :param v_out: Output voltage
    :param p_out: Output power
    :param checkOutput: True if output power of converter needs to be
limited by this model.
    :return: Array's with the losses
    '''

    '''
    Parameter input
    ---------------
    '''
    p_max = 10000  # W, Maximum output power
    vn_out = 800 # V, Nominal Dc-output power of converter
    v_in = 400 # V, DC-input voltage of converter
    fs = 50000  # Hz, Switching Frequency of MOSFETs
    i_out = p_out/v_out # DC-output current
    lLeak = 25.4981E-6  # H, Leakage inductance of transformer
    lMag = 1.6E-3  # H, Magnitizing inductance of transformer
    n = 107 / 50  # winding ratio of transfomer
    aux = 1  # Indicates that output power can not be achieved due to too
high phi_c
```

```
            # Should normally not be used since output power will always
be limited to Pmax if checkOutput is True
    rsp_on = 30E-3  # Ohm, On resistance for primary side switches
    rss_on = 16E-3  # Ohm, On resistance for secondary side switches
    rsp_tf = 70E-3  # Ohm, Transformer primary winding resistance
    Alpha = 0 # Steinmetz coefficiënt of transformer
    Beta = 0 # Steinmetz coefficiënt of transformer
    k = 0 # Steinmetz constant of transformer
    Ta = 25 # °C, starting temperature converter
    Rth_HS = 0.4 # °C/W, heat sink surface convection coefficient
    Rth_JC_p = 0.62 # °C/W, heat conduction coefficient for junction of
primary MOSFET
    Rth_JC_s = 0.27 # °C/W, heat conduction coefficient for junction of
secondary
    Rth_tp = 1.1 # °C/W
    Atf = -1 # m², Cross section of transformer core
    '''
    Calculating and limiting output power
    -------------------------
    '''

    p_out = v_out * i_out
    if checkOutput: # Limits output power to p_max and adjusts output
current
        if p_out > p_max:
            p_out = p_max
            i_out = p_max / v_out # Limits output power
            print("Current is limited so power does not surpass ", p_max, "
W")
        print("Output voltage = ", v_out, " V")
        print("Output current = ", i_out, " A")
        print("Output power = ", p_out/1000, " kW")
    '''
    Calculating phase shift between both bridges
    -------------------------------------------
    '''
    ws = 2 * math.pi * fs
    # Calculating phase shift
    sol = scipy.optimize.fsolve(lambda phi_c:
(v_in*(v_out/n))/(ws*lLeak)*(phi_c*(1-phi_c/math.pi))-p_out, 0)
    for solution in sol:
        if solution < 0 or solution > math.pi/2:
            del solution
    if not sol:
        phi_r2 = math.pi/2
        aux = 0
    else:
        phi_r2 = sol[0]
    print("Phi = ", round(phi_r2*360/(2*math.pi), 3))
    print("Phi_u = ", round(phi_r2/(2*math.pi), 3))

    # Calculating Ip and Il
    ip_phi = aux*(2*v_in*phi_r2+math.pi*(v_out/n-v_in))/(2*ws*lLeak)
    is_phi = aux*ip_phi/n
    ip_pi = aux*(v_in-v_out/n)*(math.pi-phi_r2)/(ws*lLeak)+ip_phi
    is_pi = aux*ip_pi
    print("Ip = ", ip_phi, " A")
    print("Il = ", ip_pi, " A")

    '''
    Conduction Losses
```

```
    -----------------
    '''
    # Calculating RMS-currents in AC-link
    d = v_out/vn_out
    irms_i = aux*(v_in/(ws*lLeak))*((1/(3*math.pi))*((math.pi**3*d**2)/4 -
2*d*phi_r2**3 + 3*math.pi*d*phi_r2**2-(math.pi**3*d)/2 +
math.pi**3/4))**0.5 # Primary side RMS current.
    isp_rms = aux*irms_i/math.sqrt(2) # Actual RMS current at the primary
side switches
    iss_rms = isp_rms/n # Actual RMS current at the secondary side switches

    # Calculating Conduction losses
    print("Primary effective Current = ", round(isp_rms, 2), " A")
    print("Primary RMS Current = ", round(irms_i, 2), " A")
    psp_cond = 4*rsp_on*(isp_rms**2) # Conduction losses at primary side
    pss_cond = 4*rss_on*(iss_rms**2) # Conduction losses at secondary side
    psps_cond = psp_cond+pss_cond # Total conduction losses

    '''
    Transformer Losses
    ----------------
    '''

    Bmax = irms_i * rsp_tf / (4.44 * fs * n * Atf)
    ki = k / (2 * math.pi) ** (Alpha - 1) * \
         scipy.integrate.quad(lambda x: abs(math.cos(x)) ** Alpha * 2 **
(Beta - Alpha), 0, 2 * math.pi)[
             0]  # Deciding k-factor for DAB AC-current
    ptf_iron = Atf * ki * fs * abs(4 * Bmax) ** Alpha * abs(2 * Bmax) **
(Beta - Alpha)  # Transformer iron losses
    ptf_cond = (irms_i) ** 2 * rsp_tf  # Transformer conduction losses
    ptf = ptf_cond + ptf_iron  # Total transformer losses

    '''
    Switching Losses
    ----------------
    '''
    # Hard off-switching will always occur, ZVS or not
    psp_switch_off = float(4 * turnOffModelPrimary(v_in, abs(ip_pi), fs)) #
Turn-Off switching losses for primary switches
    pss_switch_off = float(4 * turnOffModelSecondary(n*v_in*d, abs(is_pi),
fs)) # Turn-Off switching losses for secondary switches

    # Checking for zero voltage conditions
    if ip_phi > 0 and ip_pi > 0: #ZVS at both bridges
        print('ZVS at both bridges')
        psp_switch_on = 0
        pss_switch_on = 0

    else:
        if ip_pi > 0: #ZVS only at primary bridge
            print('ZVS at primary bridge')
            psp_switch_on = 0
            pss_switch_on = 4 * turnOnModelSecondary(n*v_in*d, abs(is_phi),
fs)

        else: #ZVS only at secundary bridge
            print('ZVS at secundary bridge')
            psp_switch_on = 4 * turnOnModelPrimary(v_in, abs(ip_phi), fs)
            pss_switch_on = 0
```

```
    # Calculate and print all total losses and efficiency
    pswt_p = psp_switch_off + psp_switch_on
    pswt_s = pss_switch_off + pss_switch_on
    psw_tot = pswt_p + pswt_s
    psp = pswt_p + psp_cond
    pss = pswt_s + pss_cond
    ploss_tot = psp + pss
    eff = p_out / (p_out + psp+ pss + ptf)

    if printlosses:
        print('-------------------------')
        print('Primary Turn-On losses = ', round(psp_switch_on, 2), ' W')
        print('Primary Turn-Off losses = ', round(psp_switch_off, 2), ' W')
        print('Secondary switching losses = ', round(pswt_s, 2), ' W')
        print('Primary conduction losses = ', round(psp_cond, 2), ' W')
        print('Secondary conduction losses = ', round(pss_cond, 2), ' W')
        print('Transformer conduction losses = ', round(ptf_cond, 2), ' W')
        print('Transformer iron losses = ', round(ptf_iron, 2), ' W')
        print('Total switching losses = ', round(psw_tot, 2), ' W')
        print('Total conduction losses = ', round(psp_cond+pss_cond, 2), '
W')
        print('Total transformer losses = ', round(ptf, 2), ' W')
        print('Total losses = ', round(ploss_tot, 2), ' W')
        print('Total efficiency = ', round(eff, 2), ' W')

    # Eventual temperature of MOSFETs and additional Heat sinks
    Ts_p = Ta + psp*Rth_HS # Heat Sink surface temperature
    Tj_p = Ts_p + psp/4*(Rth_JC_p+Rth_tp) # Temperature heat sink at MOSFET
junction
    Tc_p = Ts_p + psp/4*Rth_tp # Temperature of MOSFET

    if printlosses:
        print('-------------------------')
        print('Heat Sink surface temperature = ' , Ts_p, ' °C')
        print('MOSFET surface temperature = ' , Tc_p, ' °C')
        print('MOSFET junction temperature = ' , Tj_p, ' °C')
        print("*************************")

    return i_out, psp_switch_on, psp_switch_off, pss_switch_on,
pss_switch_off, psp_cond, pss_cond, ptf_cond, ptf_iron, Ts_p, Tc_p, Tj_p
```

Appendix E

Python: the model for the operating range

```
import pandas as pd
import numpy as np
import matplotlib.pyplot as plt
from matplotlib import cm
from modelConverter import ModelConverter
from turnOnLosses_model1 import turnOnLossesC3M0090K_model1 ,
turnOnLossesC3M001620KK_model1
from turnOffLosses_model1 import turnOffLossesC3M0090K_model1,
turnOffLossesC3M001620KK_model1
from turnOnLosses_model3 import turnOnLossesC3M0090K_model3_Prim,
turnOnLossesC3M001620KK_model3_Sec, turnOnLossesC3M0090K_model3_Sec
from turnOffLosses_model3 import turnOffLossesC3M0090K_model3_Prim,
turnOffLossesC3M001620KK_model3_Sec, turnOffLossesC3M0090K_model3_Sec
from turnOffLosses_model2 import turnOffLossesC3M0090K_model2,
turnOffLossesC3M001620KK_model2
from turnOnLosses_model2 import turnOnLossesC3M0090K_model2,
turnOnLossesC3M001620KK_model2

'''
------------------------------------------------------------------------
------------
Code to simulate DAB losses in an isolated DAB converter over its entire
operating range
------------------------------------------------------------------------
-------------
'''

# First some General function used to get/export information or plot it in
3D graphs
def isAlreadyInList(list, value):
    solution = False
    for i in list:
        if i == value:
            solution = True
    return solution

def plotSurface(xi, yi, zi, Xlabel, Ylabel, Zlabel, title,
amountCurrentTest, amountVoltageTest):

    x = list()
    y = list()
    z = list()

    for c in range(amountVoltageTest):
        for f in range(amountCurrentTest):
            y.append(yi[c][f])
            x.append(xi[c])
            z.append(zi[c][f])

    x = np.reshape(x, (amountVoltageTest, amountCurrentTest))
    y = np.reshape(y, (amountVoltageTest, amountCurrentTest))
    z = np.reshape(z, (amountVoltageTest, amountCurrentTest))
```

```
    x = x.astype(np.float)
    y = y.astype(np.float)
    z = z.astype(np.float)

    fig = plt.figure(figsize=[12, 8])
    ax = fig.gca(projection='3d')  # Set up axis from 3D plot
    ax.plot_surface(x, y, z, cmap=cm.coolwarm)
    ax.set_xlabel(Xlabel)
    ax.set_ylabel(Ylabel)
    ax.set_zlabel(Zlabel)
    plt.title(title)
    plt.show()

def plotSurfaceDifference(xi, yi, z1, z2, Xlabel, Ylabel, Zlabel, title,
amountCurrentTest, amountVoltageTest):

    x = list()
    y = list()
    z = list()

    for c in range(amountVoltageTest):
        for f in range(amountCurrentTest):
            y.append(yi[c][f])
            x.append(xi[c])
            z.append(z1[c][f]-z2[c][f])

    x = np.reshape(x, (amountVoltageTest, amountCurrentTest))
    y = np.reshape(y, (amountVoltageTest, amountCurrentTest))
    z = np.reshape(z, (amountVoltageTest, amountCurrentTest))
    x = x.astype(np.float)
    y = y.astype(np.float)
    z = z.astype(np.float)

    fig = plt.figure(figsize=[12, 8])
    ax = fig.gca(projection='3d')  # Set up axis from 3D plot
    ax.plot_surface(x, y, z, cmap=cm.coolwarm)
    ax.set_xlabel(Xlabel)
    ax.set_ylabel(Ylabel)
    ax.set_zlabel(Zlabel)
    plt.title(title)
    plt.show()

def exportData(xi, yi, z1, amountCurrentTest, amountVoltageTest, path):

    x = list()
    y = list()
    z = list()

    for c in range(amountVoltageTest):
        for f in range(amountCurrentTest):
            y.append(yi[c][f])
            x.append(xi[c])
            z.append(z1[c][f])

    x = np.reshape(x, (amountVoltageTest, amountCurrentTest))
    y = np.reshape(y, (amountVoltageTest, amountCurrentTest))
    z = np.reshape(z, (amountVoltageTest, amountCurrentTest))
```

```
    x = x.astype(np.float)

    df = pd.DataFrame(z)
    df.to_csv(path, index=False, header=False)

def OperatingRangetest(turnOnModelPrimary, turnOnModelSecondary ,
turnOffModelPrimary, turnOffModelSecondary, plotGraphs):
    '''
    :param turnOnModelPrimary: Name of the model which calculates the turn-
on losses in the primary bridge
    :param turnOnModelSecondary: Name of the model which calculates the
turn-on losses in the secondary bridge
    :param turnOffModelPrimary: Name of the model which calculates the
turn-off losses in the primary bridge
    :param turnOffModelSecondary: Name of the model which calculates the
turn-off losses in the secondary bridge
    :param plotGraphs: True if all 3D-plots need to be plotted.
    :return: True if completed succesfull
    '''

    '''
    Parameter input
    ---------------
    '''
    # Don't forget to specify all specifics of the converter in the
converter model!
    vn_out = 800 # V, nominal output voltage, must be the same as in the
converter model!
    p_max = 10000 # W, maximum output power, must be the same as in the
converter model!
    test = 8  # Number of voltage levels which need to be tested
    io = [1.5, 1.71, 2, 6, 7.87, 8.5, 9, 11.33, 12]  # List of possible
output currents
    d = list(np.linspace(0.25, 1.125, 8))  # List of factors d =
V_out/Vn_out

    '''
    Estimation of losses in operating range
    ---------------------------------------
    '''
    # Creating array with all output voltages
    v_out = np.multiply(d, vn_out)  # List of possible output voltages
    # Creating array with lists as elements: for each voltage, each current
is tested if possible.
    i_out = [[0] * len(io) for _ in range(test)]
    for a in range(test):
        for b in range(len(io)):
         i_out[a][b]=io[b]

    # Creating empty arrays
    p_out = [[0] * len(io) for _ in range(test)] # Output power in Watts
    phi_r2 = [[0] * len(io) for _ in range(test)] # Phase-shift in radials
    ip_phi = [[0] * len(io) for _ in range(test)] # Ip primary current,
Ampère
    is_phi = [[0] * len(io) for _ in range(test)] # IL primary current,
Ampère
    ip_pi = [[0] * len(io) for _ in range(test)] # Ip secondary current,
```

```
Ampère
    is_pi = [[0] * len(io) for _ in range(test)] # IL secondary current,
Ampère
    irms_i = [[0] * len(io) for _ in range(test)] # Primary RMS-current,
Ampère
    isp_rms = [[0] * len(io) for _ in range(test)] # Primary RMS-current
for a single MOSFET, Ampère
    iss_rms = [[0] * len(io) for _ in range(test)] # Secondary RMS-current
for a single MOSFET, Ampère
    psp_cond = [[0] * len(io) for _ in range(test)] # Total MOSFET
conduction losses in primary, Watts
    pss_cond = [[0] * len(io) for _ in range(test)] # Total MOSFET
conduction losses in secondary, Watts
    psps_cond = [[0] * len(io) for _ in range(test)] # Total MOSFET
conduction losses, Watts
    psp_switch_off = [[0] * len(io) for _ in range(test)] # Total MOSFET
turn-off losses in primary, Watts
    pss_switch_off = [[0] * len(io) for _ in range(test)] # Total MOSFET
turn-off losses in secondary, Watts
    psp_switch_on = [[0] * len(io) for _ in range(test)] # Total MOSFET
turn-on losses in primary, Watts
    pss_switch_on = [[0] * len(io) for _ in range(test)] # Total MOSFET
turn-on losses in primary, Watts
    pswt_p = [[0] * len(io) for _ in range(test)] # Total MOSFET switching
losses in primary, Watts
    pswt_s = [[0] * len(io) for _ in range(test)] # Total MOSFET switching
losses in secondary, Watts
    psw_tot = [[0] * len(io) for _ in range(test)] # Total MOSFET switching
losses, Watts
    psp = [[0] * len(io) for _ in range(test)] # Total MOSFET losses in
primary, Watts
    pss = [[0] * len(io) for _ in range(test)] # Total MOSFET losses in
secondary, Watts
    plossMOSFET_tot = [[0] * len(io) for _ in range(test)] # Total MOSFET
losses, Watts
    eff = [[0] * len(io) for _ in range(test)] # Total efficiency
    ptf_cond = [[0] * len(io) for _ in range(test)] # Total transformer
conduction losses, Watts
    ptf_iron = [[0] * len(io) for _ in range(test)] # Total transformer
iron losses, Watts
    p_tf = [[0] * len(io) for _ in range(test)] # Total transformer losses,
Watts
    Ts_p = [[0] * len(io) for _ in range(test)] # Temperature heat sink
    Tc_p = [[0] * len(io) for _ in range(test)] # Temperature heat sink-
MOSFET junction
    Tj_p = [[0] * len(io) for _ in range(test)] # Temperature MOSFET

    # Limiting of output power and eliminating unecessary tests
    for j in range(0, test):
        print("**************************")
        d[j] = d[j] # This adjustment is required considering that to
generate vector d, n was not considered altering the solutions for the
power equation
        p_out[j] = np.multiply(i_out[j],v_out[j])
        print("Test Number: ", j + 1)
        print("Output voltage = ", v_out[j])
        print("**************************")
```

```
        '''
        Calculating phase shift between both bridges
        ----------------------------------------------
        '''

        for i in range(0,len(p_out[j])):
            dontPrint = False
            print("Current Test Number: ", i+1)
            print("Output Power = ", p_out[j][i])
            if p_out[j][i] > p_max:
                print("Power has to be limited to ", p_max/1000, "kW, so
current will be reduced.")
                p_out[j][i] = p_max
                if isAlreadyInList(i_out[j], p_max / v_out[j]):
                    dontPrint = True
                i_out[j][i] = p_max / v_out[j]
                if not dontPrint:
                    print("Output Current = ", i_out[j][i])
                else:
                    print("Same as previous test.")
            else:
                print("Output Current = ", i_out[j][i])

            # Put all losses in arrays with lists
            i_out[j][i], psp_switch_on[j][i], psp_switch_off[j][i],
pss_switch_on[j][i], pss_switch_off[j][i], psp_cond[j][i], pss_cond[j][i],
\
            ptf_cond[j][i], ptf_iron[j][i], Ts_p[j][i], Tc_p[j][i],
Tj_p[j][i] = ModelConverter(turnOnModelPrimary,

turnOnModelSecondary,

turnOffModelPrimary,

turnOffModelSecondary,

False, v_out[j], p_out[j][i],

False)
            # Add some of the losses and calculate efficiency
            pswt_p[j][i] = psp_switch_off[j][i] + psp_switch_on[j][i]
            pswt_s[j][i] = pss_switch_on[j][i] + pss_switch_off[j][i]
            psw_tot[j][i] = pswt_p[j][i] + pswt_s[j][i]
            psps_cond[j][i] = psp_cond[j][i] + pss_cond[j][i]
            psp[j][i] = pswt_p[j][i] + psp_cond[j][i]
            pss[j][i] = pswt_s[j][i] + pss_cond[j][i]
            plossMOSFET_tot[j][i] = psp[j][i] + pss[j][i]
            p_tf[j][i] = ptf_iron[j][i] + ptf_cond[j][i]
            eff[j][i] = p_out[j][i] / (p_out[j][i] + psp[j][i] + pss[j][i]
+ p_tf[j][i])

    '''
    Plot results in plots
    -----------------
    '''

    if plotGraphs:
```

```
        plotSurface(v_out, i_out, psps_cond, 'Voltage (V)', 'Current (A)',
'Conduction Losses (W)',
                    'Total Conduction Losses', len(io), len(v_out))
        plotSurface(v_out, i_out, eff, 'Voltage (V)', 'Current (A)',
'Efficiency', 'Total efficiency of the Converter', len(io),
                    len(v_out))
        plotSurface(v_out, i_out, pswt_p, 'Voltage (V)', 'Current (A)',
'Switching Losses (W)',
                    'Total Switching Losses on Primary Side', len(io),
len(v_out))
        plotSurface(v_out, i_out, pswt_s, 'Voltage (V)', 'Current (A)',
'Switching Losses (W)',
                    'Total Switching Losses on Secondary Side', len(io),
len(v_out))
        plotSurface(v_out, i_out, psw_tot, 'Voltage (V)', 'Current (A)',
'Switching Losses (W)',
                    'Total Switching Losses of the Converter', len(io),
len(v_out))
        plotSurface(v_out, i_out, plossMOSFET_tot, 'Voltage (V)', 'Current
(A)', 'Switching Losses (W)',
                    'Total MOSFET Losses of the Converter', len(io),
len(v_out))
        plotSurface(v_out, p_out, eff, 'Voltage (V)', 'Power (W)',
'Efficiency',
                    'Total efficiency of the Converter', len(io),
len(v_out))


    '''
    Export data
    -----------
    '''
    exportData(v_out, i_out, eff, len(i_out[-1]), len(v_out),
               r'C:\Users\Jaan Wouters\Desktop\Efficiency.csv')
    exportData(v_out, i_out, psp_switch_on, len(i_out[-1]), len(v_out),
               r'C:\Users\Jaan Wouters\Desktop\TurnOnLossesPrimary.csv')
    exportData(v_out, i_out, psp_switch_off, len(i_out[-1]), len(v_out),
               r'C:\Users\Jaan Wouters\Desktop\TurnOffLossesPrimary.csv')
    exportData(v_out, i_out, psp_cond, len(i_out[-1]), len(v_out),
               r'C:\Users\Jaan Wouters\Desktop\ConductionPrimary.csv')
    exportData(v_out, i_out, pss_cond, len(i_out[-1]), len(v_out),
               r'C:\Users\Jaan Wouters\Desktop\ConductionSecondary.csv')
    exportData(v_out, i_out, pss_switch_off, len(i_out[-1]), len(v_out),
               r'C:\Users\Jaan Wouters\Desktop\TurnOffLossesSecondary.csv')
    exportData(v_out, i_out, pss_switch_on, len(i_out[-1]), len(v_out),
               r'C:\Users\Jaan Wouters\Desktop\TurnOnLossesSecondary.csv')
    exportData(v_out, i_out, p_tf, len(i_out[-1]), len(v_out),
               r'C:\Users\Jaan Wouters\Desktop\TransformerLosses.csv')

    print("--------------------------")
```

Appendix F

Python: calculator for experimental switching losses

```
import math
import pandas as pd
import numpy as np
import matplotlib.pyplot as plt

"""
------------------------------------------------------------------------
----------------------
--- File which calculates the experimental switching losses based on
oscilloscope output file ---
------------------------------------------------------------------------
----------------------
"""

'''
Parameter Input
---------------
'''
plotGraph = True # Plots graphs from the first TurnOn and TurnOff event
encountered
fs = 50000 # Hz, Switching frequency
Vop = 400 # V, Nominal operation voltage across MOSFET
Vgs_plus = 12 # V, Positive gate voltage
Vgs_min = -4 # V, Negative gate voltage
filename = '600V_3600W_2021_5_12.csv' # Name of the output file of the
oscilloscope, must be csv.
precision_Vds = 0.98 # As a fraction of Vop
precision_Vgs = 0.9 # As a fraction of Vgs
R_on = 30E-3  # Ohm, Turn On resistance for switch
R_tf = 70E-3  # Ohm, Transformer primary winding resistance
Vth = 2.1 # V, Threshold voltage
Vdiode = 4 # V, Forward voltage drop across body diode
trr = 24E-9 # seconds, reverse recovery time of body diode
Qrr = 536E-9 # C, reverse recovery charge of body diode
Irr_max_datasheet= 35 # A, peak reverse recovery current of body diode
Ip_pi_datasheet = 35 # A, Turn-off MOSFET current for Irr_max_datasheet

'''
Reading in of File
------------------
'''
# Skips all of the information from the oscilloscope above the values
with open(filename) as fp:
    skip = next(filter(
        lambda x: x[1].startswith('TIME'),
        enumerate(fp)
    ))[0]

df = pd.read_csv(filename, skiprows = skip)
t = df['TIME'].to_numpy()
Vds = df['CH1'].to_numpy()
Vgs = df['CH2'].to_numpy()
Itf = df['CH3'].to_numpy()
Id = df['CH4'].to_numpy()
```

```
'''
Calculating switching losses
----------------------------
'''

def CalculateHardTurnOn(i, plotGraph, plottedTurnOn):
    noPsw = False
    Id2_RMS = 0
    # Trace back where Vds started to descend, if Vop isn't approached well
enough, edit the next variable
    while Vds[i-1]>Vds[i] or Vds[i]<Vop*precision_Vds and
Vgs[i]<precision_Vgs*Vgs_min:
        i = i-1
    Ip_pi = Id[i]
    P_swBodyDiode = fs * Vop * (Ip_pi/Ip_pi_datasheet*Irr_max_datasheet *
trr + Qrr)
    begin = i+1
    #print(Vds[i]) # use this in case you think Vop isn't approached well
enough
    # Look where Vgs almost reaches its nominal value, this should take the
oscillation of Vds into account.
    while Vgs[i]<Vgs_plus*precision_Vgs:
        i = i+1
    end = i
    Eloss = 0
    for i in range(begin, end):
        Eloss = Eloss+Vds[i]*Id[i]*abs(t[i-1]-t[i])
        Id2_RMS = Id2_RMS + (abs(t[-1] - t[-2])) * Id[i] ** 2
    P_sw = fs * Eloss

    # Plot Graphs if requested
    if plotGraph and not plottedTurnOn:
        time = list()
        V = list()
        I = list()
        Vg = list()
        teller = 0
        for i in range(begin, end):
            time.append(teller*abs(t[-1]-t[-2])*1E9)
            teller = teller + 1
            V.append(Vds[i])
            I.append(Id[i])
            Vg.append(Vgs[i])
        time = np.array(time)
        V = np.array(V)
        I = np.array(I)
        Vg = np.array(Vg)
        # Plot figures in a nice format
        figure, axes = plt.subplots(nrows=3)
        ax3 = figure.add_subplot(111, zorder=-1)
        for _, spine in ax3.spines.items():
            spine.set_visible(False)
        ax3.tick_params(labelleft=False, labelbottom=False, left=False,
right=False)
        ax3.get_shared_x_axes().join(ax3, axes[0])
        ax3.grid(axis="x")
        axes[0].plot(time, Vg, 'r')
        axes[0].grid(True)
        axes[0].set_xticklabels([])
        axes[1].plot(time, V, 'b')
        axes[1].grid(True)
```

```
        axes[1].set_xticklabels([])
        axes[2].plot(time, I, 'g')
        axes[2].grid()
        axes[0].set_title("Vgs, Vds and Id vs time")
        axes[0].set_ylabel("Vgs (V)")
        axes[1].set_ylabel("Vds (V)")
        axes[2].set_ylabel("Id (A)")
        axes[2].set_xlabel("time (ns)")
        figure.tight_layout()
        plt.get_current_fig_manager().set_window_title('Experimental Turn-
On Losses')
    return P_sw, i, noPsw, P_swBodyDiode, Id2_RMS

def CalculateSoftTurnOn(i, plotGraph, plottedTurnOn):
    Id2_RMS = 0 # Begin new calculation of RMS current for MOSFET
    # Trace back where Vds started to descend, if Vop isn't approached well
enough, edit the next variable
    while Vds[i-1]>Vds[i] or Vds[i]<Vop*precision_Vds:
        i = i-1
    Ip_pi = Id[i]
    if Id[i] > 0:
        Positive = True
    else:
        Positive = False
    # print(Vds[i]) # use this in case you think Vop isn't approached well
enough
    ElossBodyDiode = 0
    if Positive:
        if Vgs[i]<Vth and not plottedTurnOn:
            print('Body diode conducts first')
        while Id[i] > 0 and Vgs[i]<Vth:
            ElossBodyDiode = ElossBodyDiode + Vdiode * abs(Id[i]) * abs(t[i
- 1] - t[i])
            i = i + 1
        if ElossBodyDiode == 0:
            print('Body-Diode MOSFET does not conduct')
            P_swBodyDiode = 0
        else:
            P_swBodyDiode = fs * Vop *
(Ip_pi/Ip_pi_datasheet*Irr_max_datasheet * trr + Qrr)
    else:
        print('MOSFET is alread forward conducting before Turn-On')
        P_swBodyDiode = 0
    begin = i
    PcondBodydiode = (fs * ElossBodyDiode)
    # Look where Vgs almost reaches its nominal value, this should take the
oscillation of Vds into account.
    while Vgs[i]<Vgs_plus*precision_Vgs:
        i = i+1
    end = i
    Eloss = 0
    if begin == end:
        P_sw = 0
    else:
        for i in range(begin, end):
            Eloss = Eloss+Vds[i]*Id[i]*abs(t[i-1]-t[i])
            Id2_RMS = Id2_RMS + (abs(t[-1] - t[-2])) * Id[i] ** 2
        P_sw = fs * Eloss

        # Plot Graphs if requested
        if plotGraph and not plottedTurnOn:
```

```
            time = list()
            V = list()
            I = list()
            Vg = list()
            teller = 0
            for i in range(begin, end):
                time.append(teller*abs(t[-1]-t[-2])*1E9)
                teller = teller + 1
                V.append(Vds[i])
                I.append(Id[i])
                Vg.append(Vgs[i])
            time = np.array(time)
            V = np.array(V)
            I = np.array(I)
            Vg = np.array(Vg)
            # Plot figures in a nice format
            figure, axes = plt.subplots(nrows=3)
            ax3 = figure.add_subplot(111, zorder=-1)
            for _, spine in ax3.spines.items():
                spine.set_visible(False)
            ax3.tick_params(labelleft=False, labelbottom=False, left=False,
right=False)
            ax3.get_shared_x_axes().join(ax3, axes[0])
            ax3.grid(axis="x")
            axes[0].plot(time, Vg, 'r')
            axes[0].grid(True)
            axes[0].set_xticklabels([])
            axes[1].plot(time, V, 'b')
            axes[1].grid(True)
            axes[1].set_xticklabels([])
            axes[2].plot(time, I, 'g')
            axes[2].grid()
            axes[0].set_title("Vgs, Vds and Id vs time")
            axes[0].set_ylabel("Vgs (V)")
            axes[1].set_ylabel("Vds (V)")
            axes[2].set_ylabel("Id (A)")
            axes[2].set_xlabel("time (ns)")
            figure.tight_layout()
            plt.get_current_fig_manager().set_window_title('Experimental
Turn-On Losses')
    return P_sw, i, PcondBodydiode, P_swBodyDiode, Id2_RMS

def CalculateTurnOff(i, plotGraph, plottedTurnOff):
    while Vgs[i-1]<Vgs[i] or Vgs[i]<precision_Vgs*Vgs_plus:
        i = i-1
    begin = i+1
    # takes the first oscillation of Vds into account
    passVop = 0
    while Vds[i]<Vop:
        i = i+1
    end = i
    Eloss = 0
    for i in range(begin, end):
        Eloss = Eloss+Vds[i]*-Id[i]*abs(t[i-1]-t[i])
    P_sw = fs * Eloss

    # Plot Graphs if requested
    if plotGraph and not plottedTurnOff:
        time = list()
        V = list()
        I = list()
```

```
        Vg = list()
        teller = 0
        for i in range(begin, end):
            time.append(teller*abs(t[-1]-t[-2])*1E9)
            teller = teller + 1
            V.append(Vds[i])
            I.append(-Id[i])
            Vg.append(Vgs[i])
        time = np.array(time)
        V = np.array(V)
        I = np.array(I)
        Vg = np.array(Vg)
        # Plot figures in a nice format
        figure, axes = plt.subplots(nrows=3, ncols=1)
        ax3 = figure.add_subplot(111, zorder=-1)
        for _, spine in ax3.spines.items():
            spine.set_visible(False)
        ax3.tick_params(labelleft=False, labelbottom=False, left=False,
right=False)
        ax3.get_shared_x_axes().join(ax3, axes[0])
        ax3.grid(axis="x")
        axes[0].plot(time, Vg, 'r')
        axes[0].grid(True)
        axes[0].set_xticklabels([])
        axes[1].plot(time, V, 'b')
        axes[1].grid(True)
        axes[1].set_xticklabels([])
        axes[2].plot(time, I, 'g')
        axes[2].grid()
        axes[0].set_title("Vgs, Vds and Id vs time")
        axes[0].set_ylabel("Vgs (V)")
        axes[1].set_ylabel("Vds (V)")
        axes[2].set_ylabel("Id (A)")
        axes[2].set_xlabel("time (ns)")
        figure.tight_layout()
        plt.get_current_fig_manager().set_window_title('Experimental Turn-
Off Losses')
    return P_sw, i

def clearOffset(Vgs, Id, Itf, turnedOn):
    difference = list()
    Vgs_mean = (Vgs_plus + Vgs_min) / 2
    i=0
    if turnedOn:
        # Go to where MOSFET turns off.
        while Vgs[i] > Vgs_mean:
            i = i + 1
        # Go 25% further in the Off state and then start measuring current
        i = i + round(0.5*0.25/(fs*abs(t[-2]-t[-3])))
        beginMeasurment = i
        while i < beginMeasurment + round(0.5**2/(fs*abs(t[-2]-t[-3]))):
            difference.append(Id[i])
            i = i + 1
        difference = np.array(difference)
        offset = difference.mean()
    else:
        # Go to where MOSFET turns on.
        while Vgs[i] < Vgs_mean:
            i = i + 1
        # Go 25% further in the ON state and then start measuring current
difference with Ith.
```

```
        i = i + round(0.5 * 0.25 / (fs * abs(t[-1] - t[-2])))
        beginMeasurment = i
        while i < beginMeasurment + round(0.5 ** 2 / (fs * abs(t[-2] - t[-
3]))):
            difference.append(Id[i]-Itf[i])
            i = i + 1
        difference = np.array(difference)
        offset = difference.mean()
        print("DC-bias offset was around ", round(offset, 2), " A")
    # Correct drain current function so it becomes 0A when switching off
and equals transformer current when on.
    i = 0
    for i in range(len(Id)):
        Id[i] = Id[i] - offset
    if plotGraph:
        id = Id[0:round(1/ (fs * abs(t[-2] - t[-3])))]
        itf = Itf[0:round(1/ (fs * abs(t[-2] - t[-3])))]
        vgs = Vgs[0:round(1/ (fs * abs(t[-2] - t[-3])))]
        vth = np.array([Vth]*round(1/ (fs * abs(t[-2] - t[-3]))))
        vds = np.multiply(Vds[0:round(1/ (fs * abs(t[-2] - t[-3])))], 0.1)
        # Plot the currents of two periods to see if the offset is applied
right
        plt.figure()
        plt.title('Make Sure Id and Itf overlap!')
        plt.xlabel('Time ns')
        plt.ylabel('Current (A) or Voltage (V)')
        plt.grid()
        time = np.array(range(round(1/(fs * abs(t[-1] - t[-2])))))
        plt.plot(time, id, label='Id (A)')
        plt.plot(time, itf, label='IRMS,transfo (A)')
        plt.plot(time, vgs, label='Vgs (V)')
        plt.plot(time, vth, label='Vth (V)')
        plt.plot(time, vds, label='Vds (10^1 V)')
        plt.legend()
        plt.get_current_fig_manager().set_window_title('Control Graph for
offset')
    return Id

'''
Begin Processing file
------------------------------------------------------------------------
-----------
'''

print('------------------------------------------------------------')
print('Beginning Processing file')
print('Estimated Turn-On and Turn-Off events: ', round(abs(t[0]-t[-
1])/(1/fs)))
# Create list with all the calculate switching losses
Psw_On = list()
Psw_Off = list()
P_cond = list()
P_condBodyDiode = list()
P_swBodyDiode = list()
Irms_MOSFET = list()
# Control variable
amountOfTurnOn = 0
amountOfTurnOff = 0
# Used so graphs are only plotted once
plottedTurnOn = False
plottedTurnOff = False
```

```
Vgs_mean = (Vgs_plus + Vgs_min) / 2
i = 0
Id2_RMS = 0
# First look if MOSFET is in the ON or OFF state, make sure the
measurements at the start aren't taken during a switching event!
if Vgs[i] > Vgs_mean:
    turnedOn = True
else:
    turnedOn = False
clearRMS = True
Id_TrueRMS = 0
Vgs_mean = (Vgs_plus + Vgs_min) / 2
Id = clearOffset(Vgs, Id, Itf, turnedOn)
i = 1
# Look if we encounter turn-on or turn-off
while i < len(Vds):
    # Encounter a turn-on
    if Vds[i] < 0 and not turnedOn:
        if Vgs[i] < Vth:
            if not plottedTurnOn:
                print("Perfect ZVS is achieved!")
            P_sw_On, end, PcondBodyDiode, PswBodyDiode, Id2_RMS =
CalculateSoftTurnOn(i, plotGraph, plottedTurnOn)
            Psw_On.append(P_sw_On + PswBodyDiode)
            P_swBodyDiode.append(PswBodyDiode) # Just to verify
            P_condBodyDiode.append(PcondBodyDiode)
        else:
            if not plottedTurnOn:
                print("No ZVS is achieved!")
            P_sw_On, end, noPsw, PswBodyDiode, Id2_RMS =
CalculateHardTurnOn(i, plotGraph, plottedTurnOn) # Conduction losses from
body diode are negligible
            Psw_On.append(P_sw_On)
            Psw_On.append(P_sw_On + PswBodyDiode)
            P_swBodyDiode.append(PswBodyDiode)  # Just to verify
        i = end
        amountOfTurnOn = amountOfTurnOn + 1
        turnedOn = True
        plottedTurnOn = True

    # Encounter a turn-off
    elif Vgs[i] < Vgs_mean and turnedOn:
        if plottedTurnOff:
            P_cond.append(math.sqrt(fs*Id2_RMS)**2*R_on)
            Irms_MOSFET.append(math.sqrt(fs*Id2_RMS))
        amountOfTurnOff = amountOfTurnOff + 1
        P_sw_Off, end = CalculateTurnOff(i,plotGraph, plottedTurnOff)
        Psw_Off.append(P_sw_Off)
        i = end + 20
        turnedOn = False
        plottedTurnOff = True

    else:
        Id2_RMS = Id2_RMS + (abs(t[-1] - t[-2])) * Id[i] ** 2
    i = i + 1

i = 0
Id2_RMS = 0
counter = 1
P_cond_tf = list()
while i<len(Itf):
```

```
    if counter >= round(1/ (fs * abs(t[-2] - t[-3]))):
        P_cond_tf.append(R_tf*math.sqrt(fs*Id2_RMS)**2)
        counter = 1
        Id2_RMS = 0
    Id2_RMS = Id2_RMS + Id[i]**2*(abs(t[-1] - t[-2]))
    i = i + 1
    counter = counter + 1

print('File Processed')
print(amountOfTurnOn, ' Turn-On events encountered.')
print(amountOfTurnOff, ' Turn-Off events encountered.')
print('RMS-value of MOSFET current = ', round(np.mean(Irms_MOSFET), 2), '
A')
print('Mean of the Turn-On Losses = ', round(4*np.mean(Psw_On),2), ' W, of
which ', round(4*np.mean(P_swBodyDiode), 2), ' W recovery losses body
diode.')
print('Mean of the Turn-Off Losses = ', round(4*np.mean(Psw_Off),2), ' W')
print('Mean of the MOSFET & Diode Conduction Losses = ',
round(4*np.mean(P_cond),2), ' W')
print('Mean of the Transformer Conduction Losses = ',
round(np.mean(P_cond_tf),2), ' W')
```

Appendix G

Experimental Results

Table 12: Experimental turn on losses.

Experimental Turn-On Losses (W)		Current (A)									
		1.33	1.53	1.7	5.94	7.79	7.93	8.81	10.97	11.46	11.96
Voltage (V)	200										
	300										
	400		0.77				1.82				
	500										
	600				0.24				2.27		
	700			1.49				4.09		4.45	
	800	0.54				3.20					13.79
	900										

Table 13: Experimental turn off losses.

Experimental Turn-Off Losses (W)		Current (A)									
		1.33	1.53	1.7	5.94	7.79	7.93	8.81	10.97	11.46	11.96
Voltage (V)	200										
	300										
	400		27.17				30.40				
	500										
	600				26.10				19.57		
	700			18.07				18.71		20.50	
	800	16.41				18.73					22.23
	900										

Table 14: Experimental Primary Body Diode Reverse Recovery Losses.

Experimental Primary Body Diode Reverse Recovery Losses (W)		Current (A)									
		1.33	1.53	1.7	5.94	7.79	7.93	8.81	10.97	11.46	11.96
Voltage (V)	200										
	300										
	400		43.7				43.5				
	500										
	600				46.1				43.9		
	700			44.5				44.8		43.6	
	800	44.7				44.0					45.7
	900										

Results Model 1

Table 15: Modeled Switching Losses for Model 1 (turn on and turn off).

Modeled Turn-On Losses (W)		Current (A)									
		1.33	1.53	1.7	5.94	7.79	7.93	8.81	10.97	11.46	11.96
Voltage (V)	200	0	0	0	0	0	0	0	0	0	0
	300	0	0	0	0	0	0	0	0	0	0
	400	0	0	0	0	0	0	0	0	0	0
	500	0	0	0	0	0	0	0	0	0	0
	600	0	0	0	0	0	0	0	0	0	0
	700	0	0	0	0	0	0	0	0	0	0
	800	0	0	0	0	0	0	0	0	0	0
	900	47.3	45.1	43.2	0	0	0	0	0	0	0

Modeled Turn-Off Losses (W)		Current (A)									
		1.33	1.53	1.7	5.94	7.79	7.93	8.81	10.97	11.46	11.96
Voltage (V)	200	236.5	236.9	237.3	246.6	251.1	251.5	253.8	260.0	261.6	263.2
	300	202.2	202.8	203.3	217.3	224.1	224.6	228.1	237.4	239.7	242.2
	400	167.9	168.7	169.4	188.0	197.1	197.8	202.4	214.8	217.9	221.1
	500	133.5	134.5	135.4	158.6	170.0	170.9	176.7	192.3	196.1	200.1
	600	99.2	100.4	101.4	129.3	143.0	144.1	151.0	169.7	174.3	179.1
	700	64.8	66.3	67.5	100.0	116.0	117.2	125.4	147.1	152.4	158.1
	800	30.5	32.1	33.5	70.7	88.9	90.4	99.7	124.5	130.6	137.1
	900	3.8	2.0	0.4	41.4	61.9	63.5	74.0	101.9	103.9	103.9

Results Model 2

Table 16: Modeled Switching Losses for Model 2 (turn on and turn off).

Modeled Turn-On Losses (W)		Current (A)									
		1.33	1.53	1.7	5.94	7.79	7.93	8.81	10.97	11.46	11.96
Voltage (V)	200	0	0	0	0	0	0	0	0	0	0
	300	0	0	0	0	0	0	0	0	0	0
	400	0	0	0	0	0	0	0	0	0	0
	500	0	0	0	0	0	0	0	0	0	0
	600	0	0	0	0	0	0	0	0	0	0
	700	0	0	0	0	0	0	0	0	0	0
	800	0	0	0	0	0	0	0	0	0	0
	900	27.8	28.4	28.9	0	0	0	0	0	0	0

Modeled Turn-Off Losses (W)		Current (A)									
		1.33	1.53	1.7	5.94	7.79	7.93	8.81	10.97	11.46	11.96
Voltage (V)	200	3.92	3.92	3.92	4.03	4.08	4.09	4.11	4.18	4.19	4.21
	300	3.49	3.50	3.50	3.68	3.77	3.77	3.82	3.93	3.95	3.98
	400	2.99	3.01	3.02	3.29	3.42	3.43	3.49	3.65	3.69	3.73
	500	2.41	2.43	2.44	2.85	3.03	3.04	3.13	3.35	3.40	3.46
	600	1.71	1.73	1.76	2.33	2.58	2.60	2.72	3.02	3.09	3.16
	700	0.83	0.87	0.90	1.72	2.07	2.09	2.26	2.65	2.74	2.84
	800	-0.31	-0.25	-0.20	0.99	1.46	1.50	1.72	2.24	2.36	2.48
	900	-1.47	-1.56	-1.64	0.09	0.74	0.79	1.08	1.77	1.81	1.81

Results Model 3

Table 17: Modeled Switching Losses for Model 3 (turn on and turn off).

Modeled Turn-On Losses (W)		Current (A)									
		1.33	1.53	1.7	5.94	7.79	7.93	8.81	10.97	11.46	11.96
Voltage (V)	200	0	0	0	0	0	0	0	0	0	0
	300	0	0	0	0	0	0	0	0	0	0
	400	0	0	0	0	0	0	0	0	0	0
	500	0	0	0	0	0	0	0	0	0	0
	600	0	0	0	0	0	0	0	0	0	0
	700	0	0	0	0	0	0	0	0	0	0
	800	0	0	0	0	0	0	0	0	0	0
	900	21.8	22.0	22.1	0	0	0	0	0	0	0

Modeled Turn-Off Losses (W)		Current (A)									
		1.33	1.53	1.7	5.94	7.79	7.93	8.81	10.97	11.46	11.96
Voltage (V)	200	57.8	58.0	58.2	63.3	66.1	66.1	67.4	71.0	71.9	72.9
	300	40.7	40.9	41.2	47.9	51.6	51.6	53.4	58.3	59.5	60.9
	400	26.2	26.5	26.8	34.3	38.7	38.7	40.8	46.7	48.2	49.8
	500	14.6	14.9	15.1	22.8	27.4	27.4	29.7	36.2	37.9	39.7
	600	5.8	6.1	6.3	13.3	17.8	17.8	20.1	26.9	28.7	30.6
	700	0.4	0.5	0.6	6.0	10.0	10.0	12.2	18.8	20.6	22.6
	800	0.0	0.0	0.0	1.0	4.1	4.1	5.9	12.0	13.7	15.6
	900	0.0	0.0	0.0	0.0	0.3	0.3	1.4	6.4	6.8	6.8

Appendix H

Experimental Results

Table 18: Experimental Efficiency.

Experimental Efficiency		Current (A)									
		1.33	1.53	1.7	5.94	7.79	7.93	8.81	10.97	11.46	11.96
Voltage (V)	200										
	300										
	400		0.75				0.93				
	500										
	600				0.95				0.97		
	700			0.90				0.98		0.97	
	800	0.89				0.98					0.97
	900										

Table 19: Experimental Primary MOSFET Conduction Losses and Experimental Transformer Conduction Losses.

Experimental Primary Conduction Losses (W)		Current (A)									
		1.33	1.53	1.7	5.94	7.79	7.93	8.81	10.97	11.46	11.96
Voltage (V)	200										
	300										
	400		28.5				37.3				
	500										
	600				16.8				40.7		
	700			4.8				25.3		45.5	
	800	1.4				20.4					55.9
	900										

Experimental Transformer Conduction Losses (W)		Current (A)									
		1.33	1.53	1.7	5.94	7.79	7.93	8.81	10.97	11.46	11.96
Voltage (V)	200										
	300										
	400		17.6				22.9				
	500										
	600				10.4				24.8		
	700			3.0				15.5		27.5	
	800	0.9				12.2					33.5
	900										

Results Model 1

Table 20: Modeled Efficiency for Model 1.

Modeled Efficiency		Current (A)									
		1.33	1.53	1.7	5.94	7.79	7.93	8.81	10.97	11.46	11.96
Voltage (V)	200	0.29	0.32	0.34	0.64	0.68	0.69	0.71	0.74	0.74	0.75
	300	0.45	0.48	0.51	0.77	0.80	0.81	0.82	0.83	0.84	0.84
	400	0.56	0.60	0.62	0.85	0.87	0.87	0.88	0.89	0.89	0.89
	500	0.70	0.73	0.75	0.90	0.91	0.91	0.91	0.92	0.92	0.92
	600	0.80	0.82	0.84	0.93	0.94	0.94	0.94	0.95	0.95	0.95
	700	0.88	0.90	0.91	0.96	0.96	0.96	0.96	0.96	0.96	0.96
	800	0.94	0.95	0.95	0.97	0.97	0.97	0.97	0.97	0.97	0.97
	900	0.95	0.96	0.97	0.98	0.98	0.98	0.98	0.97	0.97	0.97

Table 21: Modeled Conduction Losses for Model 1.

Modeled Conduction Losses (W)		Current (A)									
		1.33	1.53	1.7	5.94	7.79	7.93	8.81	10.97	11.46	11.96
Voltage (V)	200	69.3	69.4	69.4	72.0	74.2	74.4	75.7	80.1	81.3	82.6
	300	48.3	48.3	48.4	52.2	55.5	55.8	57.9	64.4	66.2	68.2
	400	31.0	31.1	31.2	36.3	40.7	41.1	43.8	52.5	54.9	57.6
	500	17.6	17.7	17.8	24.2	29.7	30.2	33.6	44.5	47.5	50.9
	600	8.1	8.2	8.3	15.9	22.6	23.2	27.3	40.3	44.0	48.0
	700	2.4	2.5	2.6	11.5	19.3	20.0	24.8	40.0	44.2	48.9
	800	0.5	0.7	0.8	11.0	19.8	20.6	26.1	43.5	48.4	53.7
	900	2.5	2.7	2.8	14.3	24.2	25.1	31.3	50.9	52.4	52.4

Table 22: Modeled Transformer Conduction Losses for Model 1.

Modeled Transformer Conduction Losses (W)		Current (A)									
		1.33	1.53	1.7	5.94	7.79	7.93	8.81	10.97	11.46	11.96
Voltage (V)	200	80,9	80,9	81,0	84,0	86,8	86,8	88,4	93,4	94,9	96,4
	300	56,3	56,4	56,4	60,9	65,1	65,1	67,5	75,1	77,2	79,6
	400	36,2	36,3	36,4	42,3	47,9	47,9	51,1	61,3	64,1	67,2
	500	20,6	20,7	20,8	28,2	35,2	35,2	39,2	51,9	55,5	59,4
	600	9,4	9,6	9,7	18,6	27,0	27,0	31,8	47,0	51,3	56,0
	700	2,8	2,9	3,1	13,5	23,3	23,3	28,9	46,7	51,6	57,1
	800	0,6	0,8	1,0	12,8	24,1	24,1	30,5	50,8	56,4	62,7
	900	2,9	3,1	3,3	16,7	29,3	29,3	36,5	59,4	61,1	61,1

Results Model 2

Table 23: Modeled Efficiency for Model 2.

Modeled Efficiency		Current (A)									
		1.33	1.53	1.7	5.94	7.79	7.93	8.81	10.97	11.46	11.96
Voltage (V)	200	0.61	0.64	0.67	0.86	0.88	0.88	0.89	0.90	0.90	0.91
	300	0.75	0.77	0.79	0.91	0.93	0.93	0.93	0.94	0.94	0.94
	400	0.84	0.85	0.86	0.94	0.95	0.95	0.95	0.95	0.95	0.95
	500	0.89	0.91	0.91	0.96	0.96	0.96	0.97	0.97	0.97	0.97
	600	0.93	0.94	0.94	0.97	0.97	0.97	0.97	0.98	0.98	0.98
	700	0.94	0.95	0.95	0.98	0.99	0.99	0.99	0.98	0.98	0.98
	800	0.95	0.95	0.96	0.99	0.99	0.99	0.99	0.99	0.99	0.98
	900	0.97	0.98	0.98	0.99	0.99	0.99	0.99	0.99	0.99	0.99

Table 24: Modeled Conduction Losses for Model 2.

Modeled Conduction Losses (W)		Current (A)									
		1.33	1.53	1.7	5.94	7.79	7.93	8.81	10.97	11.46	11.96
Voltage (V)	200	69.3	69.4	69.4	72.0	74.2	74.4	75.7	80.1	81.3	82.6
	300	48.3	48.3	48.4	52.2	55.5	55.8	57.9	64.4	66.2	68.2
	400	31.0	31.1	31.2	36.3	40.7	41.1	43.8	52.5	54.9	57.6
	500	17.6	17.7	17.8	24.2	29.7	30.2	33.6	44.5	47.5	50.9
	600	8.1	8.2	8.3	15.9	22.6	23.2	27.3	40.3	44.0	48.0
	700	2.4	2.5	2.6	11.5	19.3	20.0	24.8	40.0	44.2	48.9
	800	0.5	0.7	0.8	11.0	19.8	20.6	26.1	43.5	48.4	53.7
	900	2.5	2.7	2.8	14.3	24.2	25.1	31.3	50.9	52.4	52.4

Table 25: Modeled Transformer Conduction Losses for Model 2.

Modeled Transformer Conduction Losses (W)		Current (A)									
		1.33	1.53	1.7	5.94	7.79	7.93	8.81	10.97	11.46	11.96
Voltage (V)	200	80,9	80,9	81,0	84,0	86,8	86,8	88,4	93,4	94,9	96,4
	300	56,3	56,4	56,4	60,9	65,1	65,1	67,5	75,1	77,2	79,6
	400	36,2	36,3	36,4	42,3	47,9	47,9	51,1	61,3	64,1	67,2
	500	20,6	20,7	20,8	28,2	35,2	35,2	39,2	51,9	55,5	59,4
	600	9,4	9,6	9,7	18,6	27,0	27,0	31,8	47,0	51,3	56,0
	700	2,8	2,9	3,1	13,5	23,3	23,3	28,9	46,7	51,6	57,1
	800	0,6	0,8	1,0	12,8	24,1	24,1	30,5	50,8	56,4	62,7
	900	2,9	3,1	3,3	16,7	29,3	29,3	36,5	59,4	61,1	61,1

Results Model 3

Table 26: Modeled Efficiency for Model 3.

Modeled Efficiency		Current (A)									
		1.33	1.53	1.7	5.94	7.79	7.93	8.81	10.97	11.46	11.96
Voltage (V)	200	0.55	0.58	0.60	0.82	0.85	0.85	0.86	0.88	0.88	0.88
	300	0.70	0.73	0.74	0.89	0.91	0.91	0.91	0.92	0.92	0.92
	400	0.81	0.83	0.84	0.93	0.94	0.94	0.94	0.95	0.95	0.95
	500	0.88	0.89	0.90	0.95	0.96	0.96	0.96	0.96	0.96	0.96
	600	0.93	0.93	0.94	0.97	0.97	0.97	0.97	0.97	0.97	0.97
	700	0.94	0.95	0.95	0.98	0.99	0.99	0.99	0.98	0.98	0.98
	800	0.95	0.95	0.96	0.99	0.99	0.99	0.99	0.99	0.98	0.98
	900	0.98	0.98	0.98	0.99	0.99	0.99	0.99	0.99	0.99	0.99

Table 27: Modeled Conduction Losses for Model 3.

Modeled Conduction Losses (W)		Current (A)									
		1.33	1.53	1.7	5.94	7.79	7.93	8.81	10.97	11.46	11.96
Voltage (V)	200	69.3	69.4	69.4	72.0	74.2	74.4	75.7	80.1	81.3	82.6
	300	48.3	48.3	48.4	52.2	55.5	55.8	57.9	64.4	66.2	68.2
	400	31.0	31.1	31.2	36.3	40.7	41.1	43.8	52.5	54.9	57.6
	500	17.6	17.7	17.8	24.2	29.7	30.2	33.6	44.5	47.5	50.9
	600	8.1	8.2	8.3	15.9	22.6	23.2	27.3	40.3	44.0	48.0
	700	2.4	2.5	2.6	11.5	19.3	20.0	24.8	40.0	44.2	48.9
	800	0.5	0.7	0.8	11.0	19.8	20.6	26.1	43.5	48.4	53.7
	900	2.5	2.7	2.8	14.3	24.2	25.1	31.3	50.9	52.4	52.4

Table 28: Modeled Transformer Conduction Losses for Model 3.

Modeled Transformer Conduction Losses (W)		Current (A)									
		1.33	1.53	1.7	5.94	7.79	7.93	8.81	10.97	11.46	11.96
Voltage (V)	200	80,9	80,9	81,0	84,0	86,8	86,8	88,4	93,4	94,9	96,4
	300	56,3	56,4	56,4	60,9	65,1	65,1	67,5	75,1	77,2	79,6
	400	36,2	36,3	36,4	42,3	47,9	47,9	51,1	61,3	64,1	67,2
	500	20,6	20,7	20,8	28,2	35,2	35,2	39,2	51,9	55,5	59,4
	600	9,4	9,6	9,7	18,6	27,0	27,0	31,8	47,0	51,3	56,0
	700	2,8	2,9	3,1	13,5	23,3	23,3	28,9	46,7	51,6	57,1
	800	0,6	0,8	1,0	12,8	24,1	24,1	30,5	50,8	56,4	62,7
	900	2,9	3,1	3,3	16,7	29,3	29,3	36,5	59,4	61,1	61,1